Retinal Vascular Dysfunction Associated with Diabetes

By

Eui Seok Shin

A dissertation submitted in partial fulfillment of

the requirements for the degree of

Doctor of Philosophy

(Cellular and Molecular Biology)

at the

UNIVERSITY OF WISCONSIN-MADISON

2013

Date of final oral examination: 11/08/2013

The dissertation is approved by the following members of the Final Oral Committee:

Nader Sheibani, Professor, Ophthalmology and Visual Sciences

Ronald Magness, Professor, Obstetrics & Gynecology

Deane Mosher, Professor, Biomolecular Chemistry

Peiman Hematti, Associate Professor, Medicine

Zhen Huang, Associate Professor, Neurology

Table of Contents

List of Figures....iv

Abstract....vii

Acknowledgements....ix

1. Introduction....1

Diabetic retinopathy....3

Epidemiology of diabetic retinopathy....3

Biochemical Change in Diabetic Retinopathy....4

Vascular changes in diabetic retinopathy....10

Epigenetic changes in diabetic retinopathy....13

Blood-Retinal Barrier....14

The cellular organization of retina....14

Role of endothelial cells in retinal vasculature....18

Role of pericytes in retinal vasculature....19

Role of astrocytes in retinal vasculature....20

Physiological changes of retinal vascular cells under high glucose....21

Physiological changes in retinal endothelial cells....21

Physiological changes in retinal pericytes....23

Physiological changes in retinal astrocytes....24

Contributions to the field 26

2. STAT1-Mediated Bim Expression Promotes the Apoptosis of Retinal Pericytes under High Glucose Conditions 29

Abstract 30

Introduction 31

Material and Methods 33

Results 39

Discussion 62

3. High Glucose Attenuates the Migratory Activity of Retinal Astrocyte through Increased Inflammatory Cytokines and Oxidative Stress 68

Abstract 69

Introduction 70

Materials and Methods 72

Results 81

Discussion 108

4. Summary and Future Directions 114

Summary 115

Concluding remarks and future directions 118

Inflammation and vascular dysfunctions 118

Wnt signaling pathway and vascular dysfunction 119

Role of miRNA in vascular dysfunction 120

O-GlcNAc modification in diabetic retinopathy 121

Appendix. PEDF Expression Regulates the Pro-angiogenic and Pro-inflammatory Phenotype of the Lung Endothelium 124

Abstract 125

Introduction 126

Materials and Methods 129

Results 139

Discussion 168

References 173

List of Figures

Figure 1.1 Pathophysiology of diabetic retinopathy 9

Figure 1.2 Vascular changes in diabetic retina. 12

Figure 1.3 Cellular structure of retina. 16

Figure 1.4 Organization of blood vessels in the retina 17

Figure 2.1 Diabetes induces apoptosis of pericyte in retina vasculature. 40

Figure 2.2 Bim expression was increased in the retina of diabetic mice. 43

Figure 2.3 Signaling pathways involved in high glucose mediated apoptosis and increased ROS production in PC. 44

Figure 2.4 Impact of HG on proapoptotic pathways. 48

Figure 2.5 Attenuation of pericyte migration under high glucose conditions. 53

Figure 2.6 Bim expression is essential for high glucose mediated apoptosis and ROS production of PC. 55

Figure 2.7 Incubation of PC under high glucose conditions impacts their effect on EC function. 56

Supplementary Figure 2.1 Expression of cytokines by PC under high glucose and effect of cytokines on apoptosis and the phosphorylation of STAT1in retinal PC. 59

Supplementary Figure 2.2 The impact of high glucose on various down-stream signaling pathways. 61

Figure 2.8 A summary of signaling pathways known to participate in response to high glucose. 67

Figure 3.1 Effect of different glucose conditions on apoptosis, proliferation and GFAP expression in retinal AC. 85

Figure 3.2 Effect of different glucose conditions on the organization of retinal AC on Matrigel and migration. 86

Figure 3.3 The impact of different glucose conditions on the formation of actin stress fibers and focal adhesion in retinal AC. 88

Figure 3.4 The effect of different glucose conditions on adhesion of retinal AC to extracellular matrix (ECM) proteins. 89

Figure 3.5. The effect of glucose conditions on PDGF-mediated migration of retinal AC. 91

Figure 3.6 Expression of integrins in retinal AC under different glucose conditions. 92

Figure 3.7 The impact of high glucose on various down-stream signaling pathways. 96

Figure 3.8 Levels of inflammatory cytokines under different glucose conditions. 98

Figure 3.9 Effect of NAC on the migration of retinal AC under different glucose conditions and the interaction with retinal EC. 101

Figure 3.10 The impact of high glucose conditions on the level of ROS and nuclear localization of Nrf2 in Retinal AC. 105

Figure 3.11 Effect of different glucose conditions on the expression of antioxidant enzymes. 106

Figure 3.12 Effect of different glucose conditions on the expression and secretion of thrombospondin 1 and 2. 107

Appendix Figure 1. Isolation and characterization of mouse lung microvascular endothelial cells (EC). 140

Appendix Figure 2. Expression of EC markers and production of VEGF in lung EC. 143

Appendix Figure 3. The impact of PEDF-deficiency on the migration and formation of actin stress fibers and focal adhesions in lung EC. 146

Appendix Figure 4. The effect of PEDF deficiency on proliferation and apoptosis of lung EC. 148

Appendix Figure 5. PEDF -/- lung EC fail to undergo capillary morphogenesis. 150

Appendix Figure 6. PEDF -/- lung EC exhibited enhanced adhesion to various extracellular matrix (ECM) proteins. 151

Appendix Figure 7. Expression of integrins in retinal EC. 153

Appendix Figure 8. Cellular localizations and expression of junctional proteins 157

Appendix Figure 9. Altered production of ECM proteins in PEDF-/- EC. 158

Appendix Figure 10. Alterations in the expression of NOS in PEDF-/- lung EC. 161

Appendix Figure 11. Expression of PECAM-1 and inflammatory markers in PEDF -/- lungs. 163

Appendix Figure 12. Vascular abnormities in PEDF-/- lungs. 165

Appendix Supplementary Figure 1. Effect of PEDF re-expression in PEDF -/- EC on the expression and localization of β-catenin. 167

Abstract

Diabetic retinopathy (DR) is one of the complications of diabetes and the main cause of blindness among working-aged people. Diabetic retinopathy affects the integrity and function of vascular structure maintained by blood-retinal-barrier (BRB). In inner BRB, endothelial cell, pericytes and astrocytes are cellular components of the vascular structure. To understand the effect of high glucose conditions on the function of vascular cells, many studies have been conducted. However, detailed mechanism for the dysfunction of vascular cells, and interactions between vascular cells under high glucose conditions remain poorly defined.

Pericyte loss is a hallmark of DR and many studies have been performed to elucidate the effect of high glucose conditions on pericyte apoptosis. However, the detailed signaling mechanism for the apoptosis of pericytes under high glucose conditions has not been clearly defined. In this study, I showed that the rate of apoptosis and expression of proapoptotic protein Bim were increased in the retina of diabetic Akita/+ mice and mouse retinal pericytes under high glucose conditions. This increased level of Bim in mouse retinal pericytes was mediated by the sustained activation of STAT1 through increased production of inflammatory mediators. In addition, apoptosis and oxidative stress in pericytes deficient in Bim expression was not affected by high glucose conditions. Studies presented here demonstrate that STAT1-mediated Bim expression plays a crucial role in the dysfunction of retinal pericytes under high glucose conditions.

Astrocytes are macro glial cell and have an essential role in maintaining BRB and development of retinal vascular structure. However, cellular mechanisms underlying dysfunction of retinal astrocytes under high glucose conditions are poorly defined. In the present study, I

demonstrate that high glucose conditions affected adhesion, proliferation and migration of retinal astrocytes without affecting their apoptosis. Furthermore, high glucose conditions also affected the levels of pro-inflammatory molecules including IL-1β, TNF-α and iNOS in retinal astrocytes. Antioxidant, NAC restored the attenuated migration of retinal astrocytes under high glucose conditions, and the attenuated capillary morphogenesis of retinal endothelial cells by conditioned medium from retinal astrocytes under high glucose conditions. In addition, high glucose conditions increased the expression of antioxidant proteins including Prdx2 and HO-1 in retinal astrocytes, which were mediated by nuclear localization of Nrf2. Together, our results demonstrated that oxidative stress and inflammatory mediators are key mediators of the dysfunction of retinal vascular cells under high glucose conditions.

In the appendix, I demonstrate the impact of pigment epithelium-derived factor (PEDF) deficiency on the function of lung endothelial cells. PEDF -/- endothelial cell prepared from lung of PEDF -/- mice exhibited increased migration and decreased proliferation compared with PEDF +/+ endothelial cells. In addition, PEDF -/- endothelial cells exhibited increased level of pro-inflammatory molecules including VEGF, VCAM-1 and iNOS. Furthermore, an inflammatory phenotype was observed in the lung of PEDF -/- mice. Together, these results imply that PEDF has a crucial role in regulating inflammation and angiogenesis in the lung endothelium. In addition, its altered production in the eye may contribute to the inflammatory phenotype associated with diabetes.

Acknowledgements

I would like to express my deepest appreciation to my mentor, Dr. Nader Sheibani. He devoted himself to care for and teach graduate students. He showed me his passion for science and education. He is my role model as a mentor and scientist. He always opened his door for me and spent a huge amount of time to have discussion with me about my science and personal life. It cannot be overemphasized that he is a definitely good mentor for graduate students. I never forget his insightful, valuable advice. I also would like to thank Dr. Christine Sorenson for her advice and help for my research. She provided me with valuable materials for my research and advice in performing my research. I always appreciate her help during my graduate study.

I also would like to express my deepest appreciation to my committee members, Dr. Ronald Magness, Dr. Deane Mosher, Dr. Peiman Hematti and Dr. Zhen Huang. They gave me insightful advice and helpful feedback for my research. They also helped me to develop my career. I was very happy to have such nice committee members.

I want to say thank to former and current lab members, James Kinter, Elizabeth Scheef, Ping Fei, Wei Liu, Yenzhi Sang, Zafer Gurel, Saeed Yadranji, Shoujian Wang, Ismail Zaitoun, M Ali Saghiri, Debi Fisk, Keegan Shallow, Tammy Palenski, Yun Zhao, SunYoung Park, Nasim Jamali, and Mitra Fanoodian. They helped my research and made my life in the lab very warm and happy.

Research for my graduate study was supported by American Heart Association. I appreciate their financial support in performing my project and confidence in my research potentials and abilities.

My family always supported me. My parents and brother always showed their love to encourage me. My mother-in-law gave me very generous support. My sisters and brothers-in-law showed their love and endless support for me and my family.

First of all, I cannot find any word to express my deepest appreciation and love to my wife, Yong Ju. Without her, I could not have taken an adventure into science. I also would like to express my love and appreciation to my children, Hajin and Haseung. They are always source of my energy and motivation. Finally, thank you God for guiding me until now.

This thesis is dedicated to the late Woo-Seob Shim

1. Introduction

Retina is a specialized tissue for vision by converting visible light into the neuronal signals perceived by brain. Retina has a unique vascular system for providing nutrients and oxygen to the inner and outer retina, whose integrity is essential for sensing light (1). Thus, the retinal vascular structure acquires blood-retinal barrier (BRB) characteristics which are crucial for the integrity of retinal vascular structure and the regulation of the retinal microenvironment. In the retina, BRB consists of inner and outer components. Inner BRB consists of tight junctions between endothelial cells, and outer BRB is formed by tight junctions between retinal pigment epithelial (RPE) cells (2).

In inner BRB, endothelial cells are surrounded by pericytes and the foot processes of astrocytes (3). Astrocytes and pericytes are crucial for maintaining the structure of inner BRB (2). Dysfunction of vascular cells in inner BRB under disease state causes breakdown of BRB. This breakdown of BRB leads to a serious impairment in vision. In diabetic retinopathy (DR), the breakdown of BRB under diabetic condition results in vascular leakage and subsequent macular edema which are the cause of vision loss and blindness (4).

To understand how the breakdown of BRB progresses, the cellular mechanisms responsible for the dysfunction of retinal vascular cells including endothelial cells, pericytes and astrocytes under pathological conditions need to be elucidated. The effects of high glucose conditions caused by diabetes on the function of vascular cells, and the mechanisms for dysfunction of vascular cells under high glucose conditions have been the subject of numerous studies. However, the detailed mechanisms involved, and the identity of the primary cellular target remains unknown. These gaps in our understanding of these mechanisms have hampered our ability to develop effective therapies for diabetic retinopathy. Diabetic retinopathy is one of

the serious complications of diabetes and a leading cause of blindness among working-age people (5). Delineating the identity of cellular and molecular mechanisms leading to dysfunction of retinal vascular cells, and identification of protective mechanisms for vascular cell dysfunction under high glucose conditions will provide the rationale for development of effective treatments.

Diabetic retinopathy

Epidemiology of diabetic retinopathy

Diabetes mellitus is a worldwide serious health problem. In 2012, 371 million people were affected by diabetes and 4.7 million people died due to diabetes, including approximately 25.8 million patients in the United States (6). Prevalence of diabetes increases the risk of serious diabetes complications. Diabetic retinopathy is one of the diabetes complications and the main cause of blindness among working-age people. In the US, among patients of type 2 diabetes, estimated 40.3 % of patients have diabetic retinopathy and 8.2% of patients have vision-threatening retinopathy (7). For patients of type 1 diabetes, 86% of patients have retinopathy and 42% of patients have vision-threatening stage of DR (8). Studies based on 22,896 individuals with diabetes showed 34.6% of patients have DR and increasing risk was correlated with duration of diabetes and inappropriate control of blood glucose and blood pressure. Vision threatening stages of DR are proliferative DR and diabetic macular edema. Prevalence for proliferative DR was 6.96% and 6.81% for diabetic macular edema (9). Impairment in vision due

to DR remains a serious health issue worldwide. Tight blood glucose control and early detection and treatment of DR are effective to prevent vision loss and blindness caused by DR (10).

Biochemical Change in Diabetic Retinopathy

The pathogenesis of DR is very complex, because many factors contribute to the pathophysiology of DR. Sustained hyperglycemia in retinal vasculature leads to accumulation of advanced glycation end products (AGEs), inflammation, neuronal dysfunction and oxidative stress (11). These biochemical changes under hyperglycemia are implicated in microvascular dysfunction leading to increased vascular permeability and capillary obliteration. Consequently, these changes in retinal vasculature lead to macular edema and neovascularization in the retina (Figure 1.1) (12).

Excess glucose in blood can have non-enzymatic chemical reactions with amino groups of proteins, lipids, and nucleic acids to produce AGEs (13). This modification by AGEs causes vascular dysfunction in the diabetic retina. Accumulation of AGEs induces retinal pericytes apoptosis. In the early phase of apoptosis, caspase-10 mediates apoptosis of pericytes (73). Angiogenin II is also involved in apoptosis of pericytes. Angiogenin II elevates receptor for AGEs (RAGE) to induce pericyte apoptosis by AGEs (14). AGEs also increase vascular permeability in retinal endothelial cells. AGEs enhance translocation of PKC-δ contributing to loss of tight junctions (15). Thickening of basement membrane (BM) in capillaries is also observed in diabetic retina. AGEs are also involved in the modification of BM. Accumulation of AGEs is associated with the expansion of basement membrane and inhibitor for the accumulation of AGE prevents BM thickening (16). Furthermore, modified BM by AGE prevents survival of retinal pericytes by regulating signaling pathway mediated by platelet-

derived growth factor (PDGF) (17). Thus, AGEs affect survival of pericytes by regulating signaling pathways and BM integrity of retinal blood vessels.

Reactive oxygen species (ROS) is generated from mitochondrial electron transport chain, cytochrome p450s, the NAD(P)H oxidase and nitric oxide synthases. ROS produced by cell is required to maintain normal cellular functions. However, excess production of ROS can cause pathological conditions. These excess levels of ROS consequently results in oxidative stress (18). Diabetes causes oxidative stress, and augmented level of oxidative stress contributes to pathogenesis of diabetic vascular complications including DR (19). In diabetic retina, ROS levels are elevated and related with vascular dysfunction including, pericyte loss, acellular capillary formation, vascular leakage and thickening of BM (20, 21). Oxidative stress in the diabetic retina has causal links with metabolic dysfunction such as vascular inflammation, RAGE activation, activation of PKCs and activation of NF-κB (22-25). Photoreceptor cells have been recently shown to be a major source of oxidative stress and local inflammation in the diabetic retina. Diabetes increased generation of ROS by photoreceptor cells followed by induction of pro-inflammatory mediators including inducible nitric oxide synthase (iNOS) and intercellular adhesion molecule 1 (ICAM-1) (26).

Inflammation is one of the major factors induced during diabetes leading to macular edema, ischemia and neovascularization (10). Physiological changes in diabetic retina are associated with inflammation, and anti-inflammatory therapy ameliorates development of DR in various animal models (27). Several pro-inflammatory mediators are involved in the pathogenesis of DR. iNOS is an enzyme that catalyzes the reaction for generation of nitric oxide (NO). iNOS is upregulated in the diabetic retina and has a crucial role in the pathogenesis of

vascular lesion during the early stage of DR (28, 29). Inhibition of iNOS by aminoguanidine inhibited the progress of retinal dysfunction caused by DR in rodent model of diabetes (30).

Eicosanoids, mediators of inflammation are also affected by diabetic conditions. Eicosanoids have two major families; prostaglandin and leukotriens. Cyclooxygenase-2 (cox-2) is an enzyme that catalyzes the synthesis of prostaglandin. Cox-2 expression is up-regulated in the diabetic retina and treatment with cox-2 inhibitor prevents damage in the diabetic retina (31, 32). Furthermore, diabetic conditions increase the level of pro-inflammatory cytokines. Tumor necrosis factor-α (TNF-α) and Interleukin-1β are increased in the retinas of diabetic animals (33, 34). VEGF has a pro-inflammatory role and is elevated in diabetic retina. Increases in the VEGF level promotes neovascularization and damage in the retina (35), and its inhibition ameliorates vascular leakage in diabetic retina (36).

Anti-inflammatory molecules are also affected by diabetic conditions. Pigment epithelium-derived factor (PEDF) is a member of the superfamily of serine protease inhibitors. It has neuro-protective, anti-angiogenic, and anti-inflammatory features (37). PEDF level is attenuated in diabetic retina and associated with up-regulation of VEGF level (38). PEDF and VEGF act reciprocally in regulating retinal inflammation under diabetic conditions.

The neuronal dysfunction in the retina is also an important effect of diabetes. Neuronal functional abnormalities of diabetic retina precedes the onset of vascular structural change in the retina (39). Diabetes affects cells involved in neuro-sensory function of the retina through altered metabolisms and enhanced apoptosis (5). Apoptosis in neural retina was detected earlier than apoptosis in retinal vascular cells, and the rate of apoptosis in neural retina was not affected by the duration of diabetes (40). Neural apoptosis is associated with the breakdown of BRB and it is

mediated by inflammation and oxidative stress (41). Furthermore, extracellular glutamate is another factor that induces the apoptosis of neuronal cells. In the retina of rat, glutamate level was elevated at 2 months of diabetes (42). At the early stages of DR, the ability of Müller cell to remove glutamate from extracellular space is attenuated and glutamate homeostasis is altered. The increased level of glutamate in diabetic retina has toxic effects on retinal neurons by inducing apoptosis (43). Oxidative stress caused by diabetic conditions also increases glutamate level in diabetic retina (42). Reducing glutamate levels in the diabetic retina prevents neuronal cell death and degeneration. Neuronal cell death is closely related with retinal vascular cell death. The vascular defects appear in the same region as neuronal dysfunction in DR (44). These results imply that there are some intimate interactions between neuronal cells and vascular cells in the retina in order to maintain the integrity of BRB. These interactions need to be further elucidated, and retinal astrocytes may be a key player here.

Besides non-enzymatic protein modifications producing AGEs, diabetic conditions also affects posttranslational modifications of proteins which may play a pivotal role in the pathogenesis of DR. Uridine diphosphate (UDP) N-acetylglucosamine (GlcNAc) is an end product of the hexosamine biosynthetic pathway. This (UDP)-GlcNAc is a donor for O-GlcNAc modification of proteins (45). Diabetic conditions elevate the levels of O-GlcNAcylated proteins in retinal vascular cells more specifically in pericytes (46). Histone acetylation in retina is also affected by diabetic conditions. Diabetic conditions increase histone acetylation related with production of pro-inflammatory proteins including iNOS, ICAM-1 and VEGF in the retina (47). Moreover, high glucose conditions in the retina affect glycosylation of proteins. Synaptophysin is a presynaptic protein in synaptic vesicles and mediates release of neurotransmitters. Diabetic conditions increase mannose rich glycosylation of synaptophysin in the retina and enhances its

degradation in diabetic retina (48). Thus, high glucose conditions modulate various posttranslational modifications of proteins leading to the pathogenesis of DR. However, the impact of diabetic conditions on posttranslational modifications of target proteins in the retina needs to be further studied.

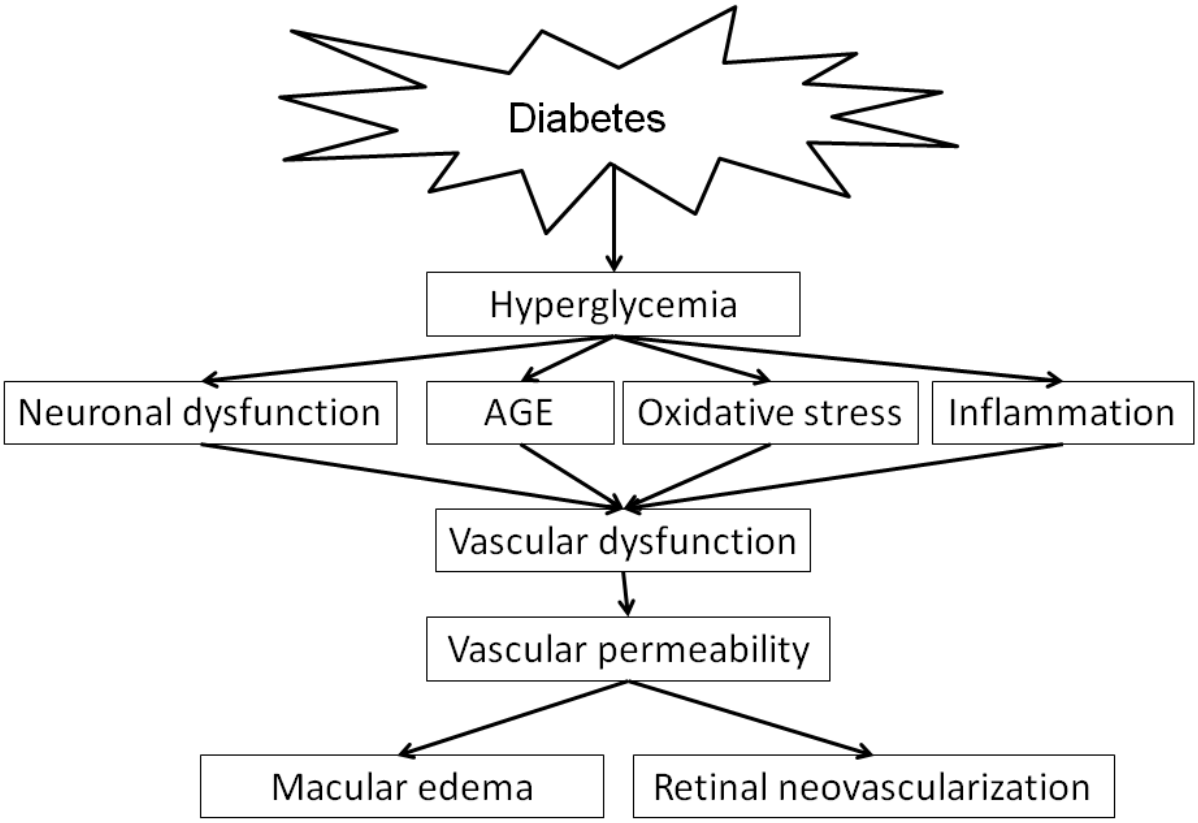

Figure 1.1 Pathophysiology of diabetic retinopathy

Hyperglycemia instigates biochemical changes leading to vascular dysfunction. Vascular dysfunction increases vascular permeability followed by macular edema and retinal neovascularization.

Vascular changes in diabetic retinopathy

Alterations in vascular structure under diabetic conditions results in the breakdown of BRB and diabetic edema (12). The vascular unit of the retina is composed of the endothelial cells, pericytes and astrocytes. Diabetic conditions affect the integrity of BRB by altering structure of neurovascular unit of the retina. In the diabetic retina, vascular endothelial growth factor (VEGF) level is increased contributing to vascular leakage (49). VEGF activates protein kinase C-β (PKC-β) which phosphorylates the tight junction protein, occludin. The phosphorylated occludin is then ubiquitinated and targeted for degradation leading to increased vascular permeability (50).

Pericytes have a crucial role in maintaining vascular stability and early depletion of pericyte is a hallmark of DR. Depletion of pericytes causes the formation of pericyte ghosts. The pericyte ghosts mark the space having pocket shape in basement membranes and is formed after pericytes have disappeared (51). While degeneration of pericytes leads to a pericyte ghost, the number of endothelial cell in retinal vessels is not affected. Pericyte loss increases proliferation of endothelial cells contributing to formation of microaneurysm in retinal vessels. The loss of pericytes in the diabetic retinal vasculature can be detected by the formation of acellular capillaries. Acellular capillaries are basement membrane tubes without cell nuclei and has at least one-fourth of the normal capillary diameter (52). Density of pericytes has an inverse correlation with vascular abnormalities in retina. Reduction of pericytes causes vascular regression leading to retinopathy (53). Loss and degeneration of pericytes affect the integrity and maintenance of BRB. Consequently, pericyte dysfunction leads to capillary dilation,

microaneurysm and increased vascular permeability leading to vascular leakage and macular edema (12).

In diabetic retina, non-perfused and obliterated microvessels are observed in early stage of retinopathy. Vessel closure promotes proliferative retinal neovascularization. The vessel closure can be observed histologically as prevalence of acellular capillary increases (54). Vessel closure contributes to poor oxygen supply to the retina leading to hypoxic conditions and proliferative vascularization.

Hypoxia acts as a primary stimulus to induce angiogenesis. The activation of angiogenesis is mediated by hypoxia-inducible factor 1-alpha (HIF-1α). HIF-1α is a transcription factor regulating transcription of various angiogenic genes including VEGF, VEGF receptor-1 (VEGFR-1) and angiopoietin-1(55). Hypoxia induces vascular abnormalities through the activation of angiogenic factors resulting in pathological vascularization under diabetic conditions. When vessel flow is blocked by vessel closure, retinal vessel leukocytes adhere to the vascular endothelium to promote angiogenesis (56). Leukocyte adhesion to retinal vessel is mediated by ICAM-1 and vascular cellular adhesion molecule-1 (VCAM-1) (57). Leukocyte adhesion to the retinal blood vessel induces endothelial cell death, pericyte loss and vascular closure leading to ischemia (12). Vascular changes in the diabetic retina promotes breakdown of BRB and macular edema leading to retinal detachment and impairment of vision (Figure 1.2).

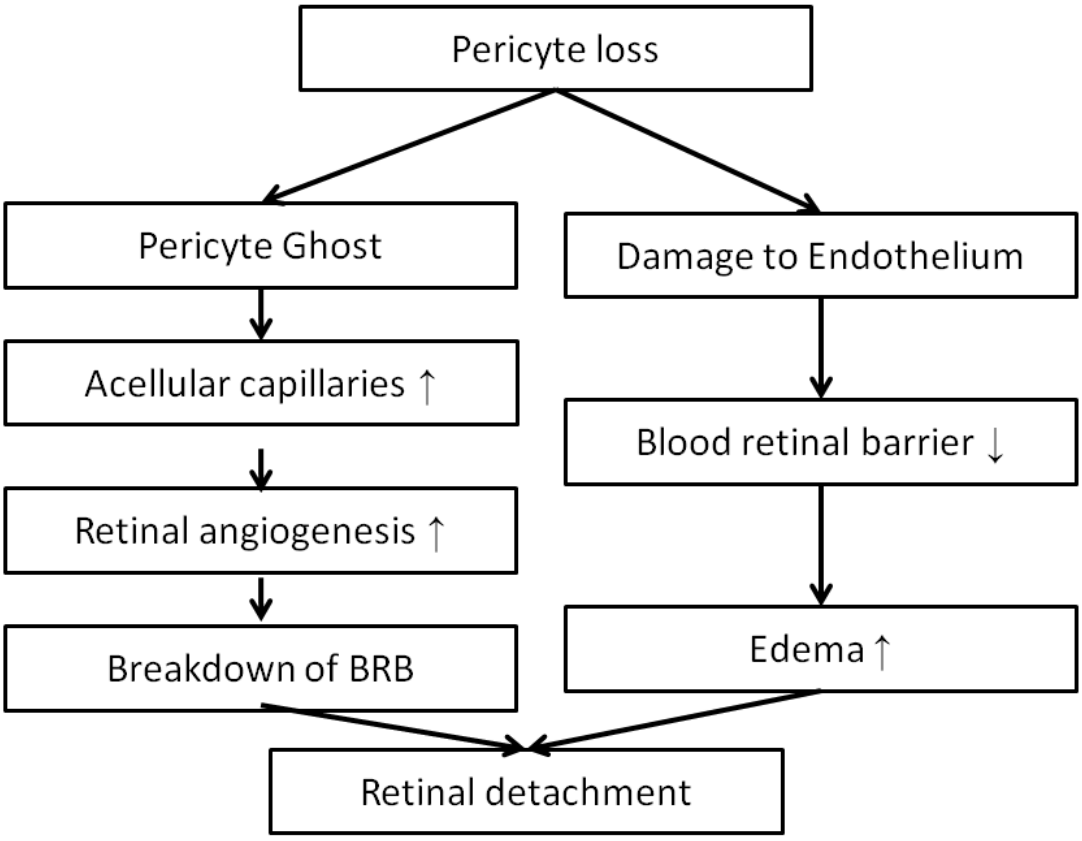

Figure 1.2 Vascular changes in diabetic retina.

Pericytes control vessel stability and proliferation of endothelial cells. Pericyte loss contributes breakdown of BRB and damage to endothelium. These vascular changes caused by pericyte loss leading to retinal detachment.

Epigenetic changes in diabetic retinopathy

Epigenetic modifications have important roles in regulation of gene expression impacting the pathogenesis of various diseases. The epigenetic changes in the development of diabetic complications including DR have been investigated (58). In human umbilical vein endothelial cell (HUVEC), high glucose conditions elevated the level of p300, a transcriptional activator with histone acetyl transferase activity. The increased p300 protein promotes its binding to promoter of genes including endothelin-1, VEGF and fibronectin. Furthermore, histone acetylation and phosphorylation of histone H2AX are upregulated by high glucose conditions (59). In the retina of diabetic rat, expression level and activity of histone deacetylases are augmented and the activities of histone acetyltransferases are decreased. These alterations in the enzymes involved in histone modifications contribute to attenuation of acetylated histone H3 level. These changes in histone acetylation are sustained even after termination of hyperglycemia (60). Furthermore, diabetic conditions regulate expression of metalloproteinase-9 (MMP-9) by epigenetic modifications. Diabetic conditions attenuated histone H3 dimethyl lysine (H3K9me2) and increased acetyl H3K9 (Ac-H3K9) in the retina. These epigenetic modifications activate MMP-9 resulting in mitochondrial damages (61).

Diabetic conditions also affect expression level of miRNA for the pathogenesis of DR (62). In the retina of streptozotocin (STZ)-induced diabetic rat, expressions of several miRNA were altered. miR-200b was attenuated under high glucose conditions accompanied by increases in VEGF levels. Injection of miR-200b mimic prevented VEGF-mediated permeability and angiogenesis (63). In another study, level of miR-200b was upregulated in the retinas of Akita/+ mice which spontaneously develop diabetes. miRNA-200b downregulated oxidation resistance 1

(Oxr1) gene expression leading to oxidative stress in human Müller cell (64). When expression profile of miRNA was investigated in the retina of normal and diabetic rat, it was found that nuclear factor-κB (NF-κB), VEGF and p53- responsive miRNAs were up-regulated (65). HIF-1α and VEGF are regulated by common miRNAs. Silencing of HIF-1α transcripts decreases expression of VEGF and vice versa. Over expression of common miRNA attenuated VEGF and HIF-1α and inhibited vascular permeability in retina of STZ-induce diabetic mice (66). Thus, regulation of gene expression by epigenetic changes under diabetic conditions also contributes to pathogenesis of DR and has been a subject of numerous studies.

Blood-Retinal Barrier

The cellular organization of retina

To understand the function of BRB in maintaining the integrity of retinal structure, understanding of the retinal vascular cell structure and organization is required. Retina is a tissue for perception of light and it converts light into electrochemical signals, which are transmitted to brain through photoreceptor and neuronal circuits for vision (5). Retina is located at the posterior area of the eye and neural tissue lined between the vitreous body and the choroid for the systemic circulation. Retina has four major cellular components which are affected by disease such as diabetes (Figure 1.3). Blood vessels are the first cellular component consisting of endothelial cells and pericytes. Pericytes are smooth muscle cell-like cells enveloping capillaries. Endothelial cells line the interior surface of blood vessels for blood-retinal barrier. Glial cells are the second component consisting of Müller cells and astrocytes. Müller cells support neuronal

cells and modulate function of neurons. Müller cells elongate from inner limiting membrane to the pigment epithelium. Astrocytes are associated with retinal blood vessels by wrapping them with their processes. Glial cells are located at the interface between the neurons and retinal blood vessels and incorporate vascular and neuronal activity of the retina. The third cellular component in the retina is neurons. Neurons are involved in photo-transduction and conveying electrochemical impulses to the brain for sensory functions. Neurons consist of five primary cell types: photoreceptors, horizontal cells, bipolar cells, amacrine cells and ganglion cells. The fourth cellular component in the retina is microglia. Microglia is involved in the modulation of immune function in the retina to maintain homeostasis of the retina. Microglia responds to stress and injury by releasing cytokine and phagocytosis to clear dead cells (5, 67).

The inner BRB is formed by retinal endothelial cells associating with astrocytes and pericytes. Anatomically, endothelial cells are surrounded by basal lamina which astrocytes and pericytes rest on (Figure 1.4). Pericytes envelop the outer side of the capillary wall and interacts with endothelial cell through peg-and-socket contacts, which contain cell junction proteins. The end-foot of astrocytes encircles capillaries and basal lamina is located between the astrocytes and pericytes. Pericytes and astrocytes provide vascular integrity by interacting with endothelial cells (68). Dysfunction in interactions among vascular cells can cause the breakdown of BRB and result in retinal diseases.

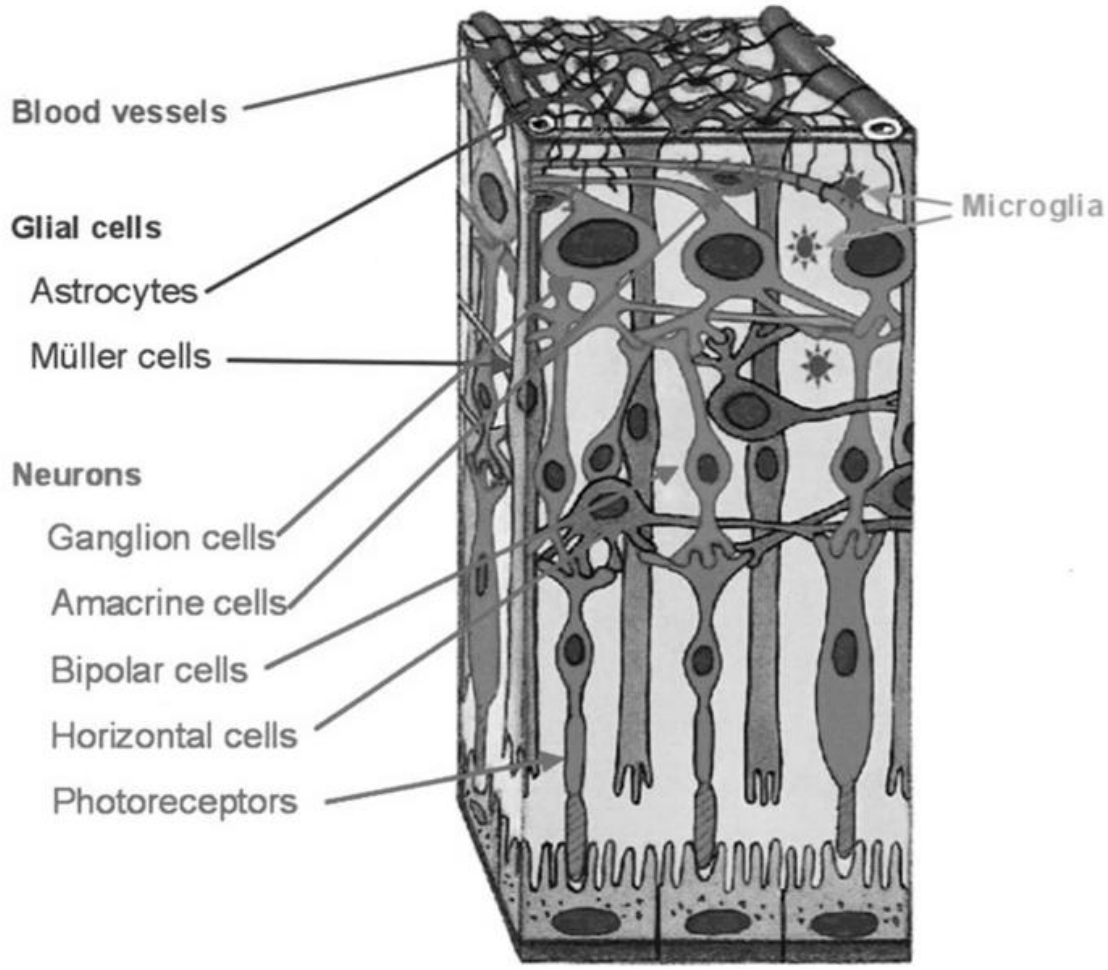

Figure 1.3 Cellular structure of retina.

Retina has four cellular components: Blood vessels, glial cells, neurons and microglia. Adapted from (5).

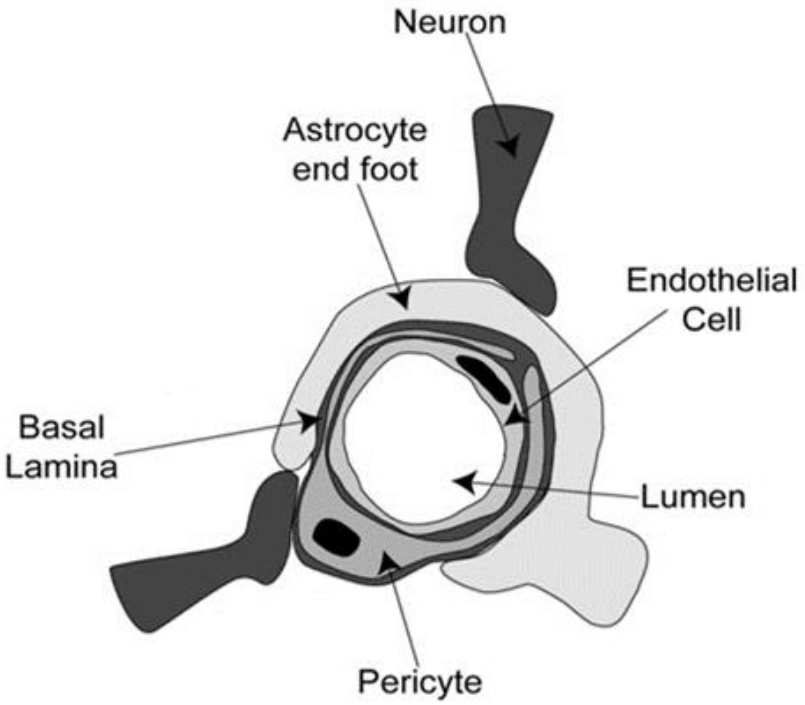

Figure 1.4 Organization of blood vessels in the retina

Endothelial cells are surrounded by basal lamina and pericytes and astrocyte rest on basal lamina. Adapted from (69).

Role of endothelial cells in retinal vasculature

In the inner BRB, retinal endothelial cells are main components to form the physical barriers between vascular lumen and the retina (70). Transport of metabolites and nutrients between blood and retina is selectively regulated by the physical barrier formed by endothelial cells to maintain homeostasis in the retina (71). This physical barrier also regulates transport of ions and fluids to provide an optimal condition, which is crucial for visual function. There are two routes for the selective transport in the retina: the paracellular aqueous pathway regulated by junctions between endothelial cells and the transcellular pathway mediated by specialized vesicles including caveolae or transport proteins (4). The junction between endothelial cells for the paracellular pathway consists of tight junctions, adherens junctions and gap junctions. These junctions at sites of attachment between endothelial cells also regulates signaling for maintaining cell position, inhibits growth by contact inhibition, and protect cell from apoptosis (72).

Endothelial cells express cell-type specific transmembrane proteins for adhesion including vascular endothelial cadherin (VE-cadherin) at adherens junctions and claudins at tight junction (73, 74). Transmembrane proteins at tight junctions include occludin, claudins and junctional adhesion molecules (75). Occludin associates with ZO-1, ZO-2 and ZO-3, which directly bind to F-actin (76). Tight junctions act as a gate for paracellular transport, and a fence for maintaining cell polarity (77). At adherens junctions, VE-cadherin is a main component and it associated with intracellular proteins including β-catenin, p120, and plakoglobin. Regulation of VE-cadherin expression can affect the overall endothelial cell junctions and vascular stability through modulation of intracellular signaling pathways (78).

At gap junctions, a hemi-channel on each of two neighboring endothelial cells makes contact. The hemi-channels consist of six connexins. Small molecules (< 1000 Da) pass freely through gap junctions. Gap junctions are involved in electrical or chemical communications (4). Gap junctions are also involved in the regulation of barrier function by modulating expression and localization of tight junction proteins such as occludin, claudin-5 and ZO-1 (79).

Role of pericytes in retinal vasculature

Pericytes have a crucial role in maintaining BRB. Pericytes or mural cells envelope capillary walls and share basal lamina with endothelial cells (Figure 1.4). Pericytes have an elongated stellate shape and extend finger-like processes to cover the capillary wall formed by endothelial cells (80). Pericytes directly interact with endothelial cell through N-cadherin and connexin-43 hemi channels (81, 82). The ratio of pericyte-to-endothelial in the retina is higher than in other organs. The ratio in the retina is approximately 1:1, whereas 1:3 in brain and 1:10 in lung (83). This higher coverage by pericyte in retinal microvessels may imply that pericytes in the retina have crucial role in maintaining BRB structure. To elucidate the pivotal role of pericytes in the regulation of retinal vascular functions many studies have been conducted.

In pericyte-deficient mice, permeability of blood barrier was increased by the up-regulation of endothelial transcytosis and abnormal polarization of astrocyte end-feet surrounding blood vessels (70). Smooth muscle α-actin (SMA) is expressed in smooth muscle cell and pericytes when activated, and related with contractile properties of these cells. In SMA null mice generated by global gene targeting, retinal structure, vascular pattern and covering vessels by mural cells were normal. However, permeability in retinal vessels was significantly increased in SMA null mice (84). These results suggest that pericytes regulate the maintenance

of blood barrier and structural integrity of blood vessels in the retina. Furthermore, pericytes regulates vessel stability by affecting survival of endothelial cells. VEGF produced by pericytes regulates the survival of endothelial cells (85). Pericytes also promote the apoptosis of endothelial cells in selective vessel patterning by expressing endosialin, a type I transmembrane glycoprotein (86). Transforming growth factor-β1 (TGF-β1) signaling between endothelial cells and pericytes are also involved in the apoptosis of retinal endothelial cells. Systemic inhibition of TGF-β signaling results in abnormalities in the retinal vascular structure including impaired perfusion of the superficial vascular plexus and vascular leakage through enhancing the apoptosis of endothelial cells (87).

Pericytes also have a crucial role in the pathogenesis of diabetes complications such as DR. In diabetic retina, pericyte loss contributes to the disruption of BRB. Apoptosis of pericytes under diabetic conditions leads to the depletion of pericytes from retinal vasculature and is a hall mark of diabetic retinopathy (88).

Role of astrocytes in retinal vasculature

Astrocytes originate from the optic nerve head and migrate into the developing retina laying down the scaffolding for retinal vascularization (89). Astrocytes are closely associated with the developing retinal vasculature with significant impact on retinal vessels function (90). Pathological conditions such as diabetes and ischemia cause degeneration of astrocytes contributing to dysfunction of retinal vasculature (91). Astrocytes are known for their interactions with blood vessels of the central nervous system and help to establish and maintain barrier properties of the vasculature (92).

Retinal astrocytes help to enhance barrier function by releasing soluble proteins. Retinal astrocytes promote the integrity of blood barrier by increasing tight junction protein expression in retinal endothelial cells (93). A-kinase anchor protein 12 (AKAP12) is derived by astrocyte. AKAP reduces VEGF level and increase thrombospondin-1(TSP1) level leading to enhanced blood barrier via the inhibition of protein kinase C ζ (PKC-ζ) phosphorylation and Rho kinase activity (94). Astrocytes regulate expression of glial cell line-derived neurotrophic factor (GDNF) and VEGF in a reciprocal manner through stimulation of retinoic acid receptor (RAR) α to antagonize loss of tight junction for maintaining vascular integrity under hyperglycemic conditions (95). In addition, astrocytes secrete sonic hedgehog (Shh) to activate Hedgehog pathway in endothelial cells, consequently decreasing permeability and pro-inflammatory mediators in endothelial cells (96). Not only secretion of proteins by astrocytes but also physical interactions between astrocytes and vascular areas in the retina is important for the integrity of barrier structure. Astrocytes provide a scaffolding for endothelial cells organization into capillaries, and enhances the tight junction between endothelial cells (97). Dysfunctions of retinal astrocytes in communication with endothelial cell and physical association with blood vessels contribute to BRB breakdown leading to pathological states (68)

Physiological changes of retinal vascular cells under high glucose

Physiological changes in retinal endothelial cells

In hyperglycemic conditions, endothelial cells in retinal blood vessels are directly exposed to a microenvironment with a high concentration of glucose. Therefore, effects of high glucose conditions on the physiology of retinal endothelial cells have been intensively studied. High glucose conditions cause loss of retinal endothelial cells or structural damage (98). The

cellular components affected by high glucose conditions are mitochondria. High glucose condition increased membrane potential and level of reactive oxygen species (ROS) in mitochondria of bovine endothelial cells. Increase in ROS level and membrane potential was correlated with the rate of cell death (99). In rat retinal endothelial cells, high glucose conditions increased mitochondrial fragmentation with concomitant increases in cytochrome c release leading to apoptosis (100). Type 2A protein phosphatase (PP2A) is also involved in the apoptosis of retinal endothelial cells induced by high glucose conditions. High glucose conditions increase PP2A activity through up-regulation of methylation followed by the activation of apoptotic proteins, superoxide, and NF-κB (101). However, apoptosis of retinal endothelial cells under high glucose is independent of caspase activity (102).

High glucose conditions also affect junctional properties in retinal endothelial cells. Connexin 43 is one of the protein components of hemi-channels which allow neighboring cells contact. High glucose conditions reduce the expression of connexin 43 and decrease cell-cell communication triggering apoptosis (103). High glucose conditions also affect tight junctions in retinal endothelial cells. In human retinal endothelial cells, high glucose conditions disrupted tight junctions by decreasing occludin expression through the activation of VEGF and insulin-like growth factor-I receptors (104). Moreover, high glucose conditions affect tight junctions by decreasing ZO-1 levels in the retina of diabetic mice (105). Consequently, high glucose conditions disturb junctional integrity leading to increased retinal endothelial cell permeability (106).

Cell adhesive and migratory activities of retinal endothelial cells are critical for angiogenesis. High glucose conditions affect migration of retinal endothelial cells. High glucose

conditions enhanced the migration of mouse and human retinal endothelial cells. This enhanced migration under high glucose condition was mediated through activation of Src, PI3K/Akt1/eNOS and ERKs pathways (107, 108). In addition, high glucose conditions enhanced the migration of retinal endothelial cells through the up-regulation of heparanase. Akt and ERK phosphorylation are also involved in the upregulation of heparanase (109). Increased migration under high glucose conditions contributes to increased angiogenic activity of retinal endothelial cells.

Physiological changes in retinal pericytes

Depletion of pericytes is a hallmark of DR and the underlying mechanisms involved have been subject of numerous investigation. Various mechanisms are involved in the progress of pericyte apoptosis under diabetic conditions. NF-κB is activated under high glucose condition leading to expression of proapoptotic protein in retinal pericytes (110). Under high glucose conditions, aldose reductase catalyzes synthesis of sugar polyol which accumulates resulting in the apoptosis of retinal pericytes (111). PKC-δ and Src homology-2 domain-containing phosphatase-1 (SHP-1) are also involved in pericytes apoptosis under high glucose conditions. PKC-δ and SHP-1 are activated by high glucose conditions resulting in pericyte apoptosis which is independent of NF-κB signaling pathway (112). Furthermore, high glucose conditions caused endoplasmic reticulum (ER) stress and oxidative stress contributing to apoptosis of pericytes (113).

Up-regulation of oxidative stress in pericytes under high glucose conditions is regulated by thioredoxin interacting protein (TXNIP) (114). Apoptosis of pericytes is also mediated by pericytes-reactive antibodies. High glucose conditions render PC more susceptible to antibody-

mediated attack leading to damage in pericytes and the damaged pericytes exhibit reduced activity in T cell inhibition (115). In addition, high glucose conditions affect morphology and function of mitochondria in pericytes. High glucose conditions disrupted mitochondrial network and enhanced its fragmentation. Membrane potential is elevated and oxygen consumption is attenuated in mitochondria under high glucose conditions. Changes in mitochondria morphology and metabolism causes apoptosis of retinal pericytes (116).

High glucose conditions induce not only apoptosis of pericytes, but also dysfunction of retinal pericytes. In bovine retinal pericytes, actin fibers were disassembled and lost under high glucose conditions (117). In diabetic mice with high blood glucose levels, pericytes in retinal vessels exhibit reduced adherence to endothelium. Angiopoietin-2 (Ang-2) was involved in this reduced adherence of pericytes to endothelium (118). In addition, pericytes protect retinal endothelial cells from inflammation-induced apoptosis by inhibiting proliferation of activated T cell. Inhibition of T cell proliferation by pericytes is attenuated under high glucose conditions (119). Thus, high glucose conditions impair survival and function of retinal pericytes leading to diabetic complications in the retina.

Physiological changes in retinal astrocytes

Astrocytes have a crucial role in the structural integrity of BRB and high glucose conditions that affect BRB structures also affect astrocytes in the retinal vasculature. Diabetic conditions contribute to reduction of astrocytes in peripapillary and far peripheral retina and inhibit astrocytes from associating with superficial large vessels (52, 120). In addition to morphological changes in astrocytes, high glucose conditions also affect cellular physiology of astrocytes. In the retina of diabetic mice, expression of glial fibrillary acidic protein (GFAP), a

marker of glial activation, is increased transiently in astrocytes but not in Müller cells (121). Aquaporins (AQP) are water channel proteins that regulate water-electrolyte balance in the retina. High glucose conditions affect the distribution of AQP1 and AQP4 in retinal astrocytes. In normal retina, AQP4 is mainly expressed around retinal blood vessels, whereas AQP1 is mainly expressed under diabetic conditions (122). Diabetic conditions also affect gap junctions in astrocytes. Connexin is an important protein in the formation of gap junction and cell-cell communication. Connexin-26 and -43 protein levels were attenuated in the astrocyte of diabetic rats. Decrease in connexin expression was followed by significant astrocyte loss (123). Moreover, high glucose conditions activate defense mechanisms against ER stress in astrocyte. Cultured astrocytes under high glucose and retinal astrocytes from diabetic rat are resistant to ER stress under high glucose conditions (124). Taken together, high glucose condition affects morphology and physiology of retinal astrocyte leading to dysfunction of retinal vasculature. However, the detailed mechanisms involved are not well defined and will be addressed in chapter 3.

Contributions to the field

Retina is a specialized organ for vision. It senses light and transmits electrochemical signal to brain. Retina has vascular structure to provide oxygen and nutrients to the retinal tissue. The integrity of vascular structure is maintained not to interfere with sensing light. Blood-retinal-Barrier (BRB) has an important role in maintaining integrity and function of vasculature in the retina. In inner BRB, blood vessels consist of endothelial cell, pericyte and astrocyte. These vascular cells have crucial roles in maintaining BRB function and integrity. Under pathological conditions, dysfunctions of vascular cells are induced leading to breakdown of BRB in the retina. Diabetic retinopathy is a serious vision threatening disease. Diabetic conditions in the retina alter integrity of BRB and destroy BRB leading to vascular leakage and edema in the retina. To understand the impact of high glucose conditions caused by diabetes on the vascular cells including endothelial cells, pericytes and astrocyte, a considerable number of studies have been conducted. From those studies, many physiological factors have been shown to be involved in the dysfunction of vascular cells under high glucose conditions. However, detailed signaling pathways for the dysfunction of vascular cells and mechanisms of interactions between vascular cells under high glucose conditions are not clearly elucidated.

Previously, our lab demonstrated the effect of high glucose conditions on the function of retinal endothelial cell isolated from mice. High glucose conditions affected migratory activity of retinal endothelial cell without affecting apoptosis. However, the impact of high glucose conditions on retinal pericytes needs further investigations. Pericyte loss is a hallmark of the pathogenesis of DR. Although many physiological factors including oxidative stress, inflammation, PKC-δ, SHP-1 and rho-associated protein kinase (ROCK) have been known to be

involved in the apoptosis of pericytes under high glucose conditions, the upstream signaling event leading apoptosis of pericytes under high glucose conditions has not been clearly defined. In chapter 2, I will address the effect of high glucose conditions on apoptosis and migration of pericytes. Furthermore, I will show how high glucose conditions affect interactions between endothelial cell and pericytes. In addition, I will further demonstrate that Bim, a proapoptotic protein, is upstream of ROS production in pericytes under high glucose conditions leading to apoptosis. I will show Bim expression is regulated by the activation of transcription factor STAT1 in response to inflammatory mediators produced under high glucose conditions. These results provide new insight into the mechanism involved in pathogenesis of DR.

Astrocytes are glial cells and have processes that associate with retinal blood vessels and retinal neurons. Astrocytes have a crucial role in maintaining the integrity of BRB and neuronal functions. It is known that high glucose conditions affect physiology of astrocytes leading to their dysfunction. However, underlying mechanisms for the dysfunction of astrocytes under high glucose conditions have not been previously defined. Our lab described a novel method to isolate and culture astrocyte from mice retina. In chapter 3, I will show how high glucose conditions affect migration, proliferation and adhesion properties of retinal astrocytes. Furthermore, the effect of high glucose on signaling pathways involved in migration and proliferation of astrocytes will be revealed. In addition, I will explain the effect of high glucose conditions on production of ROS in retinal astrocytes and how increased ROS levels in astrocytes affect migration and tube formation of retinal endothelial cells. Oxidative stress caused by high glucose conditions activate defense mechanisms in astrocytes to respond to stress. The defense mechanism against oxidative stress under high glucose conditions in retinal astrocytes will be elucidated.

Together, these studies will delineate how high glucose conditions cause dysfunction of retinal vascular cells including retinal pericytes and astrocytes, and affect interactions among vascular cells contributing to vascular dysfunction associated with diabetes.

2. STAT1-Mediated Bim Expression Promotes the Apoptosis of Retinal Pericytes under High Glucose Conditions

This work was submitted to *Cell Death and Disease.*

Abstract

Hyperglycemia impacts different vascular cell functions and promotes the development and progression of various vasculopathies including diabetic retinopathy. Although the increased rate of apoptosis in pericytes (PC) has been linked to increased oxidative stress and activation of PKC-δ and SHP-1 tyrosine phosphatase during diabetes, the detailed mechanisms require further elucidation. Here we show that the rate of apoptosis and expression of proapoptotic protein Bim were increased in the retinal PC of diabetic Akita/+ mice and mouse retinal PC cultured under high glucose conditions. Increased Bim expression in retinal PC under high glucose conditions required the sustained activation of STAT1 through production of inflammatory cytokines. Pericytes cultured under high glucose conditions also exhibited increased oxidative stress and diminished migration. Inhibition of oxidative stress, PKC-δ, or ROCK I/II was sufficient to protect PC against apoptosis under high glucose conditions. Furthermore, PC deficient in Bim expression were protected from high glucose mediated increased oxidative stress and apoptosis. However, only inhibition of PKC-δ lowered Bim levels. N-acetylcysteine didn't affect STAT1 levels suggesting that oxidative stress is downstream of Bim. PC cultured under high glucose conditions disrupted capillary morphogenesis of retinal endothelial cell (EC) in co-culture experiments. In addition, conditioned medium prepared from PC under high glucose conditions attenuated EC migration. Together our results indicate that Bim plays a pivotal role in the dysfunction of retinal PC under high glucose conditions by increasing oxidative stress and death of PC.

Introduction

Dysfunction in retinal blood vessel as well as pathological neovascularization causes blindness in patients with diabetes (125, 126). Mechanisms of vascular dysfunction in diabetes have been the subject of numerous studies. A causal link between diabetic hyperglycemia and the development of retinal vascular complications is established, considering that tight glucose control in diabetic patients reduces the progression of the disease (127). Elucidating mechanisms for dysfunction of retinal vascular cell under high glucose conditions is necessary to develop new therapeutics for diabetic retinopathy.

Pericytes (PC), smooth muscle-like cells that envelope capillaries provide vessel stability and control endothelial cell (EC) proliferation and survival. Pericytes have attracted much attention since the inception of studies to understand the pathogenesis of diabetic retinopathy. Alterations in the interactions between PC and EC play crucial roles in the development of diabetic retinopathy (128). Unfortunately, very little is known about the nature of these interactions, and how they are altered in diabetes.

Pericyte loss is considered a hallmark of early diabetic retinopathy, which can result in focal EC proliferation associated with microaneurysm formation (129). Recent studies suggest that the loss of PC contributes not only to the vasodynamic changes in the early stages of diabetic retinopathy, but also to neovascularization in proliferative diabetic retinopathy (130). In addition, several studies indicate that retinal PC selectively degenerate to form PC ghosts, while EC remain relatively constant, or pathologically proliferate when neovascularization forms (130-132). Although apoptosis of vascular cells is documented in the early stages of diabetic

retinopathy, we believe that PC sense and respond to hyperglycemia differently compared with EC.

The BCL-2 protein family regulates apoptosis by maintaining mitochondrial homeostasis through a balanced activity of pro- and anti-apoptotic family members (133). Among BCL-2 family of proteins, Bim is a proapoptotic protein with only one bcl-2 homology (BH3) domain. Bim is required for the activation of cell death pathways mediated by other bcl-2 proapoptotic family members, namely BAX and BAK (134). Bim expression is increased in the neuroretina of diabetic patients compared with non-diabetics (135). However, the role of Bim in the development and progression of diabetic retinopathy has not been previously addressed.

We recently described a novel method for isolation and culture of retinal PC from wild type and transgenic mice (136). Here we demonstrate that mouse retinal PC not only exhibited higher rates of apoptosis, as shown in PC from other species (112, 137), but also exhibited attenuation of migration under high glucose conditions. High glucose also had a significant impact on production of reactive oxygen species (ROS) and interaction of EC and PC during capillary morphogenesis. Furthermore, we uncovered that increased Bim expression required sustained activation of STAT1 through increased production of inflammatory cytokines. Furthermore, PC prepared from Bim -/- mice were protected from high glucose ill effects. Collectively, our results suggest a pivotal role for Bim expression and/or activation in the dysfunction of PC under high glucose conditions.

Material and Methods

Animals. All experiments were carried out in accordance with and approved by the Institutional Animal Care and Use Committee of the University of Wisconsin School of Medicine and Public Health. *Ins2*^{Akita} heterozygous (Akita/+) male mice on C57BL/6J background were purchased from Jackson Laboratories (Bar Harbor, ME). The diabetic (Akita/+) mice used in the experiments described here were male due to effectiveness and severity of the diabetic phenotype in males. The wild type male mice were used as control. Genomic tail DNA isolation and PCR were performed using the PCR kit (REDExtract-N-Amp™ Tissue PCR Kit, Sigma), and the transgenic Ins2Akita/+ mice were identified by PCR screening. The amplified fragments were digested with Fnu4HI and resulting bands separated on 3.0% agarose gel, as recommended (Jackson Laboratories).

Immunohistochemical staining of the frozen sections. Frozen sections from mouse eyes were prepared as previously described by us (99). 7 month old of mice were used for frozen sections. Apoptotic cell death was assessed by TdT-dUTP Terminal Nick-End Labeling (TUNEL) staining. TUNEL staining was performed using Click-iT TUNEL Alexa Fluor Imaging Assay (Invitrogen, Carlsbad, CA). Sections were then incubated with rabbit anti-PDGFRβ antibody (eBiosciences, San Diego, CA) (1:500 dilution prepared in blocking solution) or rabbit anti-Bim antibody (Cell signaling, Danvers, MA) (1:500 dilution prepared in blocking solution) for overnight at 4 ℃ in a humid environment. After three washes in PBS 5 min each, sections were incubated with appropriate CY3-conjugated secondary antibodies (Jackson ImmunoResearch, West Grove, PA). Sections were counterstained with DAPI (Invitrogen) for staining of the nuclei for 15 min. Sections were washed three times with PBS, covered with PBS:glycerol (2 vol/1vol)

and mounted with a coverslip. Sections were viewed by fluorescence microscopy, and images were captured in digital format using a Zeiss microscope (Carl Zeiss, Chester, VA).

Cell culture. Mouse retinal PC were isolated and cultured as previously described by us (136). The medium contained either 5.7 mM D-glucose (physiological/normal glucose; LG) or 40.7 mM D-glucose (hyperglycemia/high glucose; HG), or 5.7 mM D-glucose and 35 mM L-glucose (control; LG+L-glu), as previously described (138). Cells were maintained in growth medium for 5 days prior to each experiment, and the medium was changed every other day. The cells were also exposed to a cycle of high glucose for 2 days, normal glucose for 2 days, and then high glucose for 2 days prior to each experiment (fluctuation condition). Mouse retinal EC were isolated and cultured as previously described by us (139).

Apoptosis assays. Cells (0.1 ml of $1x10^5$ cells/ml) were placed on fibronectin (2 μg/ml)-coated 4-well chamber slides. After attachment, cells were cultured in medium under normal glucose or high glucose conditions or high glucose conditions containing various treatments such as the antioxidant N-acetylcysteine (NAC) (1 mM; Sigma, St. Louis, MO), PKC-δ inhibitor rottlerin (1 μM; Sigma), ROCK1/2 inhibitor Y-27632 (10 μM; Cayman Chemical, Ann Arbor, MI), SHP-1 inhibitor Sodium Stibogluconate (1 μM) (EMD, Gibbstown, NJ) or fludarabine (10 μM; Sigma) for 5 day. Apoptotic cell death was assessed using Click-iT TUNEL Alexa Fluor Imaging Assay (Invitrogen) as recommended by the manufacturer. Positive cells were counted under fluorescence microscope and the percentage of apoptotic cells relative to the total number of

cells was calculated. Concentrations for various pharmacological inhibitors were determined based on minimal effect on cell viability during the five day exposure to high glucose concentrations. The effect of cytokines on apoptosis was determined by measuring caspase activation using Caspase-Glo 3/7-assay kit as recommended by the supplier (Promega, Madison, WI). The assay provides caspase-3/7 DEVD-aminoluciferin substrate and the caspase 3/7 activity is detected by luminescent signal. For the assay, retinal PC were plated at 8×10^3 cells per well of a 96 well plate and the next day incubated with 10 ng/ml TNF-α, IL-1β or MCP-1for 24 h. Caspase activity was detected using a luminescent microplate reader (Victa2 1420 Multilabel Counter, PerkinElmer, Waltham, MA). All samples were prepared in triplicate and repeated at least three times with similar results.

Determination of oxidative stress. Cells (0.1 ml of $1x10^5$ cells/ml) were plated on fibronectin (2 μg/ml)-coated 4-well chamber slides. After attachment, cells were cultured in medium under different glucose conditions for 5 days with/without various treatments as noted above. The level of cellular reactive oxygen species (ROS) was assessed using dihydroethidium staining (DHE; Invitrogen), as previously described (140). For quantitative assessments, the images were analyzed using Image J software (National Institutes of Health, Bethesda, MD). Values were obtained from each cells captured in 5 high power fields (x400). More than forty cells per each condition were analyzed.

Transwell migration assays. The impact of high glucose on migration of PC, and the impact of conditioned medium collected from PC under various glucose conditions on the migration of EC, was assessed using transwell assays as described in (136). The method for determining the effect of PDGF-BB on the migration of PC was also described by us (136). To examine the migration of EC, 1×10^5 cells in 100 μl of medium were added to the top of each transwell membrane. Transwell inserts were placed in 24-well dishes containing conditioned medium collected from PC cultured under various glucose conditions for five days. Cells were allowed to migrate through the membrane for 3 h at 37℃. The number of migrated cells was determined as previously described (138).

Scratch wound assays. The migration of cells cultured under various glucose concentrations was also assessed by scratched wound assay as described (138). Confluent monolayers of retinal PC cultured in different glucose conditions for 5 days were wounded using a 1 ml micropipette tip and incubated with growth medium with appropriate glucose concentration. Wound closure was monitored by phase microscopy, and the wounds were photographed at 0, 24, 48 and 96 hour. Each sample was performed in triplicate on at least three independent occasions using two different isolations of PC, with similar results.

Western blot analysis. Approximately 2×10^5 cells were plated in 60-mm plates and cultured in the growth medium containing different glucose concentrations for 5 days. For cytokine treatment, retinal PC was incubated with 10 ng/ml TNF-α, IL-1β or 10ng/ml TNF-α+10ng/ml IL-

1β for 24 h after serum starvation for 24h. The cells were washed twice with cold PBS, lysed in 0.1ml of lysis buffer (20 mM Tris pH 7.4, 2 mM EDTA, 1 mM NaF, 1mM Na_3VO_4, 1% Triton X-100, 1% NP-40, 0.1% SDS and protease inhibitor cocktail (Roche) and briefly sonicated. The lysates were centrifuged and protein concentrations were determined using the BCA protein assay kit (Pierce). For the retina lysate, the retinas were lysed in the same lysis buffer and prepared as described above for cells. The protein samples were mixed with appropriate volume of 6x SDS sample buffer and analyzed using 4-20% SDS-PAGE (Invitrogen). Proteins were transferred to nitrocellulose membrane, blocked, and incubated with appropriate primary antibodies at 4 ℃ overnight. After washing, the blots were incubated with appropriate HRP-conjugated secondary antibodies and developed using ECL system (GE healthcare). The antibody to β-actin (Sigma) or β –catenin (BD Biosciences, San Jose, CA) was used to verify equal protein loading. The following primary antibodies were used: p-STAT1 (Tyr701), STAT1, p-Src (Tyr418), p-p38 (Thr180/Tyr182), p38, p-Akt1 (ser 473), Akt1, p-ERK and ERK (cell signaling, Danvers, MA), p-JNK1, and JNK1 (R&D System, Minneapolis, MN), Bim (Cell signaling) and p53 (Santa Cruz Biotechnology, Santa Cruz, CA).

Capillary morphogenesis. Capillary morphogenesis was performed as previously described by us (138). Equal numbers of retinal pericytes and endothelial cells (2×10^5) in 2 ml were applied to the Matrigel-coated plates (0.5 ml Matrigel per 35 mm dish), incubated at 37 ℃, photographed after 18 h in digital format using a Nikon microscope. For quantitative assessment of the data, the mean number of branch points was determined by counting the number of branch points in five high-power fields (×100).

RNA purification and real time qPCR analysis. The total RNA from PC was extracted using mirVana PARIS kit (Invitrogen, Carlsbad, CA). cDNA synthesis was performed from 1 μg of total RNA using Sprint RT Complete-Double PrePrimed kit (Clontech, Mountain View, CA). 1 μl of each cDNA (dilution 1:10) was used as template in qPCR assays, performed in triplicate of three biological replicates on Mastercycler Realplex (Eppendorf) using the SYBR-Green qPCR Premix (Clontech). Amplification parameters were as follows: 95 ℃ for 2min; 40 cycles of amplification (95 ℃ for 15 sec, 60 ℃ for 40 sec); dissociation curve step (95 ℃ for 15 sec, 60 ℃ for 15 sec, 95 ℃ for 15 sec). Primer sequences for TNF-α were 5′-ACCGTCAGCCGATTTGCTAT-3′ (forward) and 5′-TTGACGGCAGAGAGGAGGTT-3 (reverse). For IL-1β, 5'- GTTCCCATTAGACAACTGCACTACA-3' (forward), and 5'-CCGACAGCACGAGGC TTTT-3' (reverse); Standard curves were generated from known quantities for each of the target gene of linearized plasmid DNA. Ten times dilution series were used for each known target, which were amplified using SYBR-Green qPCR. The linear regression line for ng of DNA was determined from relative fluorescent units (RFU) at a threshold fluorescence value (Ct) to quantify gene targets from cell extracts by comparing the RFU at the Ct to the standard curve, normalized by the simultaneous amplification of RpL13a, a housekeeping gene. Primer sequences for RpL13a were 5'-TCTCAAGGTTGTTCGGC TGAA-3' (forward) and 5'-CCAGACGCCCCAGGTA-3' (reverse).

Statistical analysis. Statistical differences between control and treated samples were evaluated with student's unpaired *t*-test (2-tailed) or one-way ANOVA with post hoc Dunnett's test for multiple comparisons. Mean ±SE are shown. p values ≤ 0.05 were significant.

Results

*Apoptosis of PC was increased in the retina of diabetic mice and under high glucose conditions***.** Apoptosis of PC in mouse retina was determined in wild type and Ins2Akita/+ mice with 7 months of diabetes. Akita/+ mice carry a mutation in their insulin gene and develop diabetes by 4 weeks of age. Diabetes is more prominent in male mice. These mice do exhibit many of the early non-proliferative change in their retina. In imunofluorescence staining for TUNEL (apoptotic cells) and PDGFR-β (PC), an increase in TUNEL-positive PC in diabetic retinas was observed compared with wild type mice (Figure 2.1 A). Quantification for TUNEL-positive PC is shown in Figure 2.1 B.

We next determined the impact of high glucose on retinal PC apoptosis in culture. The effect of high glucose on mouse retinal PC has not been previously addressed. Retinal PC were cultured in medium under normal, high glucose or osmolarity control for 5 days as detailed and previously used by us and others (138, 141, 142). Consistent with previous studies (112), mouse retinal PC cultured under high glucose conditions exhibited a significantly higher rate of apoptosis compared with cells cultured under normal glucose or osmolarity control (Figure 2.1 C). A similar rate of apoptosis to that observed under high glucose conditions was noted in PC cultured under fluctuating glucose conditions (Figure 2.1 C)

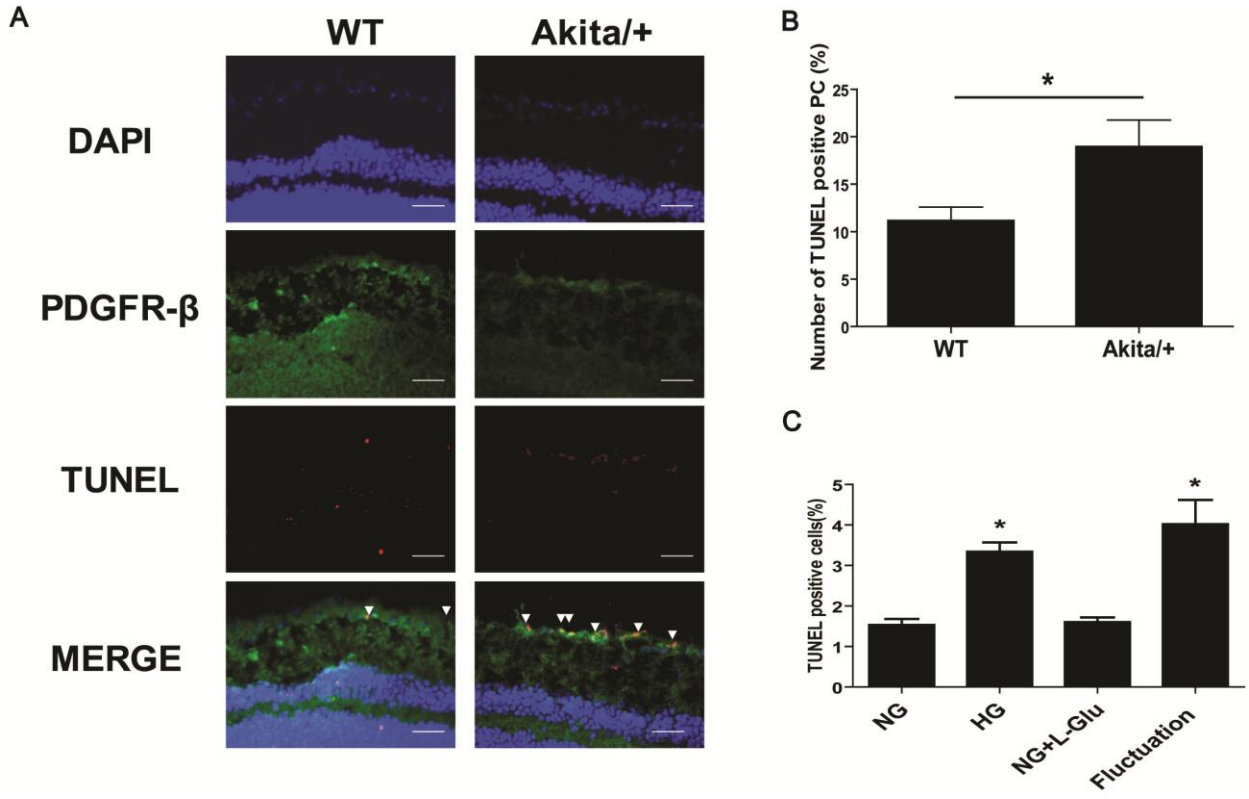

Figure 2.1 Diabetes induces apoptosis of pericyte in retina vasculature.

(A) Retinal frozen sections were prepared from wild type and Akita/+ mice. Double immunofluorescence staining was performed for PDGFR-β and TUNEL. Arrow heads indicate TUNEL and PDGFR-β positive cells in the superficial layer of the retina. Bar indicates 20 μm. (B) Quantification of TUNEL and PDGFR-β positive cells is shown. Data are presented as mean ± SEM (n=7 for wild type and n=8 for Akita/+ mice); *$p<0.05$ compared with wild type. (C) The effects of high glucose on apoptosis of retinal PC. Retinal PC cultured under high glucose conditions exhibited a significantly higher rate of apoptosis. NG: normal glucose condition and HG: high glucose. Similar results were observed under fluctuation conditions. $n \geq 3$; *$p \leq 0.05$ (NG vs. HG or Fluctuation)

Bim level was increased in retinas of diabetic mice. We next examined whether expression of bcl-2 family member Bim was altered in retinas of diabetic Akita/+ mice. Bim is a proapoptotic member of the bcl-2 family with significant role in retinal vascular homeostasis (143). The expression level of Bim in mouse retina was determined in wild type and Akita/+ mice. In immunofluorescence staining for Bim and PDGFR-β, an increase in Bim retinas was observed in diabetic compared with wild type mice (Figure 2.2 A). In superficial layer of retina, the expression level of Bim was increased in PC. To further confirm increased Bim expression in diabetic mice retina, lysates from retinas were analyzed by Western blotting. Bim level was significantly elevated in the retina of Akita/+ mice compared with wild type mice (Figure 2.2 B, 2.2 C).

Oxidative stress is an up-stream effecter of high glucose-mediated PC dysfunction. Exposure of perivascular supporting cells to high glucose generally results in increased oxidative stress and apoptosis (112, 144, 145), perhaps through activation of PKC-δ promoting diabetic retinopathy (112). To determine whether increased oxidative stress and/or activation of PKC-δ similarly contributes to high glucose-induced apoptosis of mouse retinal PC, we evaluated the rate of apoptosis in the presence of the N-acetylcysteine (NAC), an antioxidant with significant inhibitory effect on pathogenesis of diabetic retinopathy (146, 147), or Rottlerin. Rottlerin is a PKC-δ specific inhibitor with an IC_{50} of 3-6 μM for PKC-δ (148, 149). Rottlerin inhibits apoptosis of smooth muscle cells in response to oxidative stress (150). Incubation with Rottlerin or NAC protected PC from high glucose mediated apoptosis (Figure 2.3 A). Inhibition of SHP-1, as demonstrated previously (112), was also protective, although to a lesser extent (Figure 2.3 A).

RhoA/ROCK signaling pathway plays an important role in regulation of angiogenesis, and its opposition by MAPK/ERKs signaling promotes EC survival and sprouting during angiogenesis (151-153). Very little is known about the contribution of RhoA/ROCK pathway to the function of PC. We next determined the impact of ROCK I/II inhibitor, Y-27632, on PC apoptosis under high glucose conditions. Inhibition of ROCK I/II protected PC from high glucose induced apoptosis (Figure 2.3 A). Thus, activation of RhoA/ROCK pathway makes a significant contribution to the proapoptotic phenotype of retinal PC under high glucose conditions.

To examine the effect of high glucose condition on oxidative stress in PC, level of ROS was measured by dihydroethidium (DHE) staining. High glucose condition indeed elevated ROS levels in PC. NAC inhibited ROS production under high glucose condition. In contrast, Rottlerin, sodium stibogluconate (SSG; a SHP-1 specific inhibitor (154)) and Y-27632 did not affect ROS production in PC under high glucose conditions (Figure 2.3 B). Thus, oxidative stress is an up-stream effecter of high glucose mediating PC dysfunction.

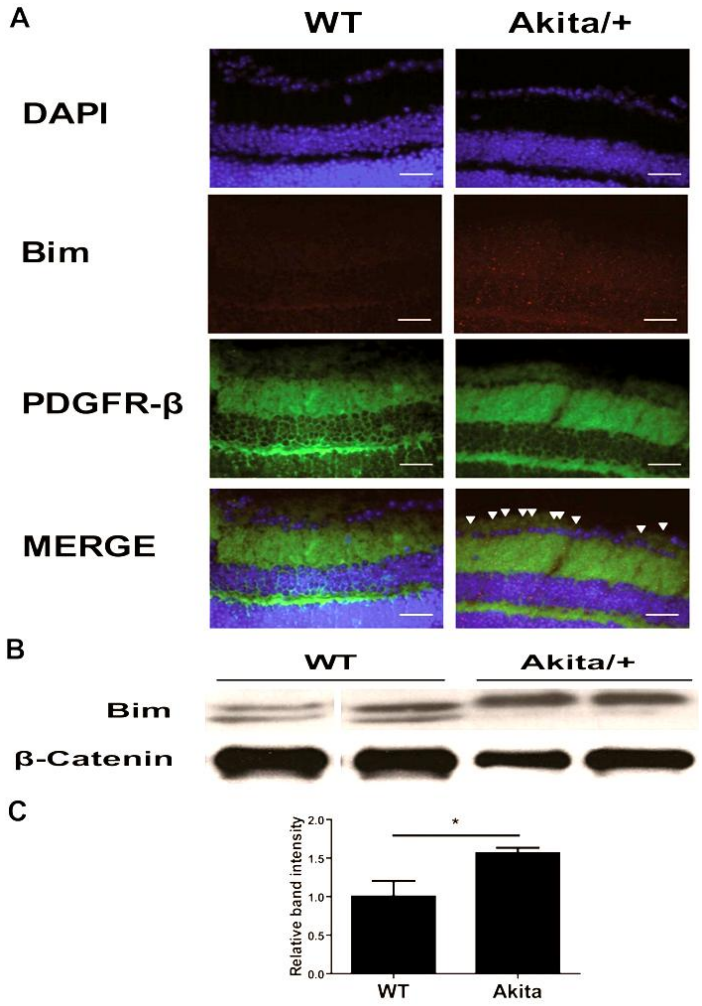

Figure 2.2 Bim expression was increased in the retina of diabetic mice.

(A) Retinal frozen sections were prepared from wild type and Akita/+ mice. Double immunofluorescence staining was performed for PDGFR-β and Bim. Arrow heads indicate Bim and PDGFR-β positive cells in the superficial layer of retina. Bar indicates 20 μm. (B) Expression of Bim in the retina of wild type and Akita/+ mice was examined by Western blot analysis. The antibody to β-catenin was used for loading control. (C) Quantification of band intensity in Western blots. $n \geq 4$; $*p \leq 0.05$ (wild type vs. Akita/+).

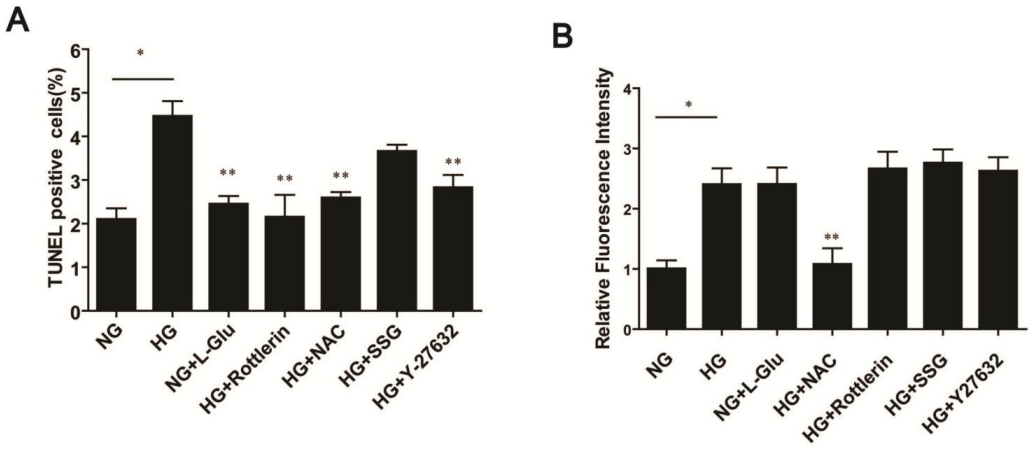

Figure 2.3 Signaling pathways involved in high glucose mediated apoptosis and increased ROS production in PC.

(A) An increase in the rate of apoptosis was observed in PC cultured under high glucose (HG) compared to normal glucose (NG) or osmolarity control (NG+L-Glu) conditions. Incubation of PC under high glucose with NAC (anti-oxidant), Rottlerin (PKC-δ inhibitor) or Y-27632 (ROCK I/II inhibitor) reduced the rate of apoptosis. SSG (SHP-1 inhibitor) had a modest effect. $n \geq 3$; *$p \leq 0.05$ (NG vs. HG); **$p \leq 0.05$ (HG vs. NG+L-Glu or HG+inhibitors). (B) Retinal PC cultured under high glucose (HG) conditions exhibited a significantly elevated level of ROS compared to normal (NG) or osmolarity control (NG+L-Glu) conditions. Incubation of PC under high glucose with NAC reduced the level of ROS. Inhibition of PKC-δ, SHP-1 and ROCK I/II had no significant effect on ROS levels under high glucose conditions. $n \geq 30$; *$p \leq 0.05$ (NG vs. HG); **$p \leq 0.05$ (HG vs.HG+NAC).

High glucose enhanced Bim expression in retinal PC. The bcl-2 protein family members play important roles in regulation of apoptosis and angiogenesis (143, 155). We also assessed p53 expression under various glucose conditions. The p53 expression was minimally affected in PC cultured under various glucose conditions (Figure 2.4 A). Although incubation of PC with NAC under high glucose conditions had no significant effect on p53 expression, incubation of PC with PKC- inhibitor resulted in a modest but significant increase in p53 expression under high glucose conditions.

We observed a significant increase in Bim expression of PC cultured under high glucose conditions compared to normal glucose or osmolarity control (Figure 2.4 B). Although incubation of PC with NAC in high glucose did not have a significant effect on Bim expression, inhibition of PKC-δ reduced Bim expression to levels comparable to that seen in cells cultured in normal glucose. Expression of Bim in pancreatic β-cells is regulated by the activation of STAT1 (156, 157). To elucidate the mechanism(s) for the up-regulation of Bim expression, we examined the level of active and total STAT1 in PC under various glucose conditions. Level of p-STAT1 in PC cultured under high glucose conditions was significantly increased compared with normal glucose or osmolarity control (Figure 2.4 C). Inhibition of ROS or PKC-δ under high glucose condition did not affect the level of p-STAT1.

We next examined if inhibition of STAT1 protects PC from apoptosis induced by high glucose conditions. Fludarabine is a purine analog and potent inhibitor of STAT1 activity(158). Inhibition of STAT1 by fludarabine protected PC against apoptosis under high glucose conditions (Figure 2.4 D). Thus, activation of STAT1, perhaps by production of inflammatory cytokines including tumor necrosis factor-α (TNF-α) and interleukin-1β (IL-1β) in PC under

high glucose conditions may occur. Supplementary Figure 2.1 A and B shows that in fact incubation of PC under high glucose conditions resulted in increased expression of TNF-α compared with normal glucose conditions.

We next examined which cytokines is required for PC apoptosis. Supplementary Figure 2.1 C shows incubation of PC with TNF-α induced PC apoptosis whereas monocyte chemotactic proteins-1 (MCP-1) and IL-1β did not have any effect. The effect of inflammatory cytokines on the activation of STAT1 was then examined in PC incubated with TNF-α and IL-1β under normal glucose conditions. TNF-α and IL-1β increased phosphorylated STAT1 level in retinal PC (Supplementary Figure 2.1 D). Thus, incubation of PC under high glucose conditions results in production of inflammatory cytokines, including TNF-α, and sustained activation of STAT1 driving Bim expression.

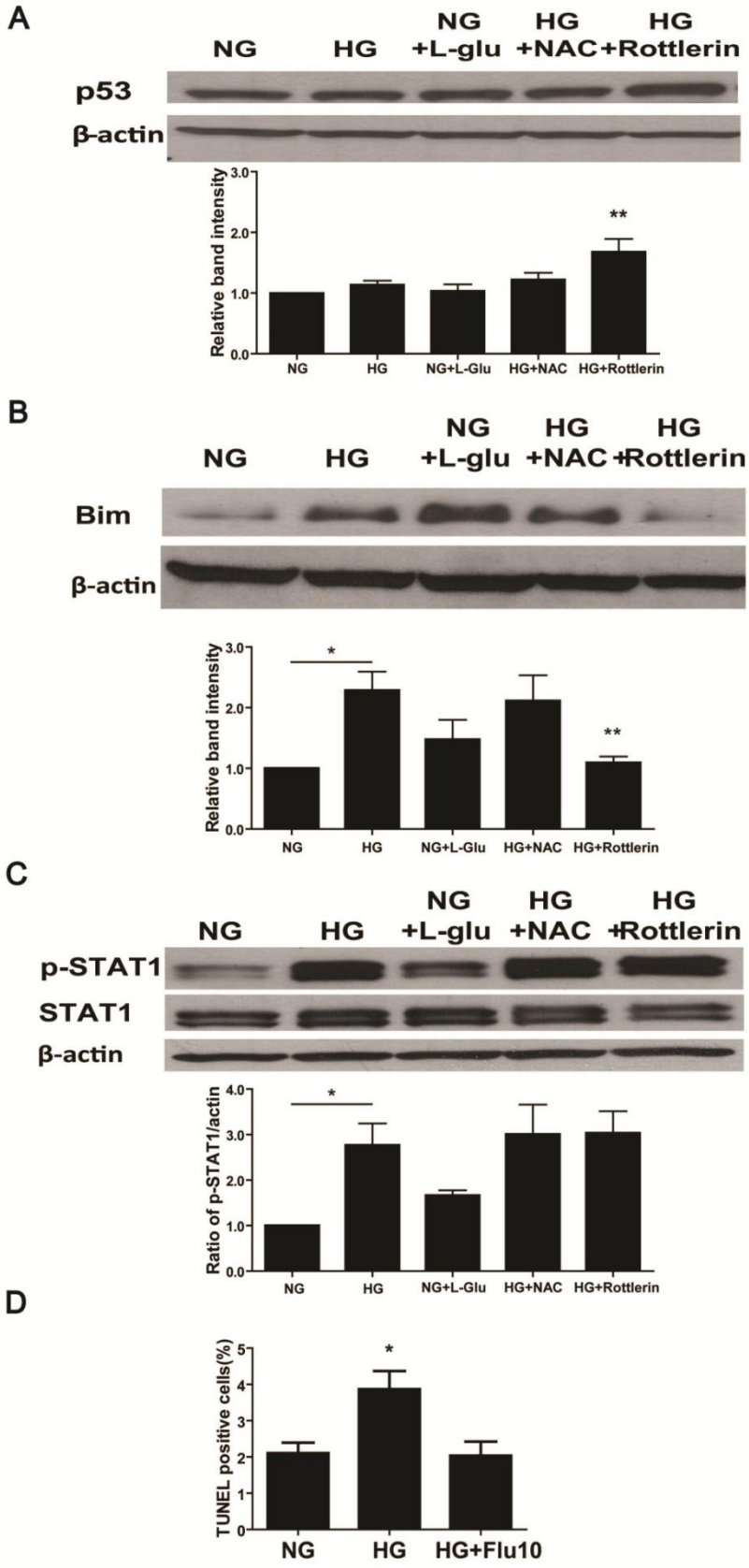
A
NG
HG
NG +L-glu
HG +NAC
HG +Rottlerin
p53
β-actin
Relative band intensity
3.0
2.0
1.0
0.0
**
NG
HG
NG+L-Glu
HG+NAC
HG+Rottlerin
B
NG
HG
NG +L-glu
HG +NAC
HG +Rottlerin
Bim
β-actin
Relative band intensity
3.0
2.0
1.0
0.0
*
**
NG
HG
NG+L-Glu
HG+NAC
HG+Rottlerin
C
NG
HG
NG +L-glu
HG +NAC
HG +Rottlerin
p-STAT1
STAT1
β-actin
Ratio of p-STAT1/actin
4.0
3.0
2.0
1.0
0.0
*
NG
HG
NG+L-Glu
HG+NAC
HG+Rottlerin
D
TUNEL positive cells(%)
5
4
3
2
1
0
*
NG
HG
HG+Flu10

Figure 2.4 Impact of HG on proapoptotic pathways.

(A) Expression of p53 was confirmed by western blot analysis. The quantitative assessment of the data is also shown. No significant change in p53 expression was observed. NAC had no effect on the level of p53 while inhibition of PKC-δ caused a modest but significant increase in p53 level. $n \geq 3$; *$p \leq 0.05$ (NG vs. HG); **$p \leq 0.05$ (HG vs.HG+Rottlerin). (B) High glucose resulted in a significant increase in Bim expression compared to normal glucose (NG) or osmolarity control (NG+L-Glu). Although incubation of PC under high glucose with NAC had no significant effect on Bim expression, inhibition of PKC-δ (Rottlerin) resulted in significant decrease in Bim expression. (C) High glucose increased p-STAT1 level significantly compared to normal glucose or osmolarity control (NG+L-Glu). NAC and Rottlerin did not affect p-STAT1 level under high glucose condition. Graphs of band intensities from three independent experiments are also shown. $n \geq 3$; *$p \leq 0.05$ (NG vs. HG); **$p \leq 0.05$ (HG vs.HG+rottlerin). (D) Fludarabine, a inhibitor for STAT1, reduced the rate of apoptosis in PC against apoptosis. High glucose (HG) condition increased the rate of apoptosis compared with normal glucose (NG) and Incubation of PC with fludarabine under high glucose condition decreased the rate of apoptosis compared with high glucose conditions. $n \geq 3$; *$p \leq 0.05$ (NG vs. HG and HG vs. HG+Flu10).

High glucose inhibited retinal PC migration. Migration of PC is essential during vascular development and stabilization of newly formed vessels (159). Alteration in migration of PC may also contribute to pathogenesis of DR (160). The impact of high glucose on migration of retinal PC has not been previously addressed. We next assessed the migratory properties of PC in transwell and scratch wound assays. We observed decreased PC migration under high glucose conditions compared with normal or control conditions in both scratch wound (Figure 2.5 A) and transwell (Figure 2.5 B) migration assays.

We next determined the downstream events that may contribute to the PC migratory defect under high glucose conditions. PC incubated under high glucose conditions, in the presence of NAC, demonstrated migration similar to that observed in PC incubated under normal glucose or osmolarity control (Figure 2.5 C). Similar results were observed in the presence of PKC-δ and ROCK I/II inhibitor (Figure 2.5 C). Furthermore, retinal PC cultured under normal glucose responded to promigratory activity of PDGF-BB, while basal and PDGF-BB-mediated migration of PC under high glucose conditions was attenuated (Figure 2.5 D). In contrast, PDGF stimulated the migration of PC in high glucose in the presence of NAC (data not shown).

The activation of PKC-α also negatively impacts migration of SMC in response to PDGF (161). We also determined whether activation of PKC-α contributes to high glucose mediated inhibition of retinal PC migration. Although inhibition of PKC-α restored basal migration of PC under high glucose conditions, it minimally affected their PDGF-mediated migration (Figure 2.5 D). Activation of SHP-1 tyrosine phosphatase is recently shown to negatively impact PDGF receptor signaling in retinal PC under high glucose conditions (112). Inhibition of SHP-1 activity

using the SHP-1-specific inhibitor sodium stibogluconate (SSG) (154, 162, 163) restored both basal and PDGF-mediated migration of PC under high glucose conditions (Figure 2.5 D).

Bim-/- PC are protected from high glucose mediated oxidative stress and apoptosis. Retinal PC isolated from Bim-/- mice were utilized to investigate the function of PC under normal or high glucose conditions. Apoptosis of Bim-/- PC was not affected under high glucose conditions, whereas high glucose increased apoptosis rate of wild type PC (Figure 6A). As indicated above, increased ROS production by high glucose is an upstream event in inducing apoptosis of PC. High glucose condition did not impact ROS production in Bim -/- PC whereas ROS production in wild type PC was increased under high glucose conditions (Figure 2.6 B).

Migratory property is crucial for the function of PC in maintaining vascular structure and function. The migration of wild type PC was attenuated under high glucose condition compared with normal glucose conditions. However, the migration of Bim-/- PC under high glucose conditions was not altered (Figure 2.6 C). Thus, Bim expression may promote PC dysfunction under high glucose conditions.

PC incubated under high glucose inhibited capillary morphogenesis and migration of EC. We recently showed that inflammatory mediators have on significant impact on capillary morphogenesis of retinal EC (164). We next determined the effects of conditioned medium collected from PC cultured under various glucose conditions on migration of retinal EC.

Conditioned medium from PC under high glucose conditions inhibited migration of EC compared with PC conditioned medium under normal glucose or control (Figure 2.7 A).

EC undergo capillary morphogenesis when grown on Matrigel, which mimics the late stage of angiogenesis (139). PC were incubated under various glucose conditions and used in co-culture experiments with retinal EC. When EC were mixed with PC cultured under high glucose conditions, capillary morphogenesis of EC was significantly inhibited compared with PC cultured under normal glucose conditions (Figure 2.7 B). Representative images of capillary morphogenesis are shown in Figure 2.7 C.

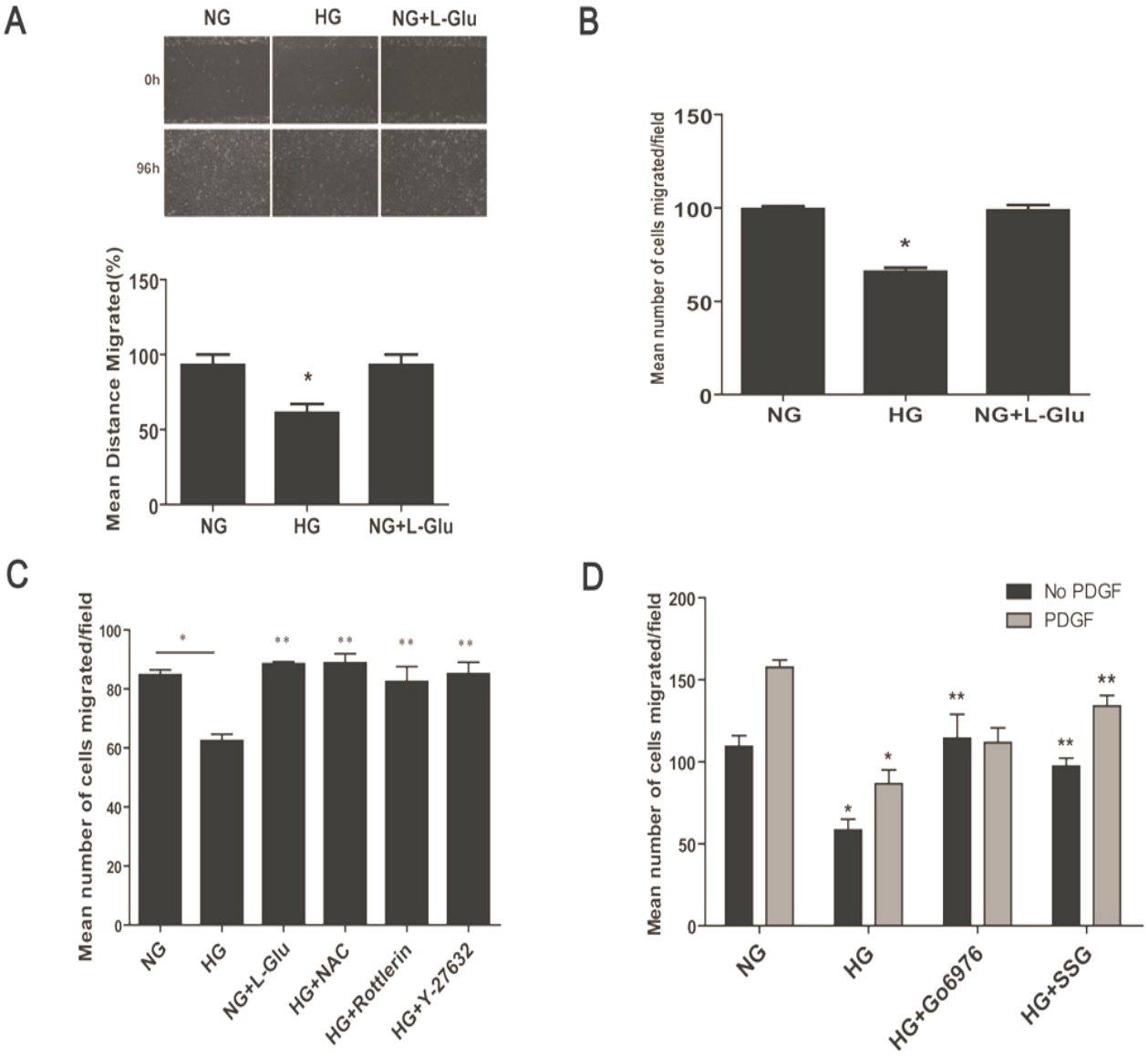
A
NG
HG
NG+L-Glu
0h
96h
Mean Distance Migrated(%)
150
100
50
0
*
NG
HG
NG+L-Glu
B
Mean number of cells migrated/field
150
100
50
0
*
NG
HG
NG+L-Glu
C
Mean number of cells migrated/field
100
80
60
40
20
0
*
**
**
**
**
NG
HG
NG+L-Glu
HG+NAC
HG+Rottlerin
HG+Y-27632
D
No PDGF
PDGF
Mean number of cells migrated/field
200
150
100
50
0
*
*
**
**
**
NG
HG
HG+Go6976
HG+SSG

Figure 2.5 Attenuation of pericyte migration under high glucose conditions.

(A) In scratch wound assays, a significant portion of wound remained uncovered in PC cultured under high glucose compared to normal (NG) or osmolarity control (NG+L-Glu) conditions. The quantitative assessment of the data is shown below. $n \geq 3$; *$p \leq 0.05$ (NG vs. HG or HG vs. NG+L-Glu). (B) A significantly lower number of PC cultured under high glucose conditions migrated through the transwell membrane compared to PC cultured under normal or osmolarity control conditions. $n \geq 3$; $p \leq 0.05$ (NG vs. HG or HG vs. NG+L-Glu). (C) Incubation of PC cultured under high glucose with NAC restored basal migration. Incubation of retinal PC under high glucose conditions with Rottlerin (PKC-δ inhibitor) or Y-27632 (ROCK I/II inhibitor) restored basal migration to levels seen in PC cultured under normal glucose or osmolarity control conditions. ($n \geq 3$; *$p \leq 0.05$ (NG vs. HG), **$p \leq 0.05$ (HG vs. NG+L-Glu or HG+NAC or HG+Rottlerin or HG+Y-27632). (D) Incubation of PC with PDGF-BB enhanced their migration under normal glucose conditions. However, PDGF-BB had a minimal effect on migration of PC cultured under high glucose. Although PCK-α inhibitor (Gö6976) restored basal migration of PC cultured in high glucose, it did not restored migratory response to PDGF-BB. The inhibition of SHP-1 (SSG) in PC cultured in high glucose restored both basal and PDGF-stimulated migration. $n \geq 3$; *$p \leq 0.05$ (NG vs. HG), **$p \leq 0.05$ (HG vs. HG+GÖ6976 or HG+SSG)

A

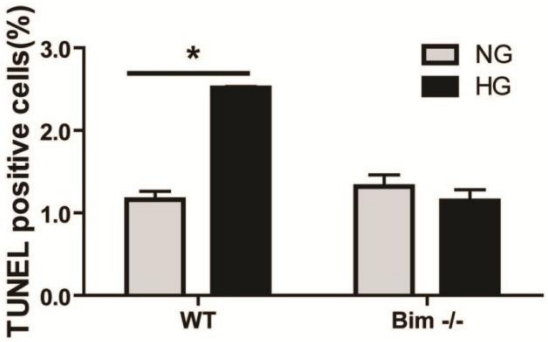
TUNEL positive cells(%)
3.0
2.0
1.0
0.0
*
NG
HG
WT
Bim -/-

B

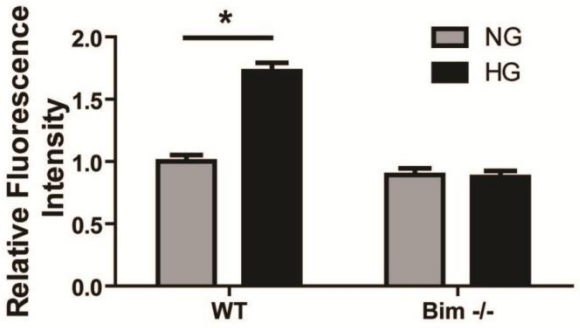
Relative Fluorescence Intensity
2.0
1.5
1.0
0.5
0.0
*
NG
HG
WT
Bim -/-

C

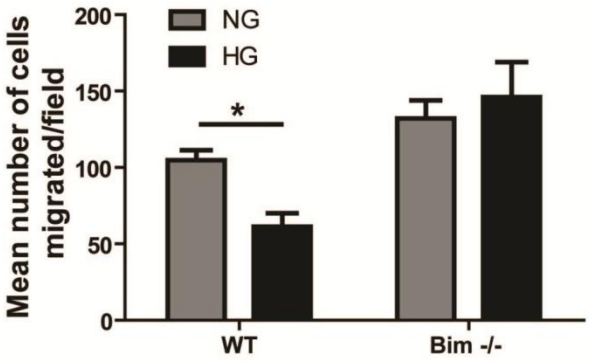
Mean number of cells migrated/field
200
150
100
50
0
NG
HG
*
WT
Bim -/-

Figure 2.6 Bim expression is essential for high glucose mediated apoptosis and ROS production of PC.

(A) Bim -/- PC were resistant to high glucose-induced apoptosis. WT and Bim -/- PC were incubated under normal (NG) or high glucose (HG) conditions for five days. High glucose did not increase the rate of apoptosis in Bim -/- PC. $n \geq 3$; $*p \leq 0.05$ (LG vs. HG). (B) Bim -/- PC generated less reactive oxygen species under high glucose conditions. $n \geq 100$; $*p \leq 0.05$ (NG vs. HG). (C) Migration of Bim -/- PC was not affected under high glucose conditions, whereas the migration of wild type PC was attenuated under high glucose condition. $n \geq 3$; $*p \leq 0.05$ (NG vs. HG).

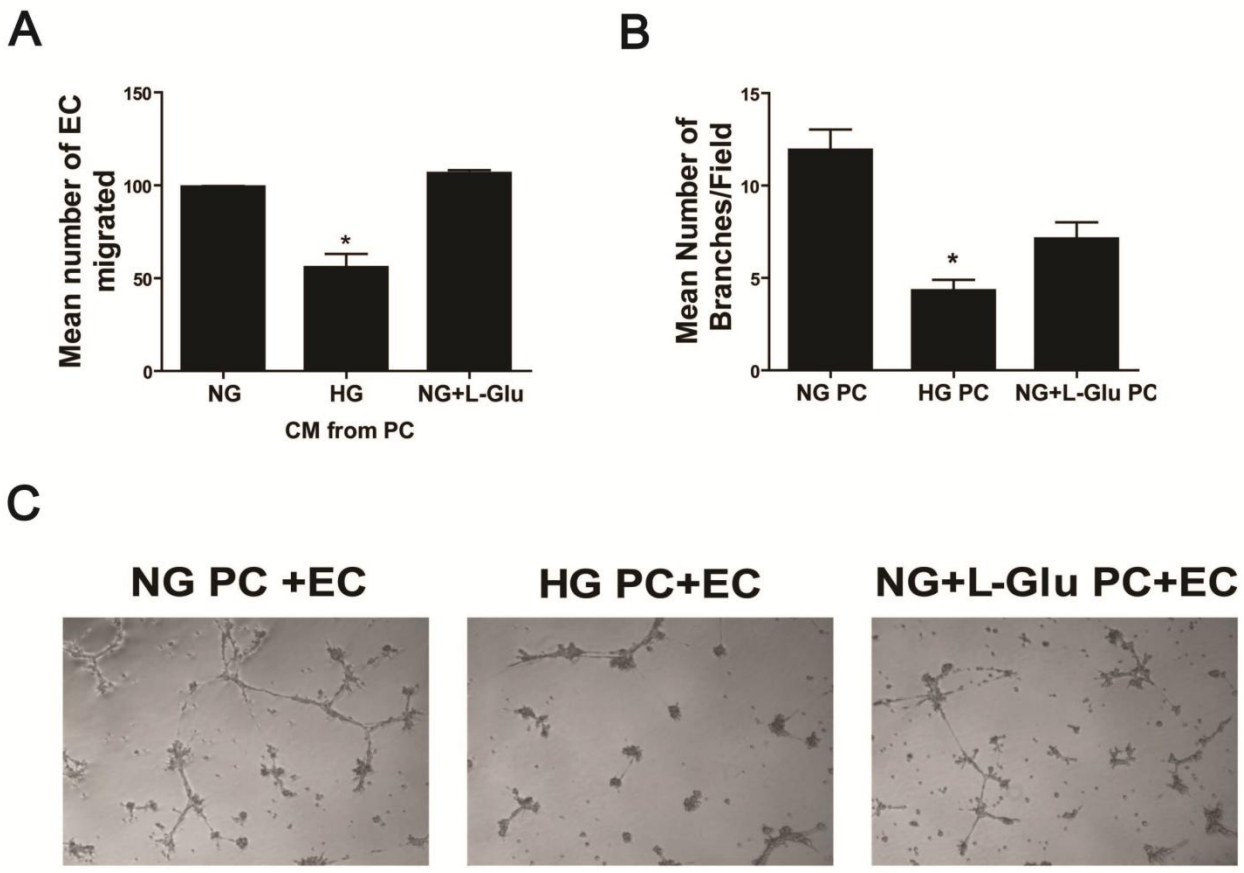

Figure 2.7 Incubation of PC under high glucose conditions impacts their effect on EC function. (A) Conditioned medium was prepared from PC incubated under normal glucose, high glucose, or control conditions for five days. The effects of this conditioned medium on the migration of retinal EC was determined in a transwell assay. Please note a significant decrease in migration of retinal EC incubated with conditioned medium from PC cultured in high glucose. $n \geq 3$; *$p \leq 0.05$ (NG vs. HG and HG vs. NG+L-Glu) (B) Retinal PC were incubated under various glucose conditions for five days and used to assess their impact on retinal EC capillary morphogenesis in co-culture (1:1) experiments. The mean number of branch points in ten high power fields (X100) was determined. Please note a significant decrease in capillary morphogenesis of retinal EC

incubated with PC under high glucose conditions. $n \geq 3$; $^{*}p \leq 0.05$ (NG vs. HG and HG vs. NG+L-Glu). Representative images for each condition are shown in (C).

Altered intracellular signaling pathways in retinal PC cultured under high glucose conditions. Increased apoptosis of PC under high glucose conditions is attributed to altered intracellular signaling pathways with important roles in cell survival, including Src/PI3 kinase, Akt, and MAP kinases (MAPKs). We determined the activities of selected signaling molecules and pathways which impact PC function. Src phosphorylation was decreased in PC under high glucose conditions compared with normal glucose or osmolarity control (Supplementary figure 2.2 A). Supplementary Figure 2.2 B also shows decreased activation of Akt1 in PC under high glucose and osmolarity control conditions compared to retinal PC under normal glucose conditions. In addition, activation of MAPK/ERKs, downstream effectors of Src kinase pathway, was also down-regulated in retinal PC under high glucose and osmolarity control compared to normal conditions (Supplementary figure 2.2 C). The levels of phosphorylated MAPK/p38 were not altered in PC under high glucose conditions (Supplementary figure 2.2 D). In contrast, MAPK/JNK1, whose activation is related to stress stimuli and increased apoptosis, was up-regulated in PC under high glucose conditions compared with normal glucose or control (Supplementary figure 2.2 E). Thus, high glucose conditions modulate various intracellular signaling pathways with significant impact on PC proliferation, migration and apoptosis.

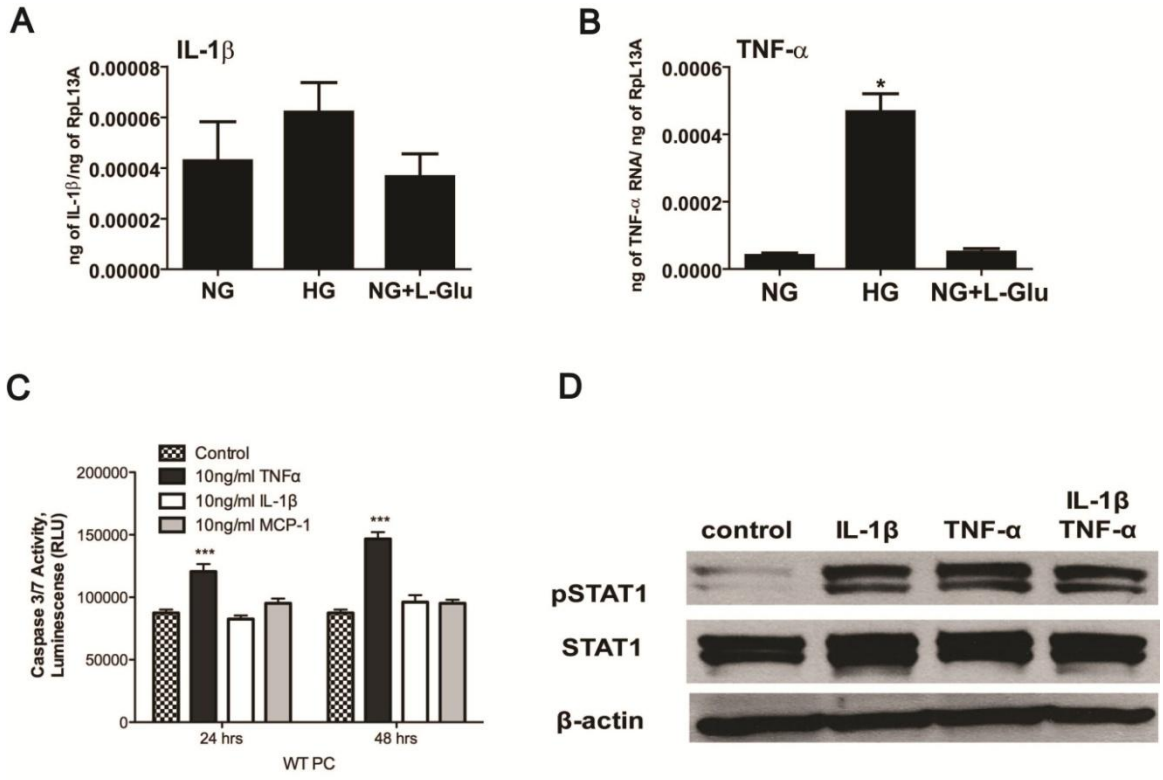

Supplementary Figure 2.1 Expression of cytokines by PC under high glucose and effect of cytokines on apoptosis and the phosphorylation of STAT1in retinal PC.

(A) and (B) Retinal PC expressed IL-1β (A) and TNF-α (B). HG conditions increased mRNA expression of TNF-α significantly compared with normal and control glucose conditions. $n \geq 3$; $*p \leq 0.05$ (NG vs. HG and HG vs. NG+L-Glu). (C) The rate of apoptosis was determined by measuring caspase activity with luminescent signal from caspase-3/7 DEVD-aminoluciferin substrate. TNF-α induced capase-3/7 activity compared to control ($N = 3$, $*p \leq 0.05$ vs. control). (D) Phosphorylation of STAT1 in retinal PC was increased by IL-1β, TNF-α and IL-1β+TNF-α.

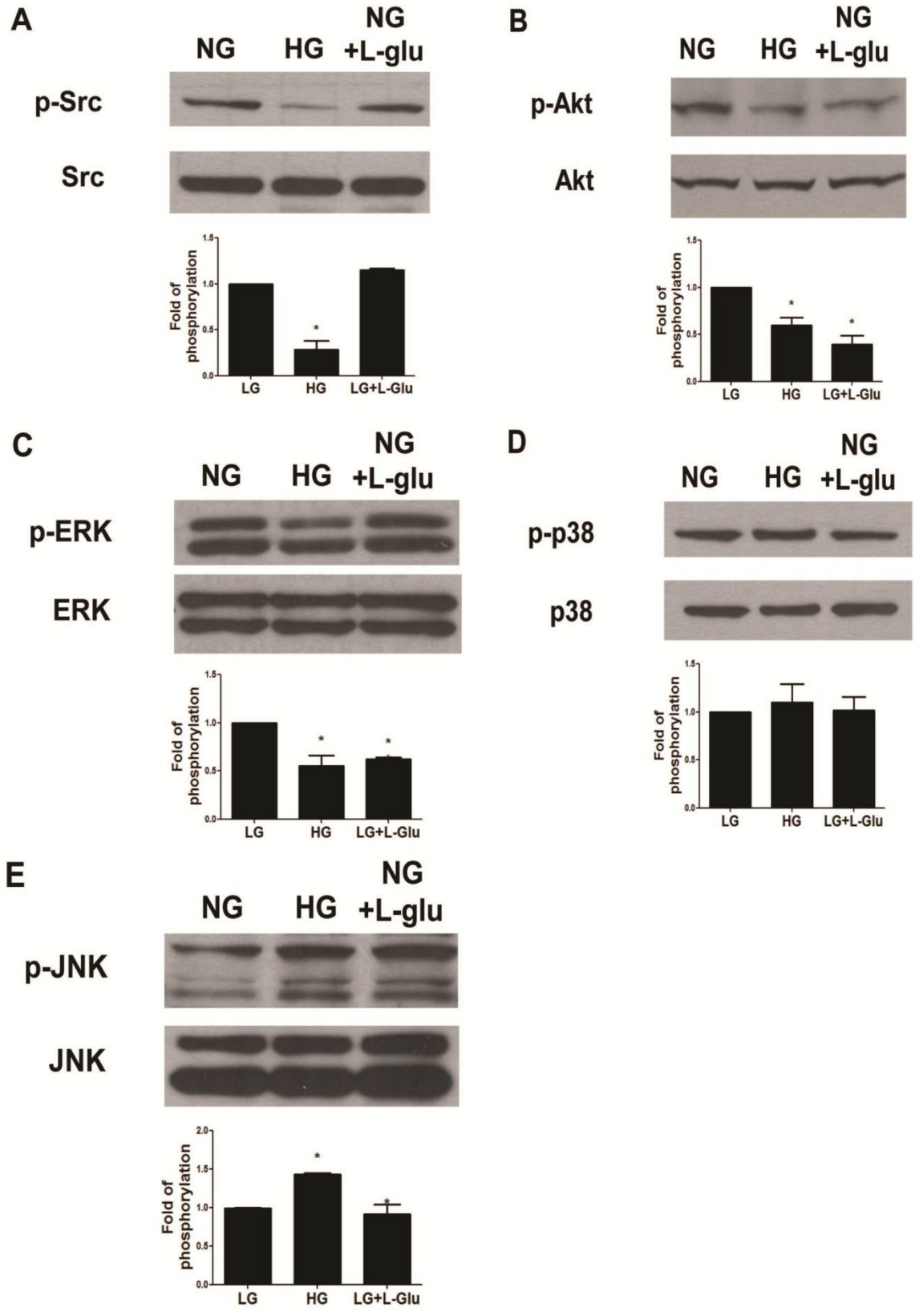
A
NG
HG
NG +L-glu
p-Src
Src
Fold of phosphorylation
LG
HG
LG+L-Glu
B
NG
HG
NG +L-glu
p-Akt
Akt
Fold of phosphorylation
LG
HG
LG+L-Glu
C
NG
HG
NG +L-glu
p-ERK
ERK
Fold of phosphorylation
LG
HG
LG+L-Glu
D
NG
HG
NG +L-glu
p-p38
p38
Fold of phosphorylation
LG
HG
LG+L-Glu
E
NG
HG
NG +L-glu
p-JNK
JNK
Fold of phosphorylation
LG
HG
LG+L-Glu

Supplementary Figure 2.2 The impact of high glucose on various down-stream signaling pathways.

The status of various signaling pathways in retinal PC under various glucose conditions was determined as described in Methods. Levels of active Src (A), Akt (B), ERK (C), P38 (D), and JNK1 (E) in retinal PC under different glucose conditions were determined by Western blot analysis from equal amounts of cell lysates. The total level for each kinase is shown in the lower part of each panel. The quantitative assessment of the data for each blot is shown below the blots. Please note decreased level of active c-Src (A), Akt1 (B) and ERKs (C) in retinal PC under high glucose conditions. No alteration in P38 MAPK was observed (D). Increased JNK1 MAPK activation was detected in the retinal PC under high glucose conditions (E). Data are presented as mean ± SEM (n=3, *$p<0.05$ NG vs. HG and HG vs. NG+L-Glu).

Discussion

Here we used mouse retinal PC to further delineate their response to high glucose and to elucidate the molecular mechanisms involved. Apoptosis of PC was significantly increased under high glucose conditions and in the retina of diabetic Akita/+ mice. We showed that high glucose conditions increased Bim expression in PC through the sustained activation of STAT1. The activation of STAT1 was mediated by the increased production of inflammatory cytokines including TNF-α under high glucose conditions. Bim is a proapoptotic protein and its level is significantly elevated in the neuroretina of diabetic patients (135). These results are consistent with increased Bim levels in the retina of diabetic Akita/+ mice and retinal PC cultured under high glucose conditions reported here. Thus, increased Bim level in the retina, and more specifically in PC, may be a crucial step in the development and progression of diabetic retinopathy.

To further demonstrate the important role of Bim in the apoptosis of PC under high glucose conditions, we determined the apoptosis rate of retinal PC prepared from Bim -/- mice under high glucose conditions. Bim deficiency protected PC from apoptosis induced by high glucose conditions and reduced ROS levels. Thus, Bim expression contributes to ROS production under high glucose conditions and promotion of PC apoptosis. To elucidate how high glucose condition may increase Bim expression, we examined the level of p-STAT1 in PC under various glucose conditions. STAT1 is a transcription factor and known regulator of Bim expression, which is activated by pro-inflammatory cytokines including TNF-α, IL-1β, and interferon-γ (IFN-γ) (156, 157). We observed that high glucose conditions resulted in increased p-STAT1 level in PC.

The increase in p-STAT1 level in PC may result from increased level of pro-inflammatory cytokines produced by PC under high glucose conditions. We observed that high glucose conditions significantly increased mRNA level of TNF-α in PC. High glucose condition is also shown to increase p-STAT1 level in renal tubular epithelial cells (165). Although NAC treatment under high glucose decreased p-STAT1 level in tubular epithelial cell, NAC treatment under high glucose did not affect p-STAT1 level in PC. This discrepancy may be attributed to the differences in duration of NAC treatment. Huang *et al*. treated with NAC for 30 min under high glucose, but here PC were exposed to NAC along with high glucose conditions for five days. Thus, chronic exposure to high glucose might contribute to sustained production of inflammatory mediators and activation of STAT1 in PC and lack of response to NAC.

STAT1 has been considered as a drug target for vascular disease and fludarabine, a nucleoside analogue, reduces STAT1 phosphorylation without affecting other STATs (166). We observed the protective effect of fludarabine against apoptosis induced by high glucose condition in PC. Fludarabine also decreased Bim expression under high glucose conditions in PC (not shown). Considering STAT1-mediated Bim expression and the role of Bim in the dysfunction of PC under high glucose conditions, compounds affecting STAT1 expression and/or activity may alleviate symptom of diabetic retinopathy.

Bim expression level is also regulated by various microRNAs. MicroRNA (miR)-24 is shown to attenuate apoptosis of cardiomyocytes by reducing Bim expression (167). In osteoblast, the microRNA cluster miR-17-92a inhibits apoptosis by reducing Bim expression level (168). However, the effect of high glucose or diabetic condition on regulation of miRNAs including

miR-17-92a and miR-24 in retinal PC remains unknown and is subject of current investigation in our laboratory.

The apoptosis of mouse retinal PC cultured under high glucose conditions was also attenuated by the inhibition of downstream signaling events including PKC-δ, ROS production and ROCK I/II activity. The activation of these pathways under high glucose was previously shown to be responsible for PC dysfunction (112, 169, 170). Only NAC reduced ROS levels in PC under high glucose, whereas the inhibition of PKC-δ, ROCK I/II or SHP-1 was ineffective. These results suggest that ROS production is an up-stream event leading to the apoptosis of PC under high glucose conditions. However, incubation of PC with NAC under high glucose conditions did not affect Bim expression. Thus, Bim activity is up-stream of ROS production.

Very few studies have systemically examined retinal PC migration under high glucose conditions. This property of PC plays critical roles during angiogenesis and the integrity of vascular function. Under high glucose conditions, the migration of wild type PC was significantly decreased. In contrast, high glucose had no significant effect on migration of Bim-/- PC. Together these results suggest that high glucose impairs PC migration and is impacted by Bim expression. Incubation of PC with NAC, Rottlerin, Y-27632 and SSG under high glucose conditions restored PC migration confirming the role of oxidative stress, PKC-δ, ROCK I/II and SHP-1 in PC migration.

PDGF-BB is secreted by EC promoting the recruitment of PC to newly formed blood vessels and their stabilization (171). We showed high glucose impaired PDGF-BB mediated migration of PC, which was reversed by inhibition of SHP-1. Thus, increased SHP-1 activity

under high glucose conditions impairs not only PDGFR-β mediated survival but also migration of PC by reducing PDGFR-β activity.

Interactions between EC and PC are crucial for their survival and maintenance of vessel structure and function. To examine the effect of high glucose conditions on the interactions between retinal EC and PC, the effect of soluble factors released in the conditioned medium of PC on migration of EC was also investigated. Conditioned medium from PC under high glucose conditions attenuated the migration of retinal EC. We also examined the effect of PC incubated under various glucose conditions on capillary morphogenesis of retinal EC in co-culture experiments. PC are able to stabilize capillary tube formation by inhibiting tube regression in EC-PC co-cultures (172). PC cultured under high glucose conditions attenuated capillary morphogenesis of retinal EC. This can be attributed to inhibition of EC migration by PC cultured under high glucose, as demonstrated here. In addition, high glucose conditions may also disturb the expression of other regulating factors including metalloproteinases and tissue inhibitor of metalloproteinase (TIMP) (173). Thus, high glucose conditions may affect secretion of soluble factors produced by PC, including inflammatory cytokines that impact EC function as we recently demonstrated (164). The identity of these factors and their regulation under various glucose conditions require further investigation.

In summary, our results demonstrate that exposure of retinal PC to high glucose results in increased Bim expression and oxidative stress, and reduced migration with a significant impact on their rate of apoptosis. We showed these effects are associated with activation of STAT1-mediated Bim expression axis in retinal PC. A summary of how high glucose conditions affect signaling pathways involved in PC migration, proliferation and apoptosis is shown in Figure 8.

Collectively we demonstrate that that increased expression of Bim through production of inflammatory cytokines and sustained activation of STAT1 is a significant pathway in modulation of PC function under high glucose conditions. Thus, targeting Bim expression and/or activity may provide a more effective modality for treatment of diabetic retinopathy.

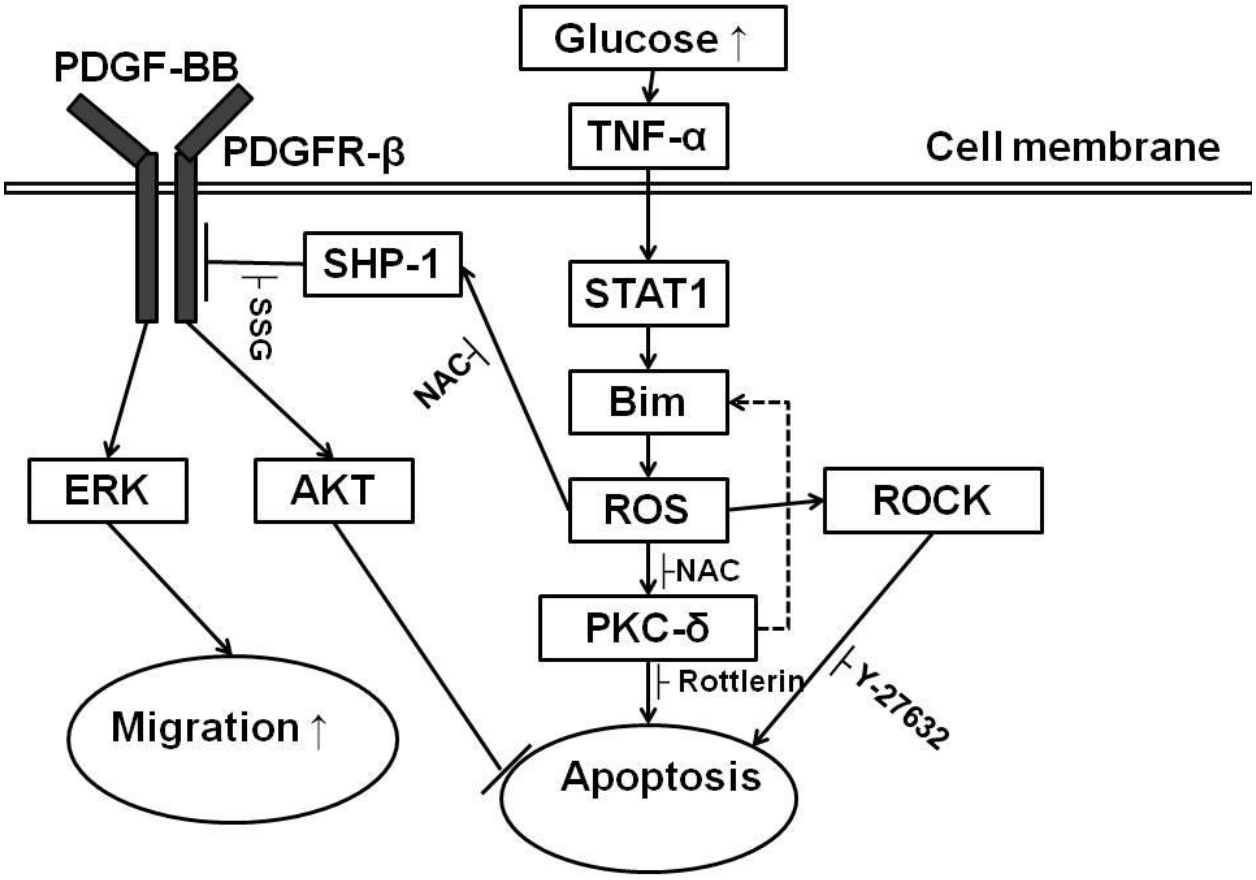

Figure 2.8 A summary of signaling pathways known to participate in response to high glucose. The exposure of PC to high glucose results in increased Bim expression and oxidative stress, which lead to activation SHP-1 and PKC-δ leading to enhanced apoptosis. Our results indicate that oxidative stress is up-stream of SHP-1 and PKC-δ activation. In addition, we showed high glucose inhibited basal and PDGF-mediated migration of PC and this can be reversed by NAC and inhibition PKC-δ or ROCKI/II.

3. High Glucose Attenuates the Migratory Activity of Retinal Astrocyte through Increased Inflammatory Cytokines and Oxidative Stress

Abstract

Astrocytes are glial cells with a crucial role in development of retinal vasculature and maintenance of blood-retina-barrier (BRB). Pathological conditions such as diabetes affect physiology and function of retinal vascular cells including astrocytes (AC) leading to breakdown of BRB. High glucose conditions caused by diabetes impact the function and morphology of retinal AC. However, the cellular mechanisms leading to dysfunction of retinal AC under high glucose conditions remain unclear. Here, we showed that high glucose conditions did not affect apoptosis of retinal AC but increased proliferation of retinal AC. In contrast, high glucose conditions through increased adhesion of retinal AC to extracellular matrix proteins. Furthermore, high glucose conditions affected intracellular signaling pathways involved in cell survival, migration and proliferation. High glucose conditions also affected expression level of inflammatory cytokines in retinal AC. In addition, we showed that the attenuation of retinal AC migration under high glucose, and retinal endothelial cell (EC) migration by conditioned medium collected from retinal AC under high glucose conditions were mediated by oxidative stress. Antioxidant proteins including heme oxygenase-1 (HO-1) and peroxiredoxin 2 (Prdx2) levels were upregulated in retinal AC under high glucose conditions through nuclear localization of transcription factor, nuclear factor-erythroid 2-related factor-2 (Nrf2). Together our results demonstrated that high glucose conditions alter function of retinal AC by increased inflammatory cytokines and oxidative stress.

Introduction

Astrocytes are glial cells with important role in retinal vascular development, and provide physical support and nutrients for neurons in the central nerve system. Astrocytes also have foot processes that envelop endothelial cells in blood vessels to maintain blood retina barrier (BRB) (4). In addition, astrocytes regulate fluid and electrolyte balance by expressing channel proteins including water channel protein, aquaporin 4 and the potassium channel Kir4.1 at the luminal spaces of endfeet (174, 175). Astrocytes regulates blood barrier function by secreting growth factors such as transforming growth factor-β (TGF-β), glial-derived neurotrophic factor (GDNF), basic fibroblast growth facor (bFGF) and angiopoetin 1(ANG1) (92). Furthermore, astrocyte secretion of sonic hedgehog (Shh) is recently shown to enhance barrier function and decrease inflammatory mediators of the endothelium (96).

Compromise in the structural integrity in BRB is crucial in the pathogenesis of retinal vascular diseases including diabetic retinopathy (DR). Pathological conditions affect physiology of cellular components of BRB including endothelial cells (EC), pericytes (PC) and astrocytes (AC) and lead to breakdown of BRB structures. In diabetic conditions, vascular cells are affected by high glucose environment. High glucose conditions promote migration of mouse retinal EC through activation of signaling pathway mediated by Src, PI3K/Akt1/eNOS and ERK (176). In contrast, high glucose conditions increased apoptosis of retinal PC by activation of Protein kinase C δ (PKC-δ) and Src homology-2 domain-containing phosphatase-1(SHP-1) (112). Diabetic conditions also affect retinal AC. In diabetic retina, morphology and viability of retinal AC were disturbed compared with normal conditions (123, 177). Although changes in AC contribute to alterations in retinal vascular structures and function under hyperglycemic conditions, the cellular mechanism leading to dysfunction of retinal AC remain poorly defined.

High glucose conditions impair various cellular functions. High glucose conditions increase apoptosis of retinal PC and inhibit migration of fibroblast. Oxidative stress caused by high glucose conditions contributes to these cellular dysfunctions (112, 178). To respond to oxidative stress, protective mechanisms have been implicated in cells exposed to high glucose conditions. The transcription of genes to protect from oxidative stress is regulated by redox-sensitive transcription factor, nuclear factor-erythroid 2-related factor-2 (Nrf2) (179). Activation of Nrf2 by oxidative stress results in its translocation into the nucleus and activation of transcription of antioxidant genes including heme oxygenase-1 (HO-1) and peroxiredoxin-2 (Prdx2) (179). Nrf2 pathway is shown to be activated to protect retinal AC from cell death mediated by oxidative stress (180). However, the effect of high glucose conditions on the activation of this defense system in retinal AC has not been determined.

We have described a novel method for isolation and culture of retinal AC from wild type and transgenic mice (181). Here we demonstrate that high glucose results in attenuation of retinal AC migration. High glucose also had a significant impact on production of reactive oxygen species (ROS) and interaction of retinal EC and AC. Furthermore, we uncovered that high glucose conditions activated protective the intracellular mechanisms via translocation of Nrf2 into the cell nucleus and increased expression of anti-oxidant proteins.

Materials and Methods

Cell Culture Conditions. Mouse retinal astrocytes (AC) were isolated and cultured as previously described (181). The cells were plated on 1% gelatin-coated 60 mm dishes and cultured in Dulbecco's Modified Eagle's Medium (DMEM) containing 10% fetal bovine serum (FBS), 2 mM L-glutamine, 2 mM sodium pyruvate, 20 mM HEPES, 1% nonessential amino acids, 100 μg/ml streptomycin, 100 U/ml penicillin, freshly added heparin at 55 U/ml (Sigma, St. Louis, MO), endothelial growth supplement 100 μg/ml (Sigma), and murine recombinant interferon-γ (R & D, Minneapolis, MN) at 44 units/ml. Cells were maintained at 33℃ with 5% CO_2. The growth medium contained either 5.7 mM D-glucose (normal glucose, NG), 40.7 mM D-glucose (hyperglycemia/high glucose, HG), or 5.7 mM D-glucose+35mM L-glucose as high osmolarity control (NG+L-glu). Cells were maintained in growth medium for 5 days prior to each experiment, and the medium was changed every other day.

Cell Proliferation and Apoptosis Assays. The rate of cell proliferation was determined using EdU DNA labeling (Click-iT EdU Flow Cytometry kit, Invitrogen, Carlsbad, CA). Cells cultured under different glucose conditions were incubated with 10 μM EdU for 1 h. Following incubation, cells were removed using cell dissociation solution (Sigma) and analyzed by FACScan caliber flow cytometer as recommended by the supplier (Becton-Dickinson, Franklin Lakes, NJ). Positive cells were calculated as a percentage of total cell number. The rate of apoptotic cell death was assessed by TdT-dUTP Terminal Nick-End Labeling (TUNEL) staining. Cells were cultured under different glucose conditions in fibronectin coated chamber slides (FN, 2 μg/ml in phosphate buffered saline) for five days. Cells were then washed twice with

phosphate buffered saline (PBS), fixed with 4% paraformaldehyde for 20 min and washed with PBS twice. Cells were permeabilized with 0.5% Triton X-100 in PBS for 10min. Apoptotic cell death was assessed using Click-iT TUNEL Alexa Fluor Imaging Assay (Invitrogen, Carlsbad, CA,) as recommended by the manufacturer. Positive cells were counted under fluorescence microscope and the percentage of apoptotic cells relative to the total number of cells was calculated.

Transwell Migration Assays. Cell migration was assessed in transwell assays as previously described (176). Briefly, transwell inserts (8-μm pore size, 6.5-mm membrane; Costar, Lowell MA) were coated with FN (2 μg/ml) in PBS on the bottom side at 4°C overnight. The next day, inserts were rinsed with PBS, blocked in PBS containing 2% BSA for 1 h at room temperature, and washed with PBS. Cells that have been cultured in medium with different glucose conditions for 5 days were removed by trypsin-EDTA, counted, and resuspended at 1×10^6 cells/ml in serum-free medium. Inserts were placed in 24-well plates (Costar) containing 0.5 ml serum-free medium, and 0.1 ml cell suspension was then added to the top of the inserts. Cells were allowed to migrate through the membrane for 4 hours at 37℃. To examine the effect of PDGF-AA or PDGF-BB on migration, transwell inserts were placed in 24-well dishes containing 0.5 ml serum-free medium or serum-free medium containing PDGF-AA or PDGF-BB (50 ng/ml; PeproTech, Rocky Hill, NJ). Following incubation, the cells on top of the filter were scraped off using a cotton swab. The membrane was fixed in 4% paraformaldehyde and stained with hematoxylin and eosin. The inserts were removed, mounted on a slide, cell side up, and the number of cells migrated to the bottom of the filter was determined by counting 10 high-power

fields (×400). To examine the migration of EC, 1×10^5 cells in 100 μl of medium were added to the top of each Transwell membrane. Transwell inserts were placed in 24-well dishes containing conditioned medium collected from RAC cultured under different glucose conditions for five days. Cells were allowed to migrate through the membrane for 3 h at 37℃. Following incubation, number of migrated cells was determined as described above.

Indirect Immunofluorescence Staining. Retinal AC (1×10^4) were plated on glass coverslips coated with 2 μg/ml of fibronectin. Cells were incubated under different glucose conditions for five days. Cells were rinsed with PBS, fixed with 3% paraformaldehyde (PFA) for 10 min on ice, washed twice with PBS. Cells were incubated in PBS containing 0.25% Triton X-100 for 15 minutes at room temperature for permeabilization. After washing cells with TBS twice, cells were incubated with anti-vinculin (1:100; Sigma), FITC-phalloidin (1:200; Sigma), and DAPI (Invitrogen, D1306; 10 μg/ml) for 40 min at 37°C. For analyzing cellular location of Nrf2, Anti-Nrf2 (Santa Cruz Biotechnology, Santa Cruz, CA) was also used. After washing three times with PBS, cells were incubated with appropriate CY3-conjugated secondary antibodies (Jackson ImmunoResearch, West Grove, PA) at 37 ℃ for 40 min. Cells were washed three times with PBS, mounted, and photographed using a Zeiss fluorescence microscope (Axiophot, Zeiss, Germany) equipped with a digital camera. Coherency of stress fiber, number of focal adhesion and intensity of signal were quantified using Image J software (NIH; http://rsb.info.nih.gov/ij).

Cell Adhesion Assays. The retinal AC adhesion to various extracellular matrix proteins was determined as recently described. Briefly, 96 well plates (Maxisorb, Nunc) were coated with various conditions of fibronectin (FN), vitronectin (VN), collagen-Ⅰ(Col-Ⅰ) and laminin (LM) (BD Biosciences, San Jose, CA) prepared in TBS (Tris-buffered saline, 20 mM Tris-HCl pH 7.6, 150 mM NaCl) with 2 mM Ca^{2+} and 2 mM Mg^{2+} (Ca/Mg) overnight at 4 ℃. The next day the plates were rinsed four times with TBS containing Ca/Mg, blocked for 1h with 200 µl of 1% BSA prepared in TBS with Ca^{2+}/Mg^{2+} for at least 1 h at room temperature. Cells cultured under different glucose conditions for 5 days were removed using cell dissociation solution (Sigma, St. Louis, MO), washed once with TBS, and resuspended in HEPES buffered saline (25 mM HEPES pH 7.6; 150 mM NaCl) containing 4 mg/ml of BSA at 5×10^5 cells/ml. Blocking solution was then removed from the coated plates and each well received 50 µl of TBS with Ca^{2+}/Mg^{2+} and 50 µl of cell suspension in triplicates. Cells were then allowed to adhere for 90 min at 37℃ and non-adherent cells were removed by gently washing the wells with 200 µl of TBS with Ca/Mg until no cells left in wells coated with BSA. The number of adherent cells in each well was quantified by measuring the cellular phosphatase activity as previously described (182). All samples were done in triplicate.

Formation of retinal AC network and capillary morphogenesis of retinal EC on Matrigel. We previously showed that retinal AC organize into a network when plated on Matrigel similar to retinal endothelial cell (EC) (181). We next determined the ability of cells cultured under different glucose conditions to organize into three dimensional networks. Approximately, 2×10^5 cells in 2ml of growth medium were plated in a 35 mm dish coated with 0.5 ml of 10 mg/ml

Matrigel (BD Biosciences, Bedford, MA), incubated at 37 ℃ for 16 to 24 h, and photographed in a digital format. For quantitative assessment, the mean number of branch points in five high power fields (×100) was determined.

For analyzing capillary morphogenesis of retinal EC, cells were removed by trypsin-EDTA, washed with DMEM containing 10% FBS, and resuspended at 2×10^5 cells/ml in conditioned medium collected from retinal AC incubated under different glucose conditions. Cells (2×10^5) in 2 ml were applied to the Matrigel-coated plates, incubated at 37 ℃, photographed after 18 h with a Nikon microscope in digital format.

FACScan Analysis. Cells cultured under different glucose conditions were washed once with PBS containing 0.04% EDTA and collected using cell dissociation solution (Sigma). Cells were washed once with DMEM containing 10% FBS and blocked in TBS with 1% goat serum for 20 min on ice. Cells were incubated with specific primary antibodies for 30min on ice. anti-cleaved caspase 3 antibody (cell signaling, Danvers, MA) or anti-GFAP (Dako, Carpinteria, CA) or anti-α5β1 integrin or anti-αvβ3 integrin (Milipore, Temecula, CA) was prepared in TBS with 1% BSA at 2 μg/ml. Following incubation, cells were then washed twice with TBS/1% BSA, and incubated with appropriate FITC-conjugated secondary antibody for 30 min on ice. The stained cells were washed twice with TBS/1% BSA and resuspended in 0.5 ml of TBS/1% BSA, and analyzed by FACScan caliber flow cytometer (Becton-Dickinson, Franklin Lakes, NJ). Cells incubated with secondary antibodies in the absence of primary antibodies were used as negative control.

*Western Blot Analysis***.** Approximately, 2×10^5 cells were plated in 60-mm plates and cultured under different glucose conditions. Cells were washed twice with cold PBS, lysed in 0.1ml of lysis buffer (20 mM Tris Ph 7.4, 2 mM EDTA, 25 mM NaF, 1mM Na_3VO_4, 1% Triton X-100, 1% NP-40, 0.1% SDS and a protease inhibitor cocktail (Roche Biochemicals, Indianapolis, IN)) and briefly sonicated. The lysates were centrifuged and protein conditions were determined using the BCA protein assay kit (Pierce, Rockford, IL). For conditioned medium, cells were rinsed once with serum free medium and incubated with serum free medium (complete medium with different conditions of glucose but no serum) for two days. The conditioned medium was collected, clarified by centrifugation. The protein samples were mixed with appropriate volume of 6X SDS sample buffer and analyzed by 4-20% SDS-PAGE (Invitrogen). Proteins were transferred to nitrocellulose membrane, blocked in TBS containing 5% BSA and 5% non-fat milk, and incubated with appropriate primary antibodies at 4 ℃ overnight. After washing with TBS containing 0.1% Tween 20, the blots were incubated with appropriate HRP-conjugated secondary antibodies (1:10,000; Jackson Immunoresearch Laboratories) and developed using ECL (Amersham). The same blot was reprobed with a monoclonal antibody to β–actin (Sigma) to verify equal protein loading in lanes with cell lysates. The antibody to β-actin (Sigma) was used to verify equal protein loading. The following primary antibodies were used: p-Src (Tyr418), p-p38 (Thr180/Tyr182), p38, p-Akt1 (ser 473), Akt1, p-ERK, ERK and HO-1 (cell signaling, Danvers, MA), p-JNK1, and JNK1(R&D System, Minneapolis, MN), Prdx2 (Pierce Biotechnology, Rockford, IL), p-p65 and p65 (Santa Cruz Biotechnology), thrombospondin (TSP1) (A6.1, Neo Markers, Fremont, CA), iNOS and TSP2 (BD Biosciences).

Immunoprecipitation of Fyn. To determine the levels of active Src family member Fyn in retinal AC under different glucose conditions, equal amount of cell lysates were used for immunoprecipitation assay. The lysates were pre-cleared with protein G-agarose (Sigma) and incubated with mouse anti-Fyn antibody (Santa Cruz Biotechnology) overnight at 4℃. Following incubation with the primary antibody, 50 µl of anti-mouse protein G agarose was added to the sample and incubated for 2 h at 4℃.The beads were centrifuged at 2,000 rpm for 5 min, and washed three times with lysis buffer. The beads were resuspended in 6x SDS sample buffer and boiled for 10 min. The immunoprecipitation eluates were separated on SDS-PAGE and transferred to a nitrocellulose membrane. The blot was probed for the activated, phosphorylated form of Fyn by using a specific antibody to the p-Src (Tyr418) (Cell signaling), and for total Fyn using anti-Fyn antibody (Santa Cruz Biotechnology).

RNA purification and real time qPCR analysis. The total RNA from retinal AC was extracted using mirVana PARIS kit (Invitrogen, Carlsbad, CA). cDNA synthesis was performed from 1 µg of total RNA using Sprint RT Complete-Double PrePrimed kit (Clontech, Mountain View, CA). 1 µl of each cDNA (dilution 1:10) was used as template in qPCR assays, performed in triplicate of three biological replicates on Mastercycler Realplex (Eppendorf) using the SYBR-Green qPCR Premix (Clontech). Amplification parameters were as follows: 95 ℃ for 2min; 40 cycles of amplification (95 ℃ for 15 sec, 60 ℃ for 40 sec); dissociation curve step (95 ℃ for 15 sec, 60 ℃ for 15 sec, 95 ℃ for 15 sec). Primer sequences for TNF-α were 5′-

ACCGTCAGCCGATTTGCTAT-3′ (forward) and 5′-TTGACGGCAGAGAGGAGGTT-3 (reverse). For IL-1β, 5’- GTTCCCATTAGACAACTGCACTACA-3’ (forward), and 5’-CCGACAGCACGAGGCTTTT-3’ (reverse); For MCP-1, 5′-GTCTGTGCTGACCCCAAGAAG-3′ (forward), and 5′-TGGTTCCGATCCAGGTTTTTA-3′ (reverse). Standard curves were generated from known quantities for each of the target gene of linearized plasmid DNA. Ten times dilution series were used for each known target, which were amplified using SYBR-Green qPCR. The linear regression line for ng of DNA was determined from relative fluorescent units (RFU) at a threshold fluorescence value (Ct) to quantify gene targets from cell extracts by comparing the RFU at the Ct to the standard curve, normalized by the simultaneous amplification of RpL13a, a housekeeping gene. Primer sequences for RpL13a were 5’-TCTCAAGGTTGTTCGGCTGAA-3’ (forward) and 5’-CCAGACGCCCCAGGTA-3’ (reverse).

Determination of oxidative stress. Cells (0.1 ml of $1x10^5$ cells/ml) were plated on fibronectin (2 μg/ml)-coated 4-well chamber slides. After attachment, cells were cultured in medium under different glucose conditions for 5 days. The level of cellular reactive oxygen species (ROS) was assessed using dihydroethidium staining (DHE; Invitrogen), as previously described (140). For quantitative assessments, the images were analyzed using Image J software. Values were obtained from each cells captured in 5 high power fields (x400). More than sixty cells per each condition were analyzed.

Statistical Analysis. Statistical differences between control and treated samples were evaluated with student's unpaired *t*-test (2-tailed) or one-way ANOVA with post hoc Dunnett's test for multiple comparisons. Mean ±SE are shown. p values ≤ 0.05 were significant.

Results

The Effects of High Glucose on Retinal AC Proliferation and Apoptosis. We determined the rate of apoptosis in retinal AC cultured under different glucose conditions as detailed in the methods section. Apoptotic cell death was determined by TdT-dUTP Terminal Nick-End Labeling (TUNEL) assay. Figure 3.1 A shows that the retinal AC under high glucose or osmolarity control exhibited a similar low rate of apoptosis as those cells cultured under normal glucose conditions. Cleaved caspase-3 level in retinal AC under different glucose conditions was determined by FACS analysis. Different glucose conditions did not affect the level of cleaved caspase-3 in retinal AC (Figure 3.1B). Thus, high glucose has minimal effect on apoptosis of retinal AC.

We next asked whether high glucose affects the rate of proliferation in retinal AC cultured under various glucose conditions. Figure 3.1C shows the mean percentage of positive cells labeled with EdU under different glucose conditions. We observed a significant increase in the rate of proliferation under high glucose or osmolarity control conditions compared to the cells cultured under normal glucose conditions. Thus, high glucose conditions result in increased proliferation of retinal AC.

Glial fibrillary acidic protein (GFAP) is a marker protein for astrocyte and known to be up-regulated by neural damage (183). We next determined the level of GFAP in retinal AC under various glucose conditions. High glucose conditions increased GFAP level in retinal AC compared with normal glucose and osmolarity control conditions (Figure 3.1D). These results are consistent with increased expression of GFAP detected in retinal section of diabetic mice (121).

Attenuation of Retinal AC network formation under High Glucose Conditions. Prior to retinal vascularization, retinal astrocytes migrate from the optic nerve to create a scaffold-like network which is utilized by EC to establish the primary retinal vascular network. We have previously shown that, like retinal EC, retinal AC do organize into a three dimensional-like network when plated on Matrigel (181). We next asked whether high glucose conditions affect retinal AC to organization into a network on Matrigel. Figure 3.2 A shows that retinal AC under normal glucose condition readily organized on Matrigel forming network. In contrast, this ability was attenuated under high glucose or osmolarity control conditions. The quantitative assessment of the data is shown in Figure 3. 2 B. Thus, early exposure of retinal AC to high glucose conditions may have significant impact on development of retinal vasculature.

High Glucose Attenuates Retinal AC Migration. The migratory properties of retinal AC were assessed using a transwell assay. Figure 3.2 C demonstrates the migratory activity of AC cultured under different glucose conditions. We observed a significant decrease in the number of cells migrated through the transwell under high glucose, compared to normal or osmolarity control conditions.

Interactions EC and AC is important during development and maintenance of blood barrier (68). To examine the effect of glucose conditions on these interactions, migration of EC was assessed using the transwell migration assay in the presence of conditioned medium collected from AC cultured under different glucose conditions. Conditioned medium from AC under high glucose conditions inhibited EC migration compared with normal glucose or osmolarity control condition (Figure 3. 2 D).

To determine the factors which affect AC migration, organization of stress fiber and focal adhesions were examined (Figure 3.3 A). Coherency of stress fiber and number focal adhesion was not affected by glucose conditions (Figure 3.3 B, 3.3 C). The migratory defects observed in retinal AC under high glucose suggest that alterations in cell adhesive mechanisms may exist. We next evaluated the adhesion of retinal AC cultured under different glucose conditions to various matrix proteins under normal or high glucose conditions. Figure 3.4 A and 3.4 B show that retinal AC adhered to fibronectin and vitronectin, and high glucose increased their adhesion to these ECM proteins. Very few cells adhered to collagen I or laminin regardless of different glucose conditions (not shown).

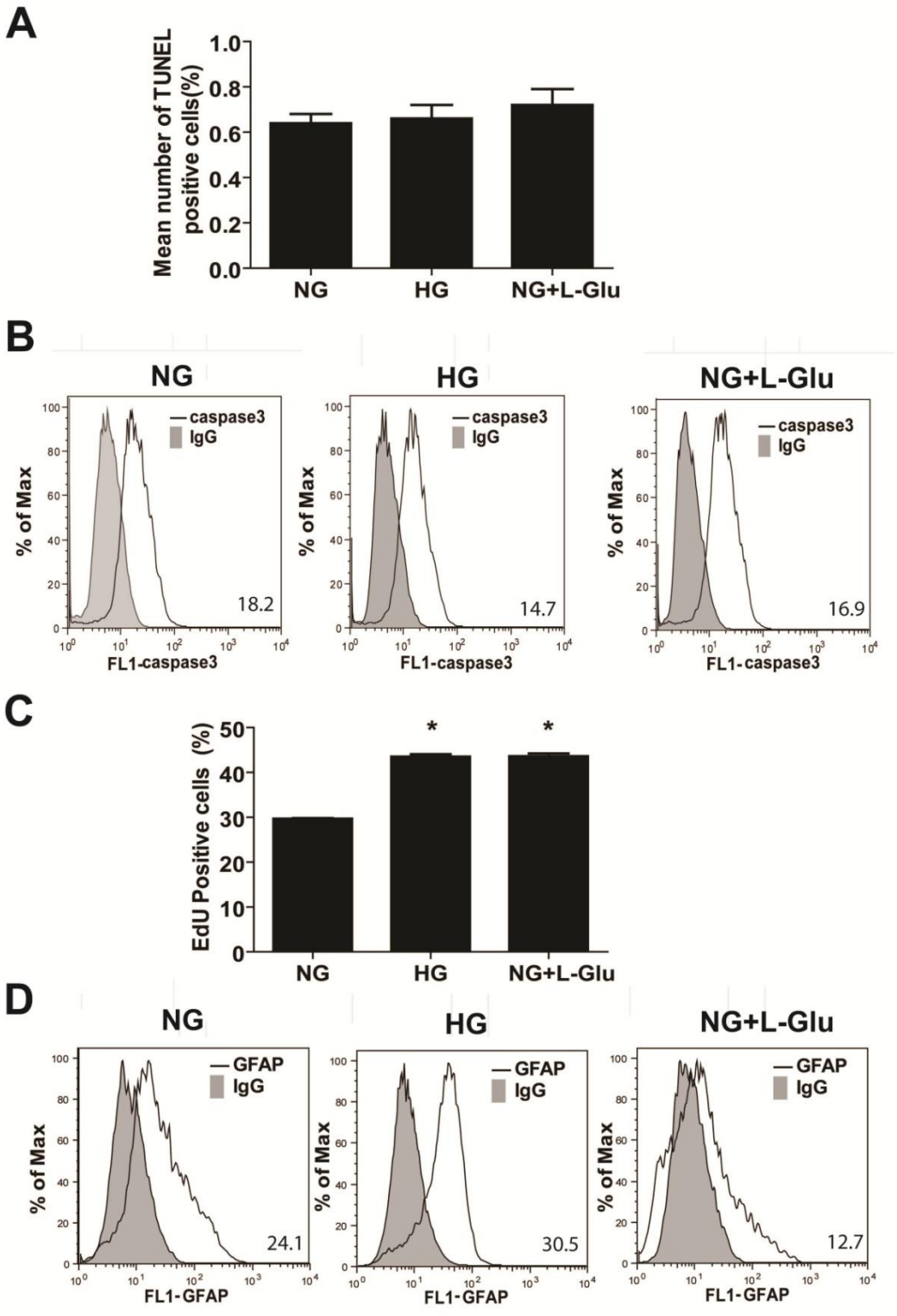
A
Mean number of TUNEL positive cells(%)
1.0
0.8
0.6
0.4
0.2
0.0
NG
HG
NG+L-Glu
B
NG
HG
NG+L-Glu
caspase3
IgG
% of Max
18.2
14.7
16.9
FL1-caspase3
C
EdU Positive cells (%)
50
40
30
20
10
0
*
*
NG
HG
NG+L-Glu
D
NG
HG
NG+L-Glu
GFAP
IgG
% of Max
24.1
30.5
12.7
FL1-GFAP

Figure 3.1 Effect of different glucose conditions on apoptosis, proliferation and GFAP expression in retinal AC.

(A) The rate of apoptosis was determined by TdT-dUTP Terminal Nick-End Labeling (TUNEL) staining. Positive cells were counted using a microscope and calculated as percentage of total cell number per field. (B) Level of cleaved caspase-3 was determined by FACS analysis. Representative mean fluorescent intensities are indicated in bottom right corner of each panel. Shaded areas show staining in the absence of primary antibody. (C) The rate of retinal AC proliferation was determined by analyzing the rate of DNA synthesis using FACScan flow cytometer. Data are presented as mean ± SEM. *$p < 0.05$; $n=3$ (NG vs. HG and NG vs. NG+L-Glu). EdU is 5-ethynyl-2′-deoxyuridine. (D) Level of GFAP in retinal AC was determined by FACS analysis. High glucose condition increased GFAP level in retinal AC compared with normal glucose and osmolarity control. Representative mean fluorescent intensities are indicated in bottom right corner of each panel. Shaded areas show staining in the absence of primary antibody.

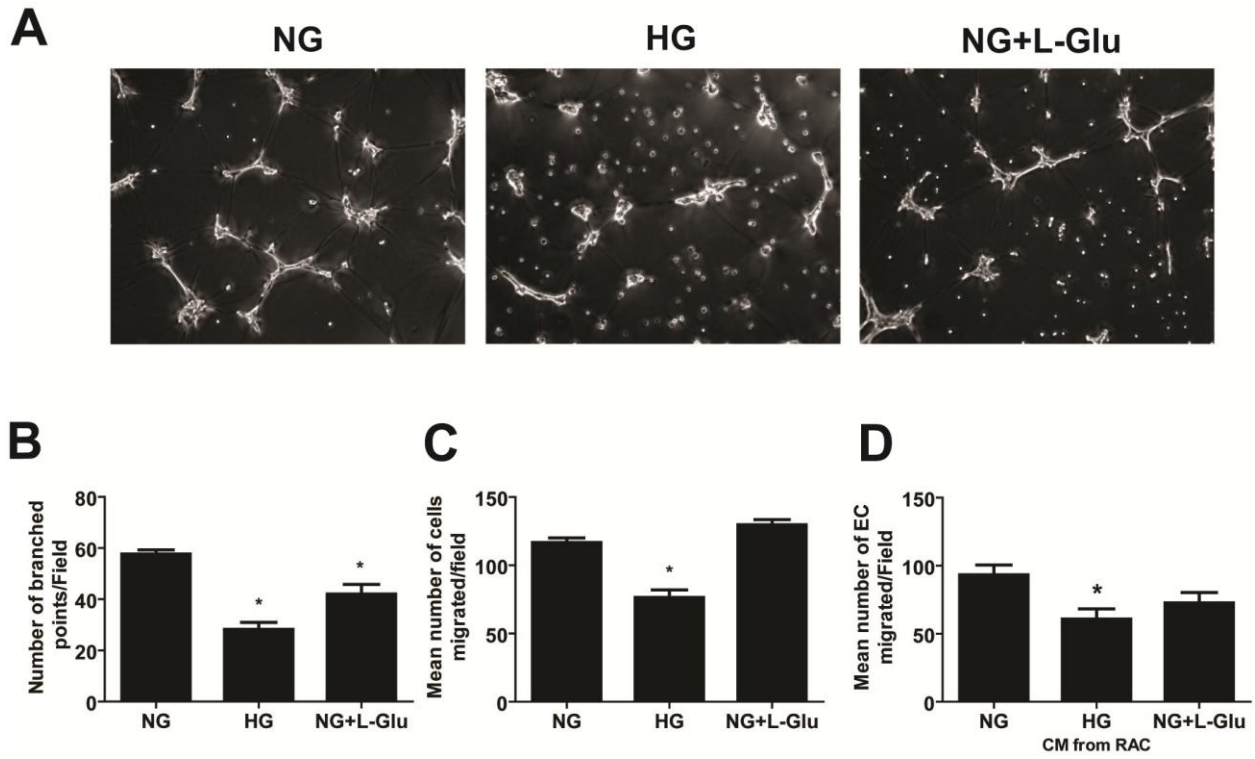

Figure 3.2 Effect of different glucose conditions on the organization of retinal AC on Matrigel and migration.

(A) High glucose conditions inhibited the organization of retinal AC on Matrigel. (B) The quantitative assessment of the organization is shown. Data are the mean number of branch points from 5 high-power fields (×100) ± SEM. *$p<0.05$; n=5 (NG vs. HG and NG vs. NG+L-Glu) (C) Transwell migration of retinal EC under different glucose conditions. High glucose conditions significantly inhibited migration of retinal AC compared with normal glucose and osmolarity control. Data are presented as mean ± SEM. n= 3,*$p < 0.05$ (NG vs. HG). (D) Conditioned medium was collected from retinal AC incubated under normal glucose, high glucose, or osmolarity control for five days. The effects of these conditioned medium on the migration of retinal EC was determined in a transwell migration assay. Please note a significant decrease in

migration of retinal EC incubated with conditioned medium from retinal AC cultured under high glucose. Data are presented as mean ± SEM. n = 3; *p<0.05 (NG vs. HG)

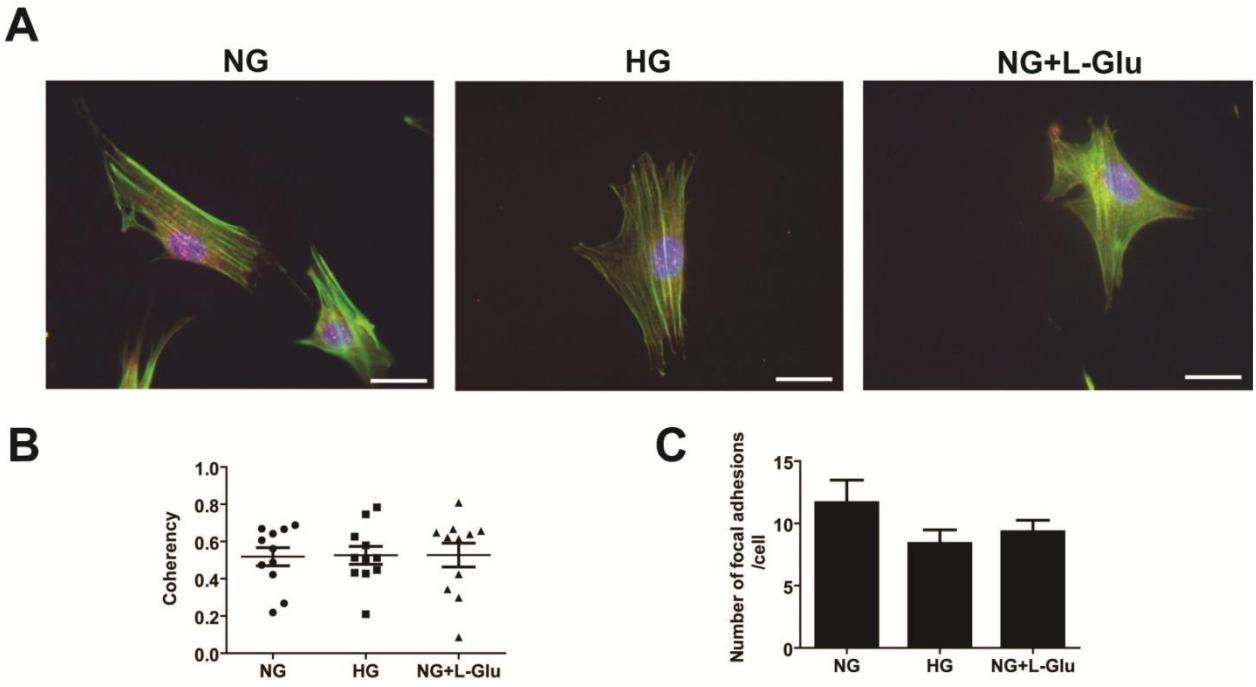

Figure 3.3 The impact of different glucose conditions on the formation of actin stress fibers and focal adhesion in retinal AC.

(A) Examination of actin stress fibers and focal adhesions in retinal AC. Retinal AC were stained with anti-vinculin (red), phalloidin (green), and DAPI (×630). Scale bar = 20 μm. (B) Coherency of stress fibers was assessed using image J software. Data are presented as each value and mean ± SEM. (C) Formation of focal adhesion was quantified. Data are presented as mean ± SEM.

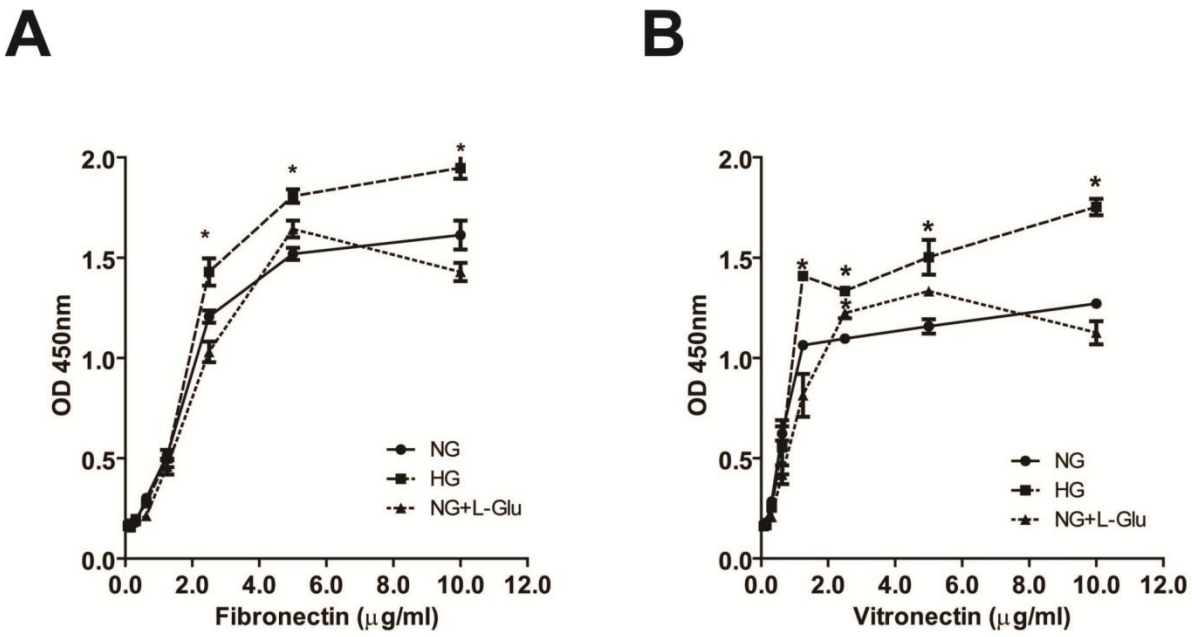

Figure 3.4 The effect of different glucose conditions on adhesion of retinal AC to extracellular matrix (ECM) proteins.

Adhesion of retinal AC to fibronectin (A) and vitronectin (B) was determined by measuring number of adherent cells in each well coated with different concentration of ECM protein. Number of adherent cells was quantified by measuring the cellular phosphatase activity as described in Methods. Data are presented as mean ± SEM. n =3; *$p<0.05$ (NG vs. HG).

The Effects of High glucose on PDGF-mediated AC migration. To elucidate the effect of glucose condition on PDGF-mediated AC migration, migratory activity of AC under various glucose conditions was investigated using a transwell migration assay with or without PDGF-AA or PDGF-BB. PDGF-AA had no effect on migration of AC cultured under normal glucose or osmolarity control conditions. However, PDGF-AA enhanced the migration of AC cultured under high glucose conditions (Figure 3.5 A). AC migration mediated by PDGF-BB was not affected under various glucose conditions (Figure 3.5 B).

The Effects of High glucose on Integrin Expression. Increase in adhesion of retinal AC to matrix proteins may be related to the enhanced expression of integrins. We determined levels of α5β1 and αvβ3 integrins by FACS analysis. α5β1integrin is a major receptor for fibronectin(184), while αvβ3 is a major receptor for vitronectin (185). α5β1 integrin level was attenuated by high glucose conditions compared with normal glucose and osmolarity control (Figure 3.6 A). However, αvβ3 level was increased under high glucose conditions compared with normal glucose conditions (Figure 3.6 B).

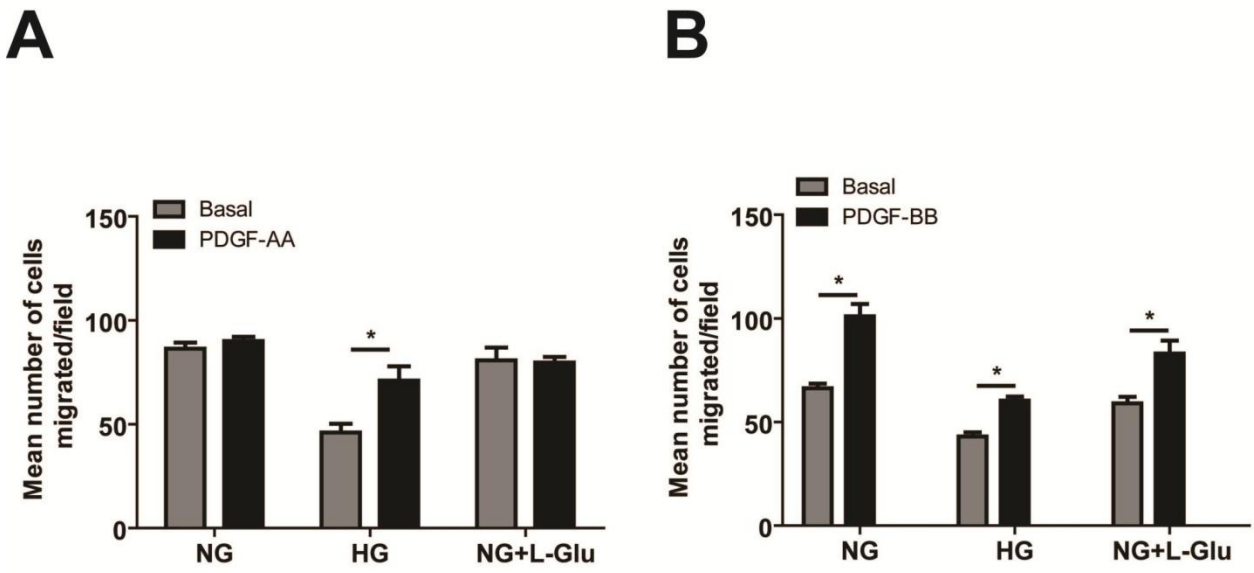

Figure 3.5. The effect of glucose conditions on PDGF-mediated migration of retinal AC. Migration of retinal AC incubated under different glucose conditions for five days was determined using transwell assay. Transwell assay was performed with basal media or media containing PDGF-AA (A) or PDGF-BB (B) in lower compartment. Data are presented as mean ± SEM. n=3; *p< 0.05 (Basal vs. PDGF-AA or PDGF-BB).

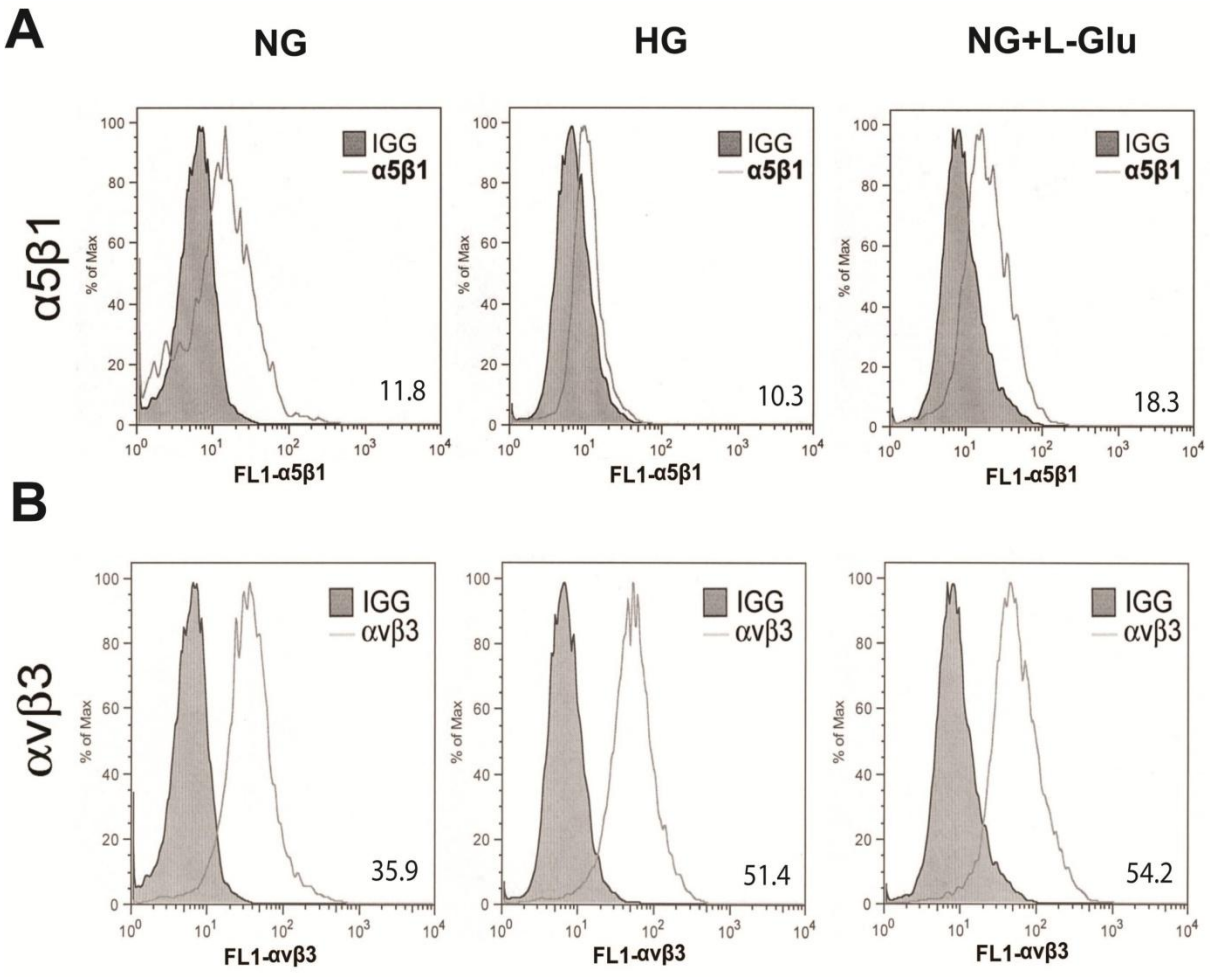

Figure 3.6 Expression of integrins in retinal AC under different glucose conditions.

Integrin α5β1 (A) and αvβ3 levels were determined by FACS analysis. Representative mean fluorescent intensities are indicated in bottom right corner of each panel. Shaded areas show staining in the absence of primary antibody.

Intracelluar Signaling Alterations in Retinal AC under High Glucose. The decreased AC migration observed in high glucose may be related to alterations in intracellular signaling pathways under high glucose conditions. These pathways play important roles in cell survival, migration, and proliferation, including Src kinase, Akt, and MAP kinases. We determined the activities of selected signaling molecules. Src phosphorylation was not affected in AC under high glucose conditions (Figure 3.7 A). In addition, activity of Akt was not affected by different glucose conditions (Figure 3.7 B). The activities of MAPKs were determined. The phosphorylation of ERK/MAP kinase was increased in retinal AC under high glucose and osmolarity control conditions compared with normal glucose condition (Figure 3.7 C). Phosphorylation of p38 MAP kinase was not affected by glucose conditions (Figure 3.7 D). Phosphorylation of JNK/MAP kinase was augmented under high glucose condition compared with normal glucose and osmolarity control conditions (Figure 3.7 E). In addition, Western blot analysis of Fyn immunoprecipitates from cell lysates, using a specific active Src antibody, showed increased activation of Fyn in retinal AC under high glucose and osmolarity control conditions compared to normal glucose conditions (Figure 3.7 F). Nuclear factor (NF)-κB has a crucial role in responding to cellular stress. To determine the effect of high glucose condition on the NF-κB signaling pathway, level of phosphorylated p65 was determined by western blot. High glucose condition increased phosphorylation of p65 compared with normal glucose and osmolarity control conditions (Figure 3.7 G).

The Effect of High Glucose on Inflammatory Cytokines. Migration of AC is related with level of inflammatory cytokines (186). We determined mRNA levels of inflammatory cytokines

including tumor necrosis factor-α (TNF-α), interleukin-1β (IL-1β) and monocyte chemotactic protein-1 (MCP-1) by quantitative real time PCR. High glucose and osmolarity control conditions increased TNF-α levels compared with normal and high glucose conditions (Figure 3.8 A). MCP-1 levels were not affected by glucose conditions (Figure 3.8 B). High glucose conditions increased mRNA levels of IL-1β compared with normal glucose and osmolarity control (Figure 3.8 C).

Inducible nitric oxide synthase (iNOS) is involved in inflammation and upregulated by inflammatory mediators including TNF-α and IL-1β (187). We next examined iNOS levels in retinal AC under various glucose conditions. High glucose conditions increased iNOS levels compared with normal glucose and osmolarity control conditions (Figure 3.8 D).

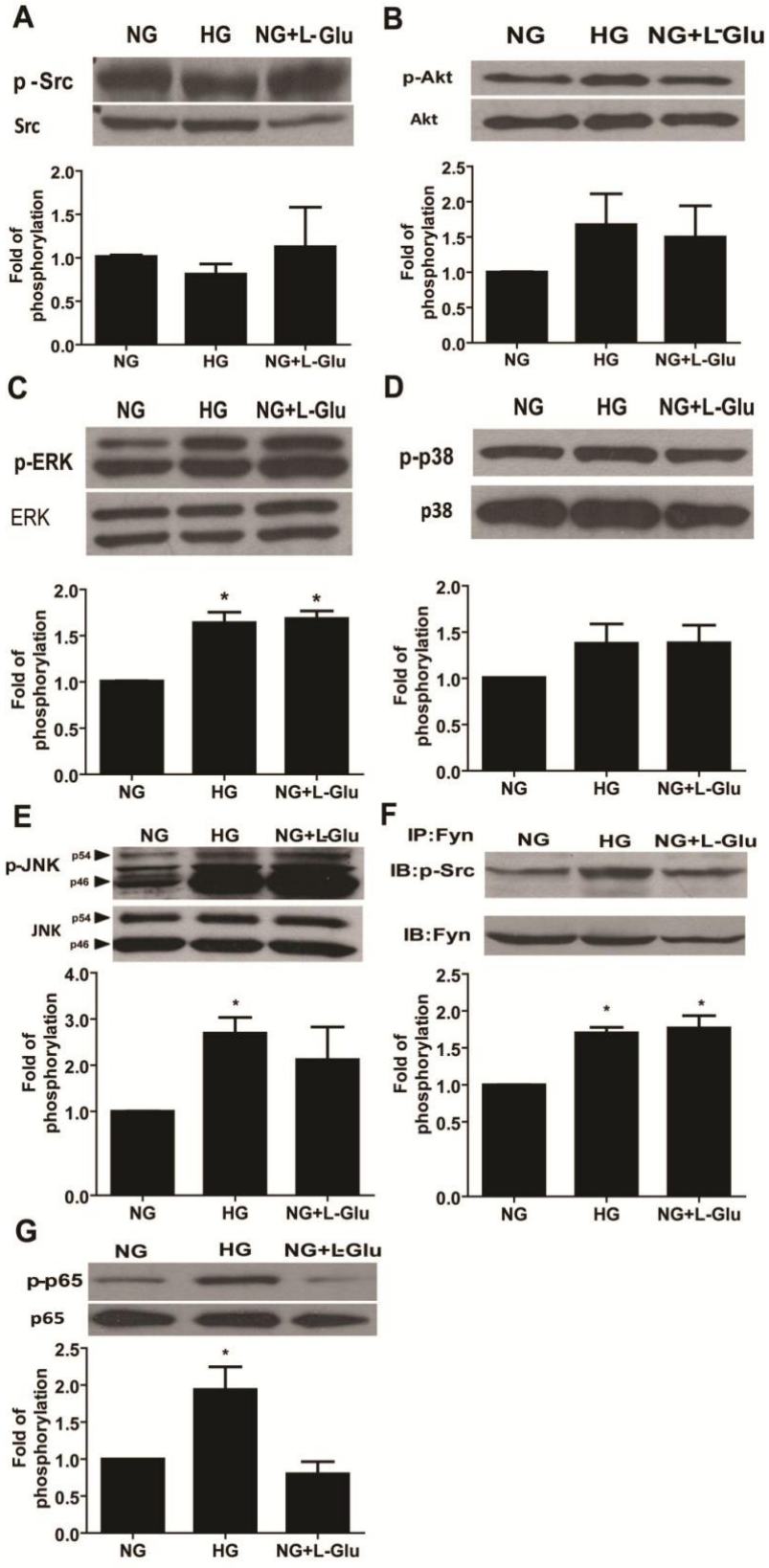
A
NG
HG
NG+L-Glu
p-Src
Src
Fold of phosphorylation
B
p-Akt
Akt
C
p-ERK
ERK
D
p-p38
p38
E
p-JNK
JNK
p54
p46
F
IP:Fyn
IB:p-Src
IB:Fyn
G
p-p65
p65

Figure 3.7 The impact of high glucose on various down-stream signaling pathways.

The status of various signaling pathways in retinal AC under various glucose conditions was determined as described in Methods. Levels of active Src (A), Akt (B), ERK (C), p38 (D), JNK1 (E), Fyn (F) and p65 (G) in retinal AC under different glucose conditions were determined by Western blot analysis from equal amounts of cell lysates. The total level for each protein is shown in the lower part of each panel. The quantitative assessment of the data for each blot is shown below the blots. Data are presented as mean ± SEM. n=3; *$p<0.05$ (NG vs. HG and NG vs. NG+L-Glu). Levels of active Fyn (F) in retinal AC under different glucose conditions was determined by Western blot analysis of immunoprecipitates from equal amounts of retinal PC lysates.

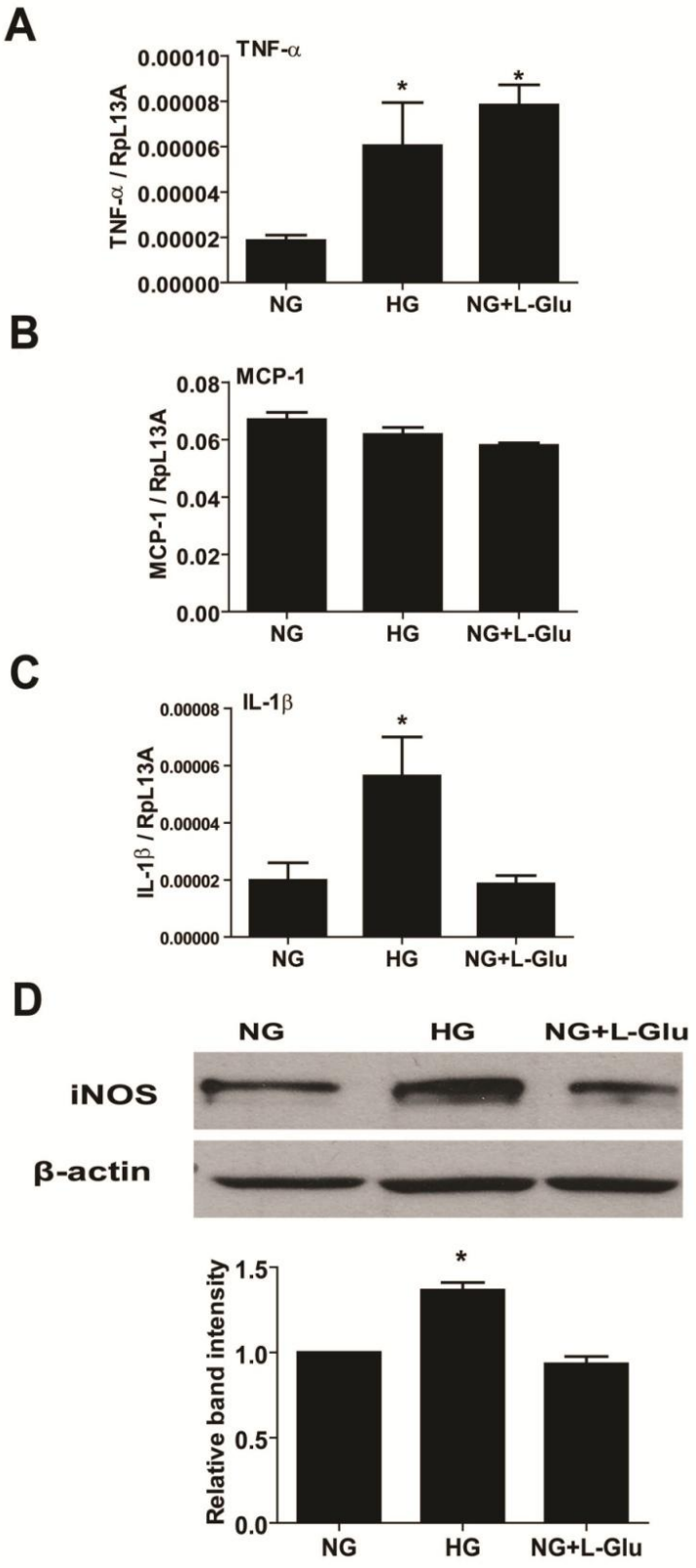
A
TNF-α
TNF-α / RpL13A
0.00010
0.00008
0.00006
0.00004
0.00002
0.00000
*
*
NG
HG
NG+L-Glu
B
MCP-1
MCP-1 / RpL13A
0.08
0.06
0.04
0.02
0.00
NG
HG
NG+L-Glu
C
IL-1β
IL-1β / RpL13A
0.00008
0.00006
0.00004
0.00002
0.00000
*
NG
HG
NG+L-Glu
D
NG
HG
NG+L-Glu
iNOS
β-actin
Relative band intensity
1.5
1.0
0.5
0.0
*
NG
HG
NG+L-Glu

Figure 3.8 Levels of inflammatory cytokines under different glucose conditions.

mRNA expressions of inflammatory cytokines in retinal AC under different glucose conditions were investigated by quantitative real time PCR method. TNF-α (A), MCP-1 (B) and IL-1β (C) levels are shown. n=5; *p<0.05 (NG vs. HG and NG vs. NG+L-Glu). (D) Protein levels of iNOS are shown. Quantification of data is also shown. β-actin was used as loading control. Data are presented as mean ± SEM. n=3; *p<0.05 (NG vs. HG and NG vs. NG+L-Glu).

Effect of antioxidant on the migration of retinal AC and capillary morphogenesis of retinal EC. High glucose conditions attenuated migration of retinal AC and increased oxidative stress in retinal AC. To determine whether oxidative stress induced by high glucose contributes to the attenuation of migration of retinal AC, Retinal AC were incubated under high glucose conditions with or without antioxidant, N-acetylcysteine (NAC) for five days. NAC restored the attenuated migration of retinal AC under high glucose conditions (Figure 3.9 A).

We next ask whether the conditioned medium collected from retinal AC under various glucose conditions affect capillary morphogenesis of retinal EC. Retinal EC were suspended in conditioned medium from AC and plated on Matrigel. Conditioned medium from AC under high glucose conditions inhibited tube capillary morphogenesis of EC compared with conditioned medium from AC cultured under normal glucose conditions (Figure 3.9 B). The quantification of tube formation is shown in Figure 3.9 C.

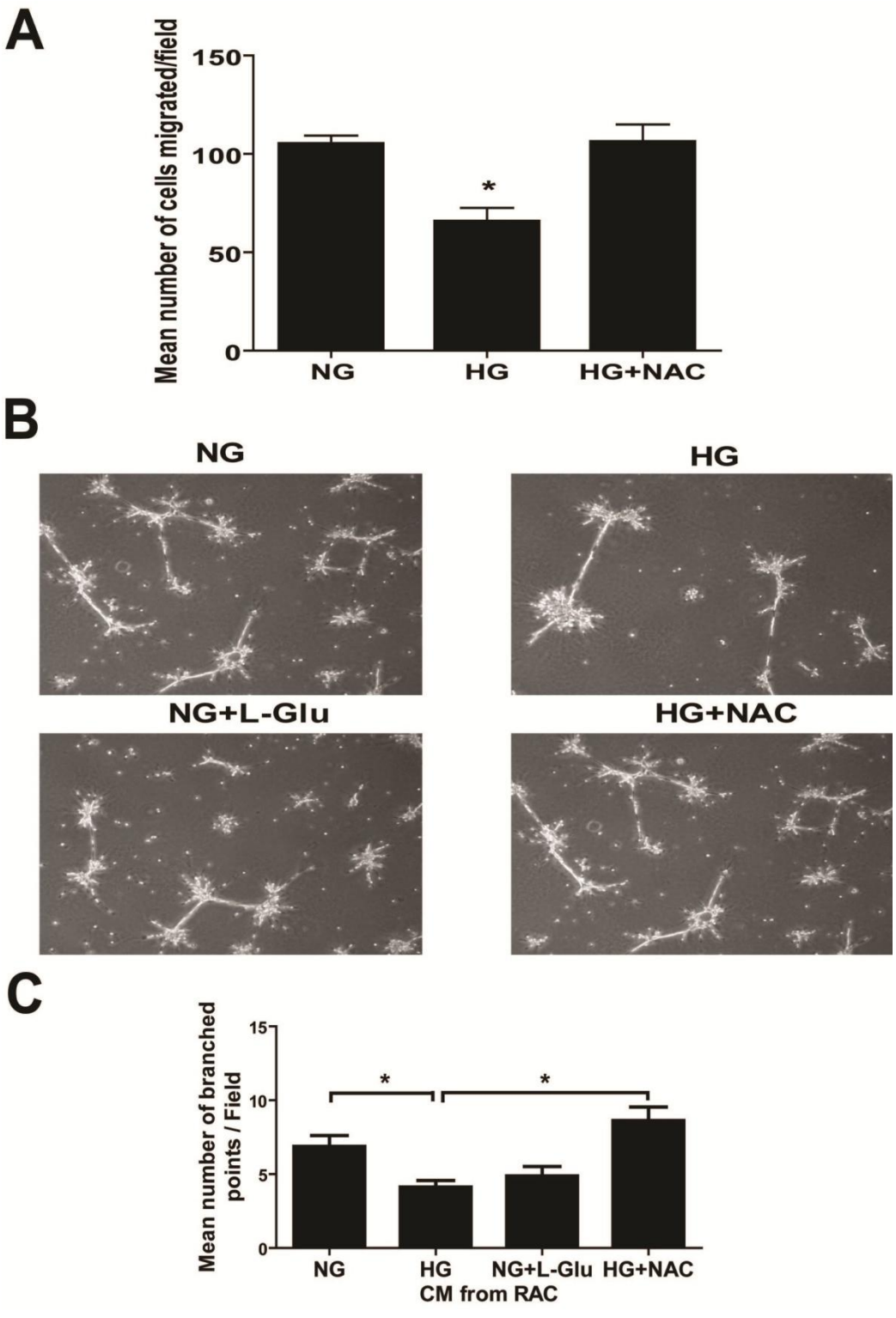
A
Mean number of cells migrated/field
150
100
50
0
*
NG
HG
HG+NAC
B
NG
HG
NG+L-Glu
HG+NAC
C
Mean number of branched points / Field
15
10
5
0
*
*
NG
HG
NG+L-Glu
HG+NAC
CM from RAC

Figure 3.9 Effect of NAC on the migration of retinal AC under different glucose conditions and the interaction with retinal EC.

(A) Incubation of retinal AC cultured under high glucose with NAC restored basal migration. Data are presented as mean ± SEM. n=3; *p <0.05 (NG vs. HG). (B) Retinal EC was suspended in conditioned medium collected from retinal AC incubated under different glucose conditions with/without NAC and grown on Matrigel to analyze tube formation. (C) The quantitative assessment of tube formation is shown. Data are the mean number of branch points from 8 high-power fields (×100) ± SEM. *p<0.05; n=8 (NG vs. HG and HG vs. HG+NAC)

Increased nuclear localization of Nrf2 in AC under High glucose conditions. High glucose conditions induce reactive oxygen species (ROS) production in brain astrocyte (188). ROS levels were determined by DHE staining of retinal AC cultured under various glucose conditions. High glucose and osmolarity control conditions increased ROS production in retinal AC (Figure 3.10 A). Nuclear factor erythroid 2-related factor 2 (Nrf2) is a transcription factor which regulates transcription of ROS-sensitive genes. Nrf2 is translocated into the nucleus to induce transcription of genes, which are involved in the protective mechanisms against oxidative stress (179). Nuclear localization of Nrf2 was examined by immunofluorescence staining. High glucose conditions increased nuclear localization of Nrf2 compared with normal glucose and osmolarity control conditions (Figure 3.10 B). Quantification of signal intensity in cell nucleus is shown in figure 10C.

Effect of high glucose on the expression of antioxidant enzymes and thrombospondins. The effects of High glucose on the expression of antioxidant enzyme including peroxiredoxin-2 (Prdx2) and heme oxygenase-1 (HO-1) were investigated by Western blot analysis. The expression of Prdx2 and HO-1 were increased in high glucose and osmolarity control conditions compared with normal glucose conditions (Figure 3.11 A and 3.11 B).

Thrombospondin 1 and 2 (TSP1 and 2) are extracellular matrix proteins and produced by various cell types including astrocyte. TSP1 and 2 have anti-angiogenic activity, and their production by AC shown to be essential for synaptogenesis of retinal ganglion cells (189). These activities are mediated by various receptors (189-191). Although, high glucose conditions increased cell-associated TSP1 and TSP2 (Figure 3.12), the secreted forms of TSP1 and TSP2

from retinal AC under high glucose and osmolarity control were decreased compared with normal glucose conditions (Figure 3.12). Thus, alteration in TSP production in AC under high glucose conditions may contribute to neuronal defects associated with diabetes.

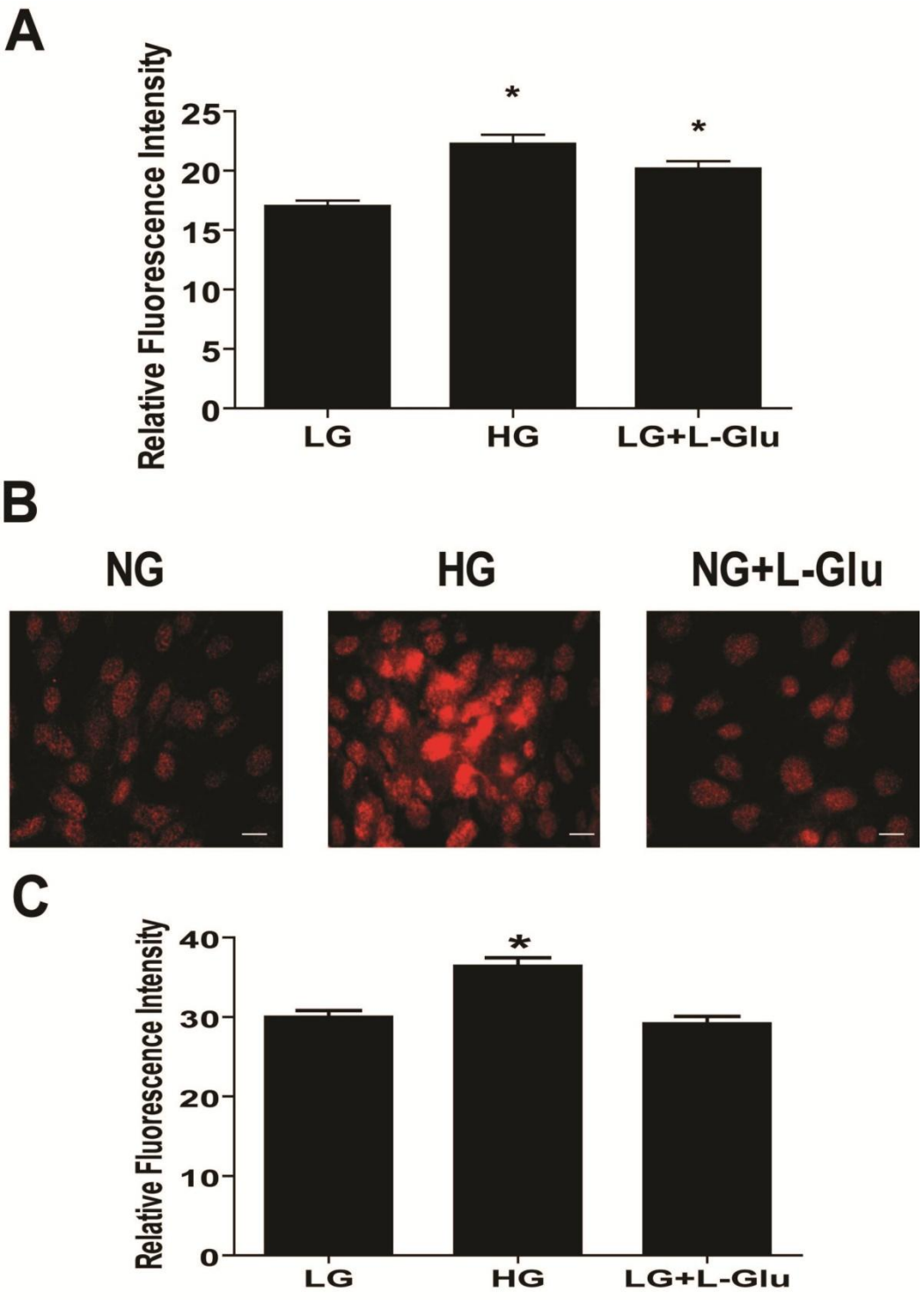
A
Relative Fluorescence Intensity
25
20
15
10
5
0
*
*
LG
HG
LG+L-Glu
B
NG
HG
NG+L-Glu
C
Relative Fluorescence Intensity
40
30
20
10
0
*
LG
HG
LG+L-Glu

Figure 3.10 The impact of high glucose conditions on the level of ROS and nuclear localization of Nrf2 in Retinal AC.

(A) Retinal AC under high glucose (HG) conditions and osmolarity control (NG+L-Glu) exhibited a significantly elevated level of ROS compared to normal glucose (NG) conditions. Data are presented as mean ± SEM. $n \geq 60$; *$p < 0.05$ (NG vs. HG and NG vs. NG+L-Glu). (B) Nuclear localization of Nrf2 in retinal AC under different glucose conditions was examined by immunofluorescence staining using antibody for Nrf2. Scale bar indicates 20 μm. (C) Nuclear localization of Nrf2 is assessed by measuring intensity of fluorescence in cell nucleus. Data are presented as mean ± SEM. $n \geq 150$; *$p < 0.05$ (NG vs. HG).

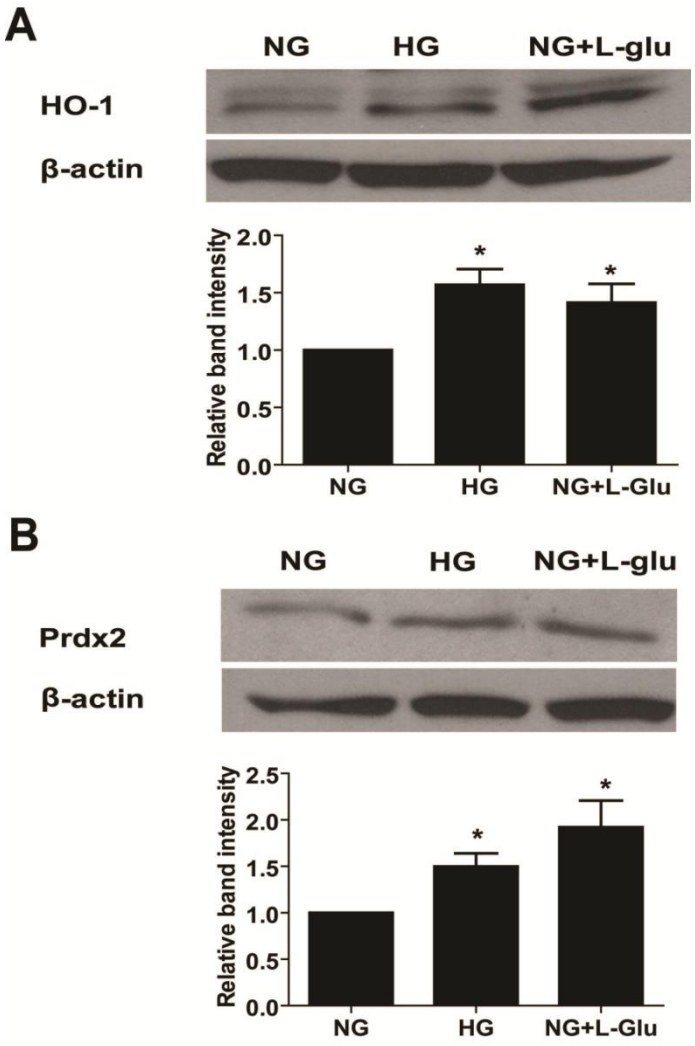

Figure 3.11 Effect of different glucose conditions on the expression of antioxidant enzymes. (A) Expression of HO-1 was determined by western blot analysis. Quantification of data is also shown. (B) Expression of Prdx2 was determined by western blot analysis. Quantification of data is also shown. β-actin was used as loading control. Data are presented as mean ± SEM. n=3; *p<0.05 (NG vs. HG and NG vs. NG+L-Glu).

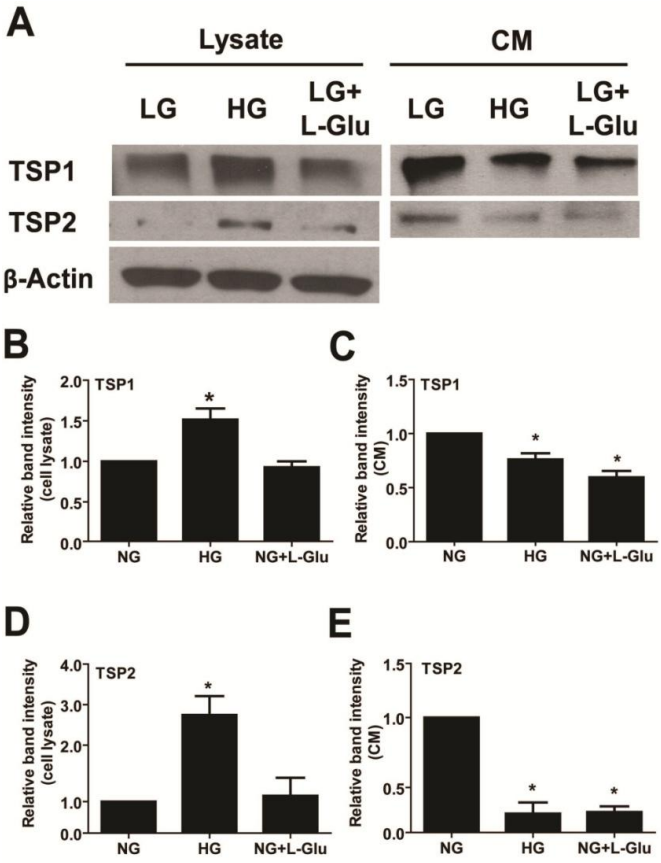

Figure 3.12 Effect of different glucose conditions on the expression and secretion of thrombospondin 1 and 2.

(A) Levels of TSP1 and TSP2 in cell lysate and conditioned medium collected from retina AC were determined by Western blot analysis. β-actin was used as loading control. Quantification for band intensity is also shown. (B) TSP1 in cell lysate. (C): TSP1 in conditioned medium. (D) TSP2 in cell lysate. (E) TSP2 in conditioned medium. Data are presented as mean ± SEM. n=3; *$p<0.05$ (NG vs. HG and NG vs. NG+L-Glu).

Discussion

Here, we determined the impact of high glucose on retinal AC properties affected. High glucose conditions did not affect retinal AC apoptosis. However, high glucose and osmolarity control conditions increased proliferation of retinal AC. High glucose conditions also increased expression of GFAP in retinal AC. Furthermore, Migration and capillary morphogenesis of AC on Matrigel was significantly attenuated under high glucose conditions. High glucose conditions also affected the activation of signaling molecules involved in migration and proliferation, and increased mRNA level of inflammatory cytokines including IL-1β and TNF-α. In addition, high glucose conditions induced production of concomitant with the activation of Nrf2, which regulates transcription of antioxidant genes. High glucose increased expression of antioxidant proteins including Prdx2 and HO-1 in AC. High glucose also inhibited the migration and capillary morphogenesis of retinal EC, which was restored by incubation with NAC. Together, our results demonstrate that high glucose conditions affect proliferation and migration of retinal AC through production of ROS and retinal AC respond to oxidative stress by increasing antioxidant enzymes.

The effect of diabetic conditions on the apoptosis of vascular cells including retinal AC has been studied. In the retina of diabetic rats, neural apoptosis level is elevated compared with non-diabetic rat. However, apoptosis of retinal AC in diabetic mice was similar to with non-diabetic mice (192). These results are consistent with our observation that high glucose conditions did not increase apoptosis of retinal AC. Thus, apoptosis of retinal AC is not affected by high glucose conditions.

GFAP has crucial roles in the intermediate filament network formation and is an essential components of the AC cytoskeleton (183). Expression of GFAP is strongly enhanced in wound area of astrocytes, and indicates damage in astrocytes (193). High glucose conditions increased GFAP level in retinal AC compared with normal glucose and osmolarity control conditions. This result implies that retinal AC are damaged/stressed under high glucose conditions. Furthermore, GFAP is also involved in retinal AC migration (183). Migration of retinal AC is important in tissue repair in response to pathogenic events (184). Increased expression of GFAP results in inhibition of cell migration (194). Thus, the attenuation of retinal AC migration might result from increased level of GFAP under high glucose conditions. Formation of stress fiber and focal adhesion are also involved in cell migration. However, different glucose conditions did not affect formation of actin stress fibers and focal adhesions in retinal AC. These results indicate that formation of stress fiber and focal adhesion is not involved in the attenuation of retinal AC migration under high glucose conditions.

The attenuated migration of retinal AC under high glucose conditions suggests that high glucose conditions may affect adhesion of retinal AC to ECM proteins. In the present study, we also observed high glucose conditions enhanced adhesion of retinal AC to ECM proteins including fibronectin and vitronectin. This enhanced adhesion of retinal AC might contribute, at least in part, to the attenuation of retinal AC migration under high glucose conditions.

Inflammatory cytokine including IL-1β and TNF-α in astrocyte have been shown to promote adhesion of astrocyte to fibronectin. IL-1β inhibits migration and TNF-α promotes migration of AC. In addition, combination of both cytokines inhibits migration of AC (186). In the present study, we observed high glucose conditions increased mRNA levels for IL-1β and

TNF-α whereas osmolarity control increased only mRNA level of TNF-α. These results imply that the attenuated migration of retinal AC under high glucose condition could be mainly attributed to enhanced level of IL-1β under high glucose conditions.

It was observed that conditioned medium collected from retinal AC under high glucose conditions inhibited migration and tube formation of retinal EC. We recently demonstrated that IL-1β and TNF-α inhibited migration and tube formation of retinal EC (195). Attenuation of migration and tube formation of retinal EC by conditioned medium collected from retinal AC under high glucose conditions may also be mediated by increased level of IL-1β in retinal AC under high glucose conditions.

Expression of IL-1β is regulated by inflammatory transcription factor NF-κB (196). Retinal AC under high glucose conditions exhibited increased phosphorylated form of p65 subunit of NF-κB. These results suggested that the activation of NF-κB by high glucose conditions is responsible for increased expression of inflammatory cytokines, IL-1β in retinal AC. The expression of TNF-α was also elevated under high glucose and osmolarity control conditions, thus implying that expression of TNF-α is regulated by osmotic stress.

Astrocytes activate repair process by undergoing proliferation when they are damaged by environmental stimuli (193). Proliferation of AC is mediated by the activation of ERK, and Fas/CD95 may be involved in the activation of ERK (197). High glucose and osmolarity control conditions increased proliferation of retinal AC. Moreover, phosphorylation of ERK was increased under high glucose and osmolarity control conditions. These results suggested that enhanced proliferation of retinal AC under osmotic stress conditions is mediated by the activation of ERK. Fas/CD95 interactions activate ERK in astrocyte (197). However, how

osmotic stress, including high glucose conditions affect Fas/CD95 expression and function need further investigation in order to elucidate the mechanisms responsible for ERK activation and enhanced proliferation.

We observed antioxidant, N-acetylcysteine (NAC), treatment restored the attenuated migration of retinal AC and capillary morphogenesis of retinal EC under high glucose conditions. These results suggest that the attenuation of retinal AC migration and inhibition of retinal EC capillary morphogenesis are mediated by oxidative stress under high glucose conditions. High glucose and osmolarity control conditions elevated ROS level, and caused oxidative stress in retinal AC. Excessive production of ROS in AC results in the activation of cellular defense system in response to oxidative stress. Nrf2 is a transcription factor that regulates the expression of antioxidant enzymes including Prdx2 and HO-1 to respond to oxidative stress. To activate transcription of antioxidant enzyme, Nrf2 is translocated into the nucleus and binds to a cis-acting antioxidant responsive element (ARE) in antioxidant genes (179, 198). Although high glucose and osmolarity control conditions increased ROS level, only high glucose conditions increased nuclear translocation of Nrf2 in retinal AC. It is possible that high glucose condition may induce more sustained activation of Nrf2 than osmolarity control conditions.

Oxidative stress induces phosphorylation of Fyn kinase. Phosphorylated Fyn kinase was increased phosphorylation of Nrf2 leading to its degradation (179). In the present study, high glucose and osmolarity conditions increased p-Fyn levels. This activation of Fyn kinase might result from oxidative stress induced by high glucose and osmolarity control conditions. Furthermore, we observed high glucose and osmolarity control conditions increased levels of

antioxidant enzymes including Prdx2 and HO-1. Heme oxygenase-1 (HO-1) is an enzyme that responds to stress and the rate-liming enzyme in heme catabolism. Induction of HO-1 in diabetic retinopathy has protective roles by anti-inflammatory, anti-apoptosis and anti-proliferative effects (199). Prdx2 is a cellular peroxidase that reduces H_2O_2 and prevents inactivation of redox-sensitive signaling pathways (200). Prdx2 has a protective effect against apoptosis in retinal photoreceptor cells (201). Upregulation of antioxidant enzyme including Prdx2 and HO-1 might be a protective mechanism for retinal AC against oxidative stress induced by osmotic stress.

Thrombospondin 1 and 2 (TSP1 and 2) are extracellular matrix glycoproteins involved in angiogenesis and neurogenesis (202). In the present study, high glucose conditions increased the levels of cell-associated TSP1 and TSP2 in retinal AC. However, levels of secreted TSP1 and TSP2 were attenuated under high glucose and osmolarity control conditions. Secretion of thrombospondin requires glycosylation at thrombospondin type 1 repeats (TSRs) (203). These results may imply that high glucose conditions affect expression of TSP1 and TSP2 in retinal AC and osmotic stress affects glycosylation of TSP1 and TSP2 for secretion.

In summary, our studies demonstrate that exposure of retinal AC to high glucose results in attenuation of migration, increased proliferation and adhesion to ECM proteins. We showed that high glucose conditions increased expression of inflammatory cytokines including IL-1β and TNF-α, and oxidative stress in retinal AC. Conditioned medium collected from retinal AC under high glucose conditions impacted on the migration and capillary morphogenesis of retinal AC. Retinal AC responded to oxidative stress by elevating the levels of antioxidant enzymes including HO-1 and Prdx2 through nuclear translocation of transcription factor Nrf2. Together,

high glucose conditions result in dysfunction of retinal AC through inflammation and increased oxidative stress.

4. Summary and Future Directions

Summary

Diabetic retinopathy (DR) is one of diabetes complications and the main cause of blindness among working-aged people. DR causes biochemical and vascular changes in retina leading to vascular leakage and edema. Retinal vasculature provides oxygen and nutrients to the inner retinal tissue. The integrity and function of vascular structure in the retina is maintained by blood-retinal-barrier (BRB). In inner BRB, endothelial cell, pericytes and astrocytes are cellular components of the vascular structure. These vascular cells have important roles for the function and integrity of BRB. Pathological conditions including diabetes affect the function and integrity of BRB through cellular dysfunction of vascular cells. High glucose conditions induced by diabetes affect the function of vascular cells including endothelial cells, pericytes and astrocyte. To understand the effect of high glucose conditions on the function of vascular cells, many studies have been conducted. From those studies, changes in vascular cells contributing to alteration in retinal vascular structure have been shown. However, detailed mechanism for the dysfunction of vascular cells and interactions between vascular cells under high glucose conditions remain poorly defined.

We have described a novel method for isolation and culture of retinal endothelial cell, pericytes and astrocytes from wild type and transgenic mice. Previously, we reported that high glucose conditions promoted migration of mouse retinal endothelial cell through activation of signaling pathways mediated by Src, PI3K/Akt1/eNOS and ERK without affecting apoptosis. Pericyte loss is a hallmark of DR and many studies have been performed to elucidate the effect of high glucose conditions on pericytes apoptosis. However, the detailed signaling mechanism for the apoptosis of pericytes under high glucose conditions has not been clearly defined. In this

study, I showed that the rate of apoptosis and expression of proapoptotic protein Bim were increased in the retina of diabetic Akita/+ mice and mouse retinal pericytes under high glucose conditions. This increased level of Bim in mouse retinal pericytes was mediated by the sustained activation of STAT1. High glucose conditions increased oxidative stress in retinal pericytes and attenuated migration of retinal pericytes. Pharmacological inhibitions of oxidative stress, PKC-δ or ROCK I/II protected retinal pericytes against apoptosis under high glucose conditions. In co-culture experiments of retinal endothelial cells and pericytes, pericytes under high glucose conditions inhibited capillary morphogenesis of retinal endothelial cells. Furthermore, conditioned medium collected from pericytes under high glucose conditions attenuated migration of retinal endothelial cells. In addition, apoptosis and oxidative stress in pericytes deficient in Bim expression was not affected by high glucose conditions. However, N-acetylcysteine did not affect Bim expression in retinal pericytes. These results imply that Bim is upstream of oxidative stress. Studies presented here demonstrate that STAT1-mediated Bim expression plays a crucial role in the dysfunction of retinal pericytes under high glucose conditions.

Astrocytes are glial cells and have an essential role in maintaining BRB and development of retinal vascular structure. High glucose conditions caused by diabetes affect morphology and function of retinal astrocytes leading to dysfunction and breakdown of BRB. However, cellular mechanisms underlying dysfunction of retinal astrocytes under high glucose conditions are poorly defined. In the present study, I demonstrate that high glucose conditions affected proliferation and expression of GFAP in retinal astrocytes without affecting apoptosis. High glucose conditions increased adhesion of retinal astrocytes to extracellular matrix proteins including fibronectin and vitronectin. In addition, high glucose conditions altered signaling pathways involved in migration, proliferation and survival. Furthermore, high glucose

conditions also affected levels of pro-inflammatory molecules including IL-1β, TNF-α and iNOS in retinal astrocytes. To delineate the mechanism for attenuated migration of retinal astrocytes, astrocytes were incubated with NAC under high glucose conditions. NAC restored the attenuated migration of retinal astrocytes under high glucose conditions. Conditioned medium collected from retinal astrocytes under high glucose conditions inhibited capillary morphogenesis of retinal astrocytes and NAC treatment recovered capillary morphogenesis of retinal endothelial cells. In the present study, I demonstrated that high glucose conditions increased expression of antioxidant proteins including Prdx2 and HO-1. The increased expression of antioxidant protein was mediated by nuclear localization of Nrf2. Together, results in the present study demonstrated that oxidative stress and inflammatory mediators are involved in the dysfunction of retinal astrocytes under high glucose conditions.

In the appendix, I demonstrate the impact of pigment epithelium-derived factor (PEDF) deficiency on the function of lung endothelial cells. PEDF -/- endothelial cell prepared from lung of PEDF -/- mice exhibited increased migration and attenuated proliferation compared with PEDF +/+ endothelial cells. In addition, PEDF -/- endothelial cells exhibited increased level of pro-inflammatory molecules including VEGF, VCAM-1 and iNOS. PEDF -/- endothelial cells also showed alterations in junctional organization. PEDF -/- endothelial cells were more adhesive to extracellular matrix proteins and showed alterations in expression of extracellular matrix proteins. Furthermore, I demonstrated that the inflammatory phenotypes in the lung of PEDF -/- mice. Lung of PEDF -/- mice exhibited increased level of macrophage marker protein, F4/80 accompanied by increased thickness of vessel walls and expression of inflammatory cytokines. Together, these results imply that PEDF has a crucial role in regulating inflammation and angiogenesis in the lung endothelium.

Concluding remarks and future directions

Inflammation and vascular dysfunctions

Inflammation is a nonspecific protective response against injury induced by pathogens. Acute inflammation has beneficial effect, but persistent inflammation has detrimental effects (27). Inflammation can cause biochemical changes in diabetic retina leading to vascular dysfunctions and breakdown of BRB. Inflammatory mediators including VEGF, iNOS, ICAM-1 and COX-2 are upregulated in the diabetic retina (204). Moreover, anti-inflammatory treatments, inhibiting inflammatory mediators, ameliorate development of diabetic retinopathy (29, 32). In the present study, I showed that inflammatory cytokines were up-regulated in retinal vascular cells including pericytes and astrocytes under high glucose conditions, and inflammatory cytokines activated a transcription factor, STAT1 to induce apoptosis of pericytes. In addition, pericytes are the major source of inflammatory cytokines in response to high glucose. Furthermore, we have shown that the inflammatory cytokines including TNF-α and IL-1β inhibit migration and capillary morphogenesis of retinal endothelial cells (195). These results suggest that inflammation caused by high glucose conditions has a crucial role in the dysfunction of retinal vascular cells, and retinal pericytes are the primary target.

Expression of pro-inflammatory genes is regulated by transcription factor NF-κB. The activation of NF-κB requires pathogen recognition by innate immune system. This recognition by innate immune system is mediated by pathogen recognition receptors including toll-like receptors (TLR) and receptor for advanced glycation endproducts (RAGE) (27). The effect of high glucose conditions on RAGE has been recognized. However, how high glucose condition affect TLR in retina has not been studied. Thus, elucidating the impact of high glucose

conditions on the expression and function of TLR, especially in pericytes, will provide new insight into the regulation of inflammation and pathogenesis of DR.

In separate study, I showed that PEDF has anti-inflammatory activity and its deficiency induced vascular inflammation and abnormalities in the lung. A considerable number of studies have demonstrated that PEDF inhibits retinal inflammation and neovascularization. Therefore, PEDF has been studied as a potential therapeutical target for treatment of diabetic retinopathy (37). Peptide fragments from PEDF inhibit progression of diabetes complications including DR in animal models (205). Development of method for increasing PEDF level in the retina may provide novel modalities for treating diabetic retinopathy.

Thrombospondin-1 (TSP1) is an anti-angiogenic factor and we have shown that the level of TSP1 was attenuated in diabetic patients and rat compared with non-diabetic subject (206, 207). Furthermore, we have demonstrated that the lack of TSP1 expression in retinal vascular endothelium of diabetic mice promoted the progression of diabetic retinopathy (208). However, the role of TSP1 in pericytes associated with apoptosis under high glucose conditions has not been examined. The role of TSP1 in the apoptosis of pericytes under high glucose needs to be elucidated to understand the role of anti-angiogenic factors in the pathogenesis of diabetic retinopathy.

Wnt signaling pathway and vascular dysfunction

Wnt proteins are ~40 kDa in size and cysteine- rich glycoproteins. Wnt proteins bind to the frizzled (Fz) receptors or complex of receptors consisting of Fz and low-density lipoprotein receptor-related protein 5/6 (LRP5/6) to activate canonical Wnt signaling pathway (209).

Binding of Wnt ligands to complex of receptors stabilize β-catenin leading to accumulation and nuclear translocation of β-catenin. The nuclear β-catenin activates transcription of various target gens including inflammatory mediators (210). PEDF binds to LRP6 receptor and inhibits Wnt signaling pathway through blocking the formation of receptor complex (211). I have demonstrated that the lack of PEDF in the lung endothelial cell increased β-catenin level and nuclear translocation of β-catenin. Thus, anti-inflammatory activity of PEDF is not specific to retinal endothelial cells, and it is mediated by inhibition of canonical Wnt pathway.

Wnt pathway also has a crucial role in the development of DR. Wnt pathway is activated in the diabetic retina and inhibition of Wnt pathway ameliorates retinal inflammation and neovascularization (209, 212). High glucose conditions increased β-catenin level in endothelial cells and inhibition of Wnt pathway attenuated the increased migration of endothelial cells under high glucose conditions. However, inhibition of Wnt did not affect pericyte loss in the diabetic retina (209). These imply that Wnt signaling pathway acts differently in pericytes and endothelial cells in inducing inflammation and dysfunctions. The role of Wnt pathway in retinal pericytes associated with apoptosis and inflammation under high glucose conditions has not been elucidated. The regulation and role of Wnt pathway in retinal pericytes leading to dysfunction and apoptosis under high glucose conditions need to be investigated to understand pathogenic role of Wnt in DR.

Role of miRNA in vascular dysfunction

microRNAs (miRNA) are a family of non-coding RNAs with 20~22 nucleotides in length. miRNAs are implicated in the regulation of mammalian gene expression by inhibiting

translation or inducing degradation of target RNA. miRNAs are involved in the regulation of key cellular functions including apoptosis (213). Bim is a proapoptotic protein and its level is regulated by miRNAs (214). Here, I showed that Bim has a crucial role in increasing oxidative stress under high glucose conditions leading to apoptosis of retinal pericytes. These results suggest that Bim expression under high glucose conditions could be attenuated by miRNA expression. There are several miRNAs involved in the regulation of Bim expression (214, 215). Identifying miRNA involved in the regulation of Bim expression in retinal pericytes under high glucose conditions will provide novel insight into regulation apoptosis in retinal pericytes

I have shown that oxidative stress induced by high glucose conditions is crucial for dysfunction of retinal pericytes and astrocytes. It has been found that miR-200b expression was upregulated in the retina of diabetic mice and the miRNA-200b inhibited expression of antioxidant protein, oxidation resistance 1 (Oxr1) contributing to apoptosis of retinal cells (64). Thus, examining miRNA expression profiles associated with oxidative stress in retinal vascular cells under high glucose conditions may provide novel miRNAs as biomarkers and therapeutic targets for detection and treatment for DR.

O-GlcNAc modification in diabetic retinopathy

O-linked GlcNAc modification is a specific posttranslational modification which occurs in various proteins with different functions. This modification attaches a single N-acetylglucoamine (GlcNAc) to hydroxyl groups of serine and threonine amino acids of proteins and it is catalyzed by the enzyme O-linked N-acetylglucosaminyl transferase (OGT) (216). Diabetic conditions increase O-GlcNAc modifications in proteins which may contribute to pathogenesis of diabetic complications (46). O-GlcNAc modification is important in modulating

protein functions, and cellular localizations. Some transcription factors including NF-κB have been known for their O-GlcNAc modification, and regulation of their activity. NF-κB is a regulator of inflammatory cytokines including IL-1β (217). NF-κB p65 subunit is modified by O-GlcNAc modification under high glucose conditions, and this modification increases transcriptional activity of NF-κB p65 subunit under high glucose conditions (218). In the present study, I demonstrated that high glucose conditions increased phosphorylation of NF-κB p65 subunit in retinal astrocytes. The role of O-GlcNAc modification in modulation of NF-κB activity in retinal vascular cells needs to be investigated.

I also demonstrated that high glucose conditions increased phosphorylation of STAT1 in retinal pericytes leading to increased Bim expression. STAT1 is also modified by O-GlcNAc modification for transcriptional regulation (219). The effect of high glucose conditions on the posttranslational modification of STAT1 under high glucose conditions in retinal vascular cells needs to be examined. Thus, investigating O-GlcNAc modifications of transcription factors in retinal vascular cells under high glucose conditions will offer novel insight into the regulatory mechanisms that impact vascular dysfunction.

Here, I demonstrated that the production of inflammatory mediators is a primary result with crucial roles in loss of pericytes under high glucose conditions. The regulatory mechanisms for inflammation leading to vascular dysfunction during diabetes are not fully defined. Elucidating mechanisms responsible for vascular inflammation associated with diabetes will facilitate our understanding of the pathogenesis of the disease and development of new modalities for treatment. Furthermore, I demonstrated that phosphorylation of transcription factors including NF-κB p65 subunit and STAT1 is important for vascular dysfunction under

high glucose conditions. Regulation of gene transcription through posttranslational modifications of transcription factors and miRNA expression under high glucose conditions needs to be further investigated. These investigations are essential for delineation the regulatory mechanisms of gene expression, which contributes to vascular dysfunctions associated with diabetes.

Appendix. PEDF Expression Regulates the Pro-angiogenic and Pro-inflammatory Phenotype of the Lung Endothelium

This work was submitted to *American Journal of Physiology-Lung Cellular and Molecular Physiology* and under revision.

Abstract

Pigment epithelium-derived factor (PEDF) is a multifunctional protein with important roles in regulation of inflammation and angiogenesis. It is produced by various cell types including endothelial cells (EC). However, the cell autonomous impact of PEDF on EC function needs further investigation. Lung EC prepared from PEDF -/- mice were more migratory and failed to undergo capillary morphogenesis in Matrigel compared to PEDF +/+ EC. Although no significant differences were observed in the rates of apoptosis in PEDF -/- EC compared to PEDF +/+ cells under basal or stress conditions, PEDF -/- EC proliferated at a slower rate. The PEDF -/- EC also expressed increased levels of proinflammatory markers including vascular endothelial growth factor, inducible nitric oxide synthase, vascular cell adhesion molecule-1, as well as altered cellular junctional organization, and nuclear localization of β-catenin. The PEDF -/- EC were also more adhesive, expressed decreased levels of thrombospondin-2, tenascin-C and osteopontin, and increased fibronectin. Furthermore, we showed lungs from mice deficient in PEDF (PEDF -/-) exhibited increased expression of macrophage marker F4/80 along with increased thickness of the vascular walls consistent with a pro-inflammatory phenotype. Together our data suggest that the PEDF expression makes significant contribution to modulation of the inflammatory phenotype and angiogenic phenotype in the lung endothelium.

Introduction

Angiogenesis is a multistep process involving the growth of new blood vessels from pre-existing capillaries, and it is crucial for the normal development and function of lung. Angiogenesis is tightly regulated by a balanced production of pro- and anti-angiogenic factors. Alterations in this balance may impact pro-angiogenic and pro-inflammatory properties of vasculature, and contribute to various pathologies (220). Survival, adhesion, proliferation, tube formation and migration of endothelial cells (EC) are essential in angiogenesis (221). Function of EC in angiogenesis are modulated by production of various pro- and anti-angiogenic factors including vascular endothelial growth factor (VEGF), thrombospondin-1 (TSP1), and pigment epithelium derived factor (PEDF) (222-224). However, the contribution of these factors to regulation of lung vascular homeostasis and pathologies remain poorly understood.

Pigment epithelium derived factor (PEDF) is a 50-kDa glycoprotein and belongs to serine protease inhibitor family of proteins (225, 226). It was first identified in cultured fetal retinal pigment epithelial (RPE) cells (227). PEDF is also expressed in other ocular cell types including Müller cells, pericytes and EC (228). PEDF influences the function and pathogenesis of various tissues including liver, kidney, heart, prostate and lung due to its various biological activities (229-232). PEDF is an endogenous inhibitor of angiogenesis and it is neuroprotective. PEDF inhibits the migration of EC in response to proangiogenic factors (233), and induces apoptosis of human EC by activating p38 mitogen activated protein kinase and caspases (230, 234). Increased expression of PEDF in the retina results in attenuation of neovascularization through modulation of canonical Wnt signaling (235). PEDF also has anti-inflammatory activity and its expression in

diabetic rat inhibits the expression of pro-inflammatory factors through inhibition of NF-κB activity (236).

PEDF plays an important role in regulation of angiogenesis and inflammation through its coordinated activity with pro-angiogenic and inflammatory factors including VEGF. Alterations in this coordinated activity and dysfunction in the regulation of VEGF and PEDF expression have been implicated in pathogenesis of various diseases with neovascular components including age-related macular degeneration (AMD), diabetic retinopathy (DR), and cancer. These alterations have been generally associated with increased expression of VEGF, while that of PEDF is suppressed (223, 237), favoring a pro-angiogenic and inflammatory state. However, the contribution such alterations to various lung pathologies require further investigation.

An important role for VEGF in lung development, integrity, and function has been previously demonstrated. Attenuation of VEGF activity through inhibition of its receptor in the lung results in increased apoptosis and development of emphysema (238). However, the role of PEDF in lung development and vascular homeostasis has not been previously studied. To gain new insight into PEDF function in the lung, we investigated the specific role of PEDF in the lung endothelium. We prepared lung EC from PEDF +/+ and PEDF -/- mice. Here we show PEDF-deficiency increased EC migration along with increased adhesion to various extracellular matrix (ECM) proteins. We also showed that PEDF-deficiency was associated with attenuation of capillary morphogenesis of lung EC. Mechanistically, PEDF-/- lung EC expressed increased levels of inflammatory markers including VEGF, VCAM-1, and iNOS concomitant with increased NO production. Furthermore, we showed that levels of inflammatory proteins were altered, and the thickness of vessel wall was increased in lungs from PEDF-/- mice. Thus,

endothelium expression of PEDF is essential for maintaining the inflammatory and angiogenic properties of the lung.

Materials and Methods

Experimental Animals and Culture of Lung EC. All experiments were carried out in accordance with and approved by the Institutional Animal Care and Use Committee of the University of Wisconsin School of Medicine and Public Health. Immortomice expressing a temperature-sensitive SV40 large T antigen were purchased from Charles River Laboratories (Wilmington, MA). The PEDF -/- mice were crossed with the Immortomice and screened as previously described (182). Lungs from three 4-week-old wild-type and PEDF -/- Immortomice were dissected and kept in serum free-Dulbecco's Modified Eagle's Medium (DMEM) containing penicillin and streptomycin (Sigma; St. Louis, MO). The lungs were pooled, rinsed with DMEM, minced into small pieces in a 60-mm tissue culture dish using sterile razor blades, and digested with 5 ml of collagenase type I (1 mg/ml in serum-free DMEM; Worthington, Lakewood, NJ) for 45 min at 37 ℃. After digestion, DMEM with 10% heat-inactivated fetal bovine serum (FBS) was added and cells were collected by centrifugation. The cellular digests were filtered through a double layer of sterile 40-μm nylon mesh (Sefar America, Hanover Park, IL) and centrifuged at 400 xg for 10 min to collect cells. Cells were washed twice with DMEM containing 10% FBS and were resuspended in 1.5 ml of medium (DMEM with 10% FBS) containing anti-rat magnetic beads coated with anti-PECAM-1 antibody (MEC13.3; BD Biosciences, Bedford, MA) as previously described (139). The cells and beads were incubated at 4^{o}C for 1h with continuous mixing. After affinity binding, magnetic beads were washed six times with DMEM with 10% FBS. The bound cells were plated into a single well of a 24-well plate coated with 2 μg/ml of human fibronectin (BD Biosciences) using 0.5 ml of EC growth medium. The EC growth medium is DMEM containing 10% FBS, 2 mM L-glutamine, 2 mM sodium pyruvate, 20 mM HEPES, 1% nonessential amino acids, 100 μg/ml streptomycin, 100 U/ml penicillin, freshly

added heparin at 55 U/ml (Sigma), 100 μg/ml endothelial growth supplement (Sigma), and murine recombinant interferon-γ (R&D Systems, Minneapolis, MN) at 44 U/ml. Cells were incubated at 33 ℃ with 5% CO_2 and progressively passaged to larger plates. Cells were normally maintained in 60-mm dishes coated with 1% gelatin prepared in phosphate buffered saline (PBS). The majority of experiments described here were performed with two separate isolations of cells and repeated twice.

RNA purification and real time qPCR analysis. The total RNA from PEDF +/+ and PEDF -/- EC was extracted using mirVana PARIS kit (Invitrogen, Carlsbad, CA). To extract total RNA from lung tissue, lung was removed from postnatal *day 28* (P28) PEDF +/+ and PEDF -/- mice. Total RNA was extracted from lung tissue using using mirVana PARIS kit (Invitrogen). cDNA synthesis was performed from 1 μg of total RNA using Sprint RT Complete-Double PrePrimed kit (Clontech, Mountain View, CA). 1 μl of each cDNA (dilution 1:10) was used as template in qPCR assays, performed in triplicate of three biological replicates on Mastercycler Realplex (Eppendorf) using the SYBR-Green qPCR Premix (Clontech). Amplification parameters were as follows: 95 ℃ for 2min; 40 cycles of amplification (95 ℃ for 15 sec, 60 ℃ for 40 sec); dissociation curve step (95 ℃ for 15 sec, 60 ℃ for 15 sec, 95 ℃ for 15 sec). Primer sequences for PEDF were 5'-GCCCAGATGAAAGGGAAGATT-3' (forward) and 5'-GAGGGCACTGGGCATTT-3' (reverse). For IL-1β, 5'-GTTCCCATTAGACAACTGCACTACA-3' (forward), and 5'-CCGACAGCACGAGGCTTTT-3' (reverse); For MCP-1, 5′-GTCTGTGCTGACCCCAAGAAG-3′ (forward), and 5′-TGGTTCCGATCCAGGTTTTTA-3′ (reverse). Standard curves were generated from known quantities for each of the target gene of

linearized plasmid DNA. Ten times dilution series were used for each known target, which were amplified using SYBR-Green qPCR. The linear regression line for ng of DNA was determined from relative fluorescent units (RFU) at a threshold fluorescence value (Ct) to quantify gene targets from cell extracts by comparing the RFU at the Ct to the standard curve, normalized by the simultaneous amplification of RpL13a, a housekeeping gene. Primer sequences for RpL13a were 5'-TCTCAAGGTTGTTCGGCTGAA-3' (forward) and 5'-CCAGACGCCCCAGGTA-3' (reverse).

Cell Proliferation and Apoptosis. For cell proliferation assays, cells (1×10^4) were plated in triplicate in multiple sets of 60-mm tissue culture plates. Cells were fed every other day for two weeks, and the cell numbers were determined on the days not fed in triplicates using a hematocytometer. Apoptotic cell death was determined by TdT-dUTP Terminal Nick-End Labeling (TUNEL) staining. TUNEL staining was performed using Click-iT TUNEL as recommended by the supplier (Invitrogen). Positive cells were counted using a fluorescence microscope and reported as a percentage of apoptotic cells. The rate of DNA synthesis was measured using Click-iT™ EdU Alexa Fluor 488 kit as recommended by the supplier (Invitrogen). The assay measures incorporation of 5-ethynyl-2'-deoxyuridine (EdU), a nucleoside analogue of thymidine, during cell proliferation. PEDF +/+ and PEDF -/- lung EC were plated at $5x10^5$ cells on 60 mm tissue culture dishes and were incubated with 10 μM EdU in PC medium for 1 h at 33 ℃. DNA synthesis was analyzed by measuring incorporated EdU using the FACSscan Caliber flow cytometer (Becton-Dickinson, Franklin Lakes, NJ). Ten thousand

cells were analyzed for each sample and three independent experiments were performed with two different isolation of EC.

Indirect Immunofluorescence Staining. Lung EC (1 x10^5) were plated on glass coverslips coated with 2 μg/ml of fibronectin. The next day, cells were rinsed with PBS, fixed with 3% paraformaldehyde (PFA) for 10 min on ice, washed twice with PBS. Cells were incubated in PBS containing 0.25% Triton X-100 for 15 minutes at room temperature for permeabilization. After washing cells with TBS twice, cells were incubated with anti-vinculin (1:100; Sigma), FITC-phallodin (1:200; Sigma), and DAPI (Invitrogen, D1306; 10 μg/ml) for 40 min at 37°C. Anti-VE-cadherin (Santa Cruz Biotechnology, Santa Cruz, CA) and β-catenin (BD Biosciences) were also used. After washing three times with PBS, cells were incubated with appropriate CY3-conjugated secondary antibodies (Jackson ImmunoResearch, West Grove, PA) at 37 ℃ for 40 min. Cells were washed three times with PBS, mounted, and photographed using a Zeiss fluorescence microscope (Axiophot, Zeiss, Germany) equipped with a digital camera.

Scratch Wound Assays. Cells (4 ×10^5) were plated on 60-mm tissue culture dishes and allowed to reach confluence (2–3 days). After aspirating the medium, cell layers were wounded using a 1-ml micropipette tip. Plates were then rinsed with PBS fed with growth medium containing 5-FU (100 ng/ml, Sigma) to exclude the potential contribution of differences in cell proliferation. The wounds were photographed at 0, 24 and 48 hour. The distance migrated as percent of total distance was determined by taking five equally spaced measurements at time 0 and at each subsequent time point for each wound and calculating the distance migrated as a percent of the

total wounded area. Each sample was performed in triplicate on at least three independent occasions using two different isolations of EC, with similar results.

Transwell Migration Assays. Transwell filters (Costar 3422) were coated with 2 μg/ml of fibronectin in PBS overnight at 4 ℃, rinsed with PBS, and then blocked with 2% BSA for 1h at room temperature. Serum-free DMEM (0.5 ml) was added to a well of 24-well plate and the Transwell was inserted into each well. Cells (1×10^5) in 100 μl of serum free-medium were added to the top of each Transwell membrane and incubated for 3 h at 37 ℃ in a tissue culture incubator. Following incubation, the medium was aspirated and the upper side of the membrane wiped with a cotton swab. The cells that had migrated through the membrane were fixed with 4% paraformaldehyde and stained with hematoxylin and eosin. Ten high power fields (x200) were counted for each condition and the average number of cells migrated per field was determined.

Capillary Morphogenesis Assay. Tissue culture plates (35 mm) were coated with 0.5 ml of Matrigel (10 mg/ml; BD Biosciences) and allowed to harden at 37 ℃ for at least 30 min. Cells were removed by trypsin-EDTA, washed with DMEM containing 10% FBS, and resuspended at 2×10^5 cells/ml in EC growth medium without serum. Cells (2×10^5) in 2 ml were applied to the Matrigel-coated plates, incubated at 33 ℃, photographed after 18 h with a Nikon microscope in digital format. For quantitative assessment of the data, the mean numbers of branch points were determined by counting the number of branch points in five high-power fields (×100). Longer incubation times did not further improve the degree of capillary morphogenesis.

Cell Adhesion Assays. Various concentrations of fibronectin, vitronectin, collagen type I, and Collagen type IV (BD BioSciences) prepared in TBS (Tris Buffered Saline, 20mM Tris-HCl, 150mM NaCl, pH 7.4,) with Ca^{2+} and Mg^{2+} (2 mM each; TBS with Ca^{2+}/Mg^{2+}) were coated on 96-well plates (50 µl/well; Nunc Maxisorbe plates, Fisher Scientific) overnight at 4°C. Plates were rinsed four times with 200 µl of TBS with Ca/Mg and blocked with 200 µl of 1% BSA prepared in TBS with Ca/Mg for at least 1 h at room temperature. Cells were prepared using 2 ml of cell dissociation solution (Sigma), washed with TBS, and resuspended at 5×10^5 cells/ml in freshly prepared HBS (20 mM HEPES, 150 mM NaCl, pH 7.6, and 4 mg/ml BSA). After blocking, plates were rinsed with TBS with Ca/Mg once, and 50 µl of cell suspension was added to each well containing 50 µl of TBS with Ca/Mg. The cells were allowed to adhere to the plate for 2 h at 37 ℃. The non-adherent cells were removed by gently washing the plate four times with TBS containing Ca/Mg until no cells left in wells coated with BSA. The number of adherent cells in each well was quantified by measuring the cellular phosphatase activity as previously described (182). All samples were done in triplicates.

FACScan Analysis. Monolayers of lung EC on 60-mm tissue culture dishes were washed once with PBS containing 0.04% EDTA and incubated with 2 ml of non-enzymatic cell dissociation solution (Sigma). Cells were removed from the dish, washed with PBS, fixed with 2% paraformaldehyde on ice for 30 min and washed with PBS. Cells were pelleted, resuspended in 0.5 ml of TBS with 1% BSA containing an appropriate dilution of primary antibodies, as recommended by the supplier, and incubated on ice for 30 min. For vascular EC markers, cells were incubated with anti-PECAM-1, anti-endoglin, anti-ICAM-2 (BD Biosciences), anti-VE-cadherin (Enzo Life Sciences), anti-ICAM-1 (Santa Cruz), anti-VCAM-1 (Millipore), anti-VEGF

receptors (VEGFR1 and VEGFR2; R&D Systems), or FITC-conjugated B4 lectin (Sigma). For integrin expression analysis, anti-α_1-integrin (BD Biosciences), anti- α_2-, α_{3-}, α_5-, α_6-, α_7, β1, β8-integrin (Santa Cruz) and $\alpha_v\beta_3$-integrin (Millipore) antibodies were used. The cells were washed with TBS containing 1% BSA and then incubated with the appropriate secondary antibody (1:200) on ice for 30 min. After the incubation, the cells were washed twice with TBS containing 1% bovine serum albumin (BSA) and resuspended in 0.5 ml of TBS containing 1% BSA. FACScan analysis was performed on a FACScaliber flow cytometer (Becton-Dickinson, Franklin Lakes, NJ).

Western Blot Analysis. Cells (6×10^5) were plated in 60-mm tissue culture dishes and incubated until it reaches about 90% confluence (2-3 days). The cells were then rinsed once with serum-free DMEM and incubated in EC growth medium without serum for 2 days. Conditioned medium (CM) was collected and centrifuged to remove cell debris. The cells were also lysed in 0.1 ml of lysis buffer [50 mM HEPES pH 7.5, 100 mM NaCl, 0.1 mM EDTA, 1mM $CaCl_2$, and 1 mM $MgCl_2$, with 1% Triton X-100, 1% NP-40, and protease and phosphatase inhibitor cocktail (Thermo Scientific, Rockford, IL)]. For lysate from lung tissue, lung was removed from postnatal day 28 (P28) PEDF +/+ and PEDF -/- mice. Lung tissue was rinsed with TBS and lysed in 1ml of lysis buffer. Protein concentrations were determined using BCA protein assay (Bio-Rad, Hercules, CA). Samples were adjusted for protein content, mixed with an appropriate volume of 6 × SDS-sample buffers, and analyzed by SDS-PAGE (4–20% Tris-Glycine gels, Invitrogen). Proteins were transferred to nitrocellulose membrane, and the membrane was blocked with blocking buffer (0.05% Tween 20 and 5% skim milk in TBS). For phospho-eNOS, the membrane was blocked in 5% BSA in TBS buffer containing 0.05% Tween 20 (TBST). The

following primary antibodies were used: Anti-tenacin-C (Millipore), fibronectin and eNOS (Santa Cruz), osteopontin and SPARC (R&D Systems), thrombospondin-1 (A6.1, Neo Markers, Fremont, CA), phospho-eNOS (Ser 1177), (Cell Signaling, Danvers, MA), β-catenin, iNOS, nNOS and TSP2 (BD Biosciences), ZO-1 and occludin (Invitrogen), F4/80(eBioscience, San Diego, CA) and MFG-E8 (R&D Systems). Primary antibodies were diluted in blocking buffer (as recommended by the supplier) and incubated with the membrane overnight at 4℃. Blots were washed with TBST and incubated with appropriate secondary horseradish peroxidase-conjugated antibody. The blots were then washed with TBST and developed by enhanced chemiluminescence method (GE Healthcare, UK). The blot was stripped and incubated with anti-β-actin (Sigma) antibody for loading control.

PEDF expression. The lenti viruses expressing GFP or PEDF were obtained from Dr. Olga Volpert (Northwestern University). For transduction of PEDF -/- lung EC, lenti viruese at multiplicity of infection (MOI) of 20 or 40 were added to the culture medium in the presence of 8 μg/ml of polybrene (Sigma) for overnight. The next day medium was removed and cells were fed with fresh medium. After 72h, PEDF level was determined by Western blot analysis.

Analysis of VEGF Levels. VEGF protein levels produced by PEDF +/+ and PEDF -/- EC were determined using a Mouse VEGF Immunoassay kit (R&D Systems). Cells were plated at $6x10^5$ cells on 60-mm tissue culture dishes and allowed to reach approximately 90% confluence. The cells were then rinsed once with serum-free DMEM and were grown in serum-free medium for 2 days. Conditioned medium was centrifuged at 400 x*g* for 5 min to remove cell debris, and 50 μl was used in the VEGF Immunoassay. The assay was performed in triplicates as recommended by

the manufacturer and was normalized to the number of cells. The amount of VEGF was determined using a standard curve generated with known amounts of VEGF in the same experiment. These experiments were repeated three times with two different isolations of cells.

Analysis of Nitric Oxide Levels. Lung EC (5×10^3 cells in 100 μl per well) were plated on black wall clear bottom 96-well plates to measure nitric oxide level and cell number. The next morning, the medium was changed to EC medium containing 30 μM DAF-FM diacetate (Invitrogen; D-23842). Following 40-min incubation at 33 ℃, the medium was replaced with fresh EC medium, and the incubation continued for 20 min. The wells were washed with TBS, each well was resuspended in 100 μl of TBS, and the absorbance was read at 495/515 nm in triplicates and repeated twice with similar results. The number of viable cells in each well was measured by a colorimetric determination at 490 nm using CellTiter 96 Aqueous Non-Radioactive Cell proliferation assay (Promega, Madison, WI).

Processing of Lungs for Histological Studies and Immunohistochemistry. Lungs from postnatal *day 28* (P28) PEDF +/+ and PEDF -/- mice were removed, inflated and fixed with formalin overnight, and processed for paraffin sectioning. Sections (5 μm each) were placed on slides, and some slides were stained with movat pentachrome. Four PEDF +/+ and PEDF -/- mice were sacrificed and two sections were prepared from each mouse. Pictures of randomly selected pulmonary arterial and venule in matched regions of slides were taken in eight different high power fields (x200). Areas of inner and outer vessel were measured using Image J software (NIH; http://rsb.info.nih.gov/ij). Vessel thickness was calculated by subtracting the area of inner vessel from the area of outer vessel. For immunohistochemical staining, four PEDF +/+ and

PEDF -/- mice were sacrificed and multiple sections from same regions per each mouse were examined. Paraffin sections were deparaffinized with xylene and rehydrated. Antigen unmasking was performed using antigen-unmasking solution (Vector Laboratories, Burlingame, CA) according to the manufacturer's instructions. The sections were then washed in PBS and incubated for 15 min in PBS blocking buffer (PBS containing 1% BSA, 0.3% Triton X-100, and 0.2% skim milk powder). The sections were incubated overnight with anti-PECAM-1 (1:150; R&D Systems). The sections were then incubated with indocarbocyanine (CY3)-labeled secondary antibody (Jackson ImmunoResearch) and photographed. The intensity of signal was determined by measuring the area of fluorescence via Image J and the ratio of vascular area was determined via AngitoTool (239), using equal-timed exposures of four high-power fields (×400).

Statistical Analysis. Statistical differences between two groups were evaluated with Student's unpaired *t*-test (2-tailed). Mean values ± SE are shown. $p<0.05$ is considered significant.

Results

Isolation and characterization of lung EC from PEDF +/+ and PEDF -/- mice. Figure 1A shows the morphology of EC prepared from PEDF +/+ and PEDF -/- immortomice. PEDF +/+ EC showed more elongated and spindly morphology compared with PEDF -/- EC when plated on gelatin-coated plates. Next, we determined mRNA expression level of PEDF in both PEDF +/+ and PEDF -/- EC by real time qPCR analysis. In PEDF +/+ EC, mRNA of PEDF was expressed, whereas not expressed in PEDF -/- EC as expected (Figure 1B). We also determined the levels of PEDF secreted by PEDF +/+ and PEDF -/- EC. In conditioned medium from PEDF +/+ EC, PEDF was detected by Western blot analysis, but not detected in conditioned medium from PEDF -/- EC as expected (Figure 1C). We measured expression levels of EC markers to confirm that these cells maintain their EC characteristics (Figure 1D). PEDF +/+ and PEDF -/- EC exhibited similar level of VE-cadherin expression, while endoglin and B4-lectin levels were lower in PEDF -/- EC compared to PEDF +/+ cells. PECAM-1 expression was also lower in PEDF -/- EC compared to PEDF +/+ EC (Figure 1D). Furthermore, we determined the expression level of ICAM-1 and ICAM-2 by FACS analysis. PEDF +/+ and PEDF -/- cell showed similar level of ICAM-1 and ICAM-2 expression (Figure 2A). However, the level of VCAM-1 in PEDF -/- EC was higher than in PEDF +/+ EC (Figure 2A). We also measured expression levels of VEGFR1 and VEGFR2 in both cell types. Expression levels of VEGFR1 and VEGFR2 were similar in PEDF +/+ and PEDF -/- EC (Figure 2A). However, PEDF -/- EC secreted four times more VEGF compared with PEDF +/+ EC (Figure 2B).

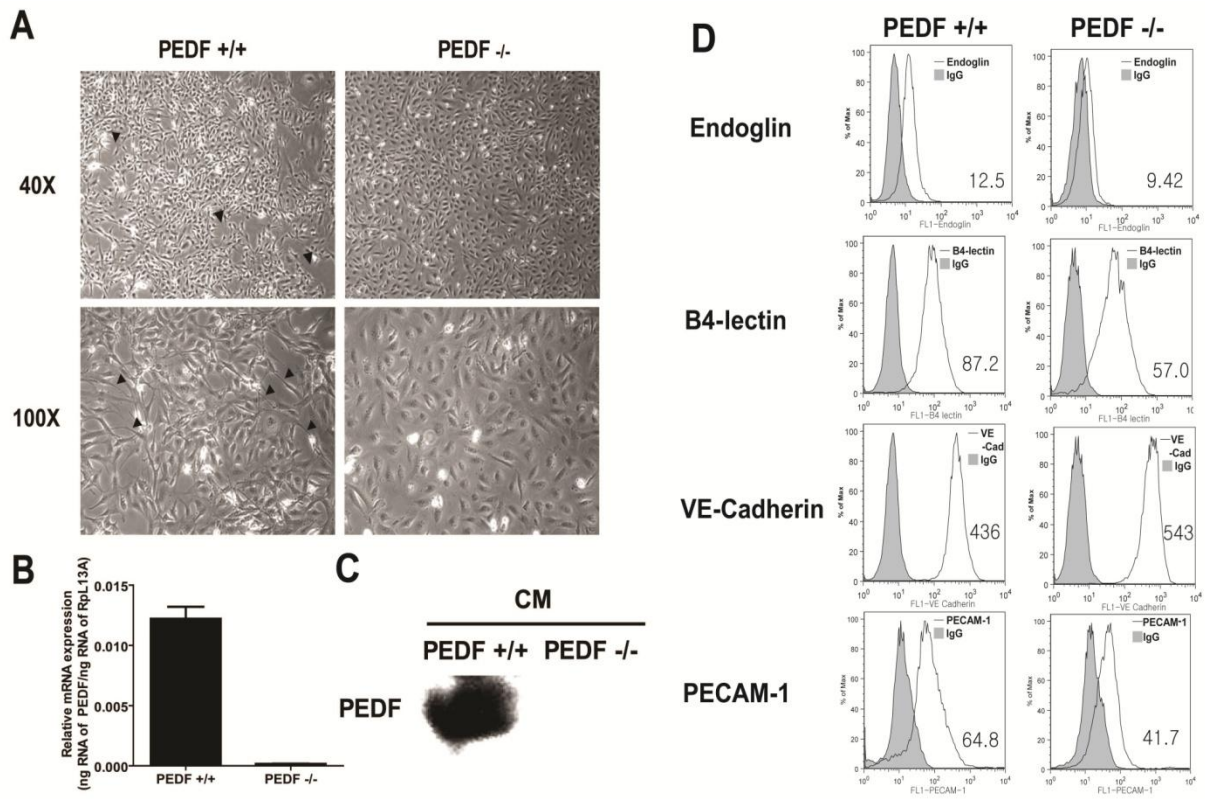

Appendix Figure 1. Isolation and characterization of mouse lung microvascular endothelial cells (EC).

A: PEDF +/+ and PEDF -/- lung EC cultured on gelatin-coated plates. Cells were photographed using a phase microscope in digital format at low magnification (top; ×40) and high magnification (bottom; ×100). Please note the elongated, spindly morphology of PEDF +/+ cells compared with PEDF -/- cells (arrows). B: mRNA expression of PEDF in lung EC prepared from PEDF +/+ and PEDF −/− mice. Three independent experiments were performed with triplicate samples (n=3, $p<0.05$). C: level of PEDF in conditioned medium collected from lung EC. PEDF +/+ lung EC secreted PEDF in conditioned medium, whereas PEDF -/- lung EC did not. D: lung EC prepared from PEDF +/+ and PEDF −/− mice were examined for expression of endoglin, B4-lectin, VE-cadherin and PECAM-1 by FACScan analysis. The shaded areas show staining in the

presence of control IgG. The geometric mean values are shown in the bottom corner of each graph. Similar results were observed with another isolation of EC.

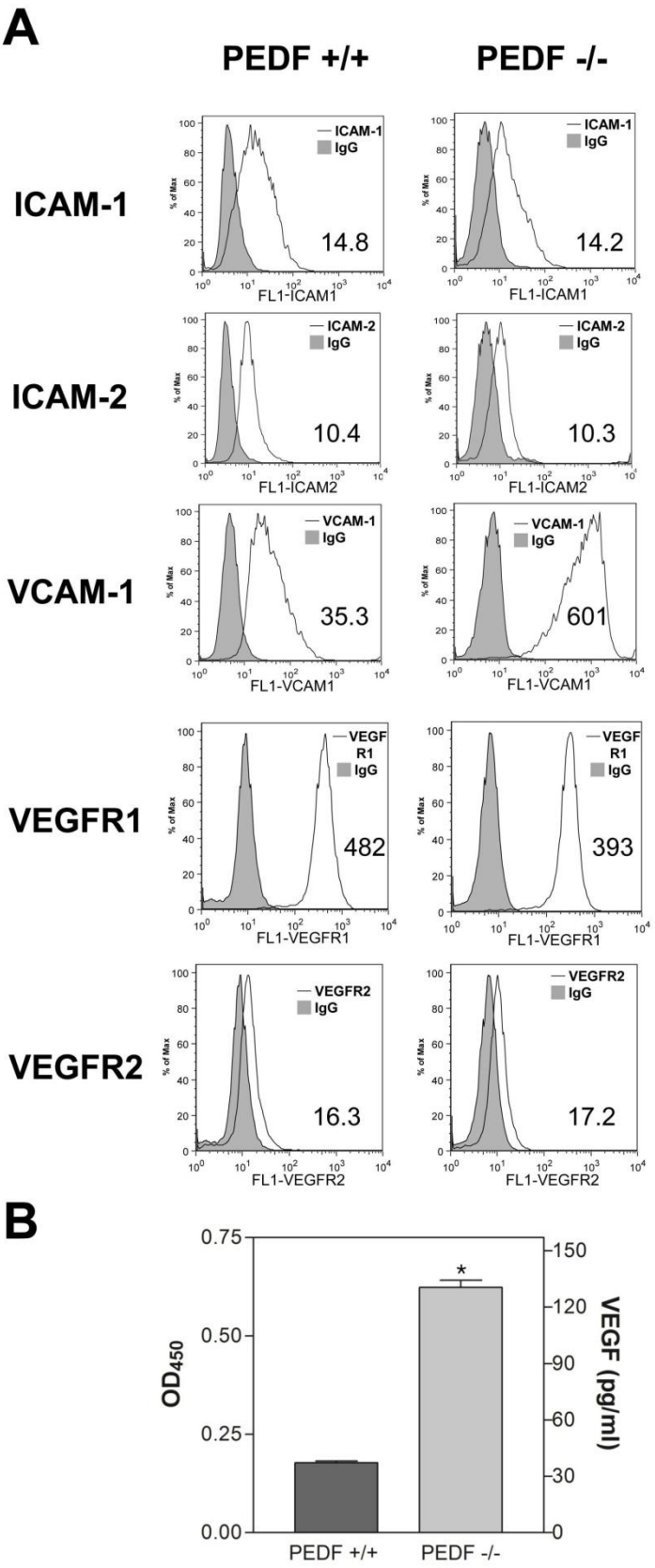
A
PEDF +/+
PEDF -/-
ICAM-1
ICAM-2
VCAM-1
VEGFR1
VEGFR2
ICAM-1
IgG
14.8
14.2
FL1-ICAM1
ICAM-2
10.4
10.3
FL1-ICAM2
VCAM-1
35.3
601
FL1-VCAM1
VEGF R1
482
393
FL1-VEGFR1
VEGFR2
16.3
17.2
FL1-VEGFR2
% of Max
B
OD450
VEGF (pg/ml)
0.75
0.50
0.25
0.00
150
120
90
60
30
0
*
PEDF +/+
PEDF -/-

Appendix Figure 2. Expression of EC markers and production of VEGF in lung EC.

A: The expression of ICAM-1, ICAM-2, VCAM-1, VEGFR1 and VEGFR2. Expression level was determined by FACS analysis using specific antibodies. Shaded areas show control IgG staining. The geometric mean values are shown in the bottom corner of each graph. B: Production of VEGF in PEDF +/+ and PEDF -/- Lung EC. Level of VEGF was determined using an ELISA method ($n=3, *p < 0.05$).

PEDF -/- lung EC are more migratory. Migratory activity of EC is crucial during angiogenesis and generally suppressed in the presence of endogenous inhibitors of angiogenesis including PEDF. We next asked whether lack of PEDF impacts the migration of EC. Confluent monolayers of PEDF +/+ and PEDF -/- EC were wounded and wound closure was monitored over time. A significant wound closure was observed in PEDF -/- EC after 72 h whereas wounds in PEDF +/+ EC were not completely closed (Figure 3A). The quantification of wound closure is shown in Figure 3B. Similar results were observed in transwell migration assays (Figure 3C). The enhanced migratory activity of PEDF -/- EC was further confirmed by examining the organization of actin and focal adhesions. More actin stress fibers and fewer focal adhesions were visible in PEDF -/- EC compared with PEDF +/+ EC (Figure 3D).

PEDF -/- EC grow at a slower rate. The impact of PEDF deficiency on proliferation of EC was determined by counting the number of cells for two weeks. Figure 4A shows a significant decrease in the growth of PEDF -/- EC compared with PEDF +/+ EC. To examine whether the decreased growth in PEDF -/- EC was due to a decrease in the rate of DNA synthesis, the percentage of cells undergoing active DNA synthesis was determined by measuring the percentage of EdU positive cells by FACS analysis. PEDF -/- EC showed decreased rate of DNA synthesis compared with PEDF +/+ EC (Figure 4B). The effect of PEDF deficiency on apoptosis of EC was also examined by TUNEL assay. PEDF -/- EC exhibited similar level of apoptosis compared with PEDF +/+ EC. When EC were challenged with H_2O_2 there was no significant difference in apoptosis rate between the two cell types (Figure 4C). Similar results were also observed by examining the level of cleaved caspase-3 (not shown).

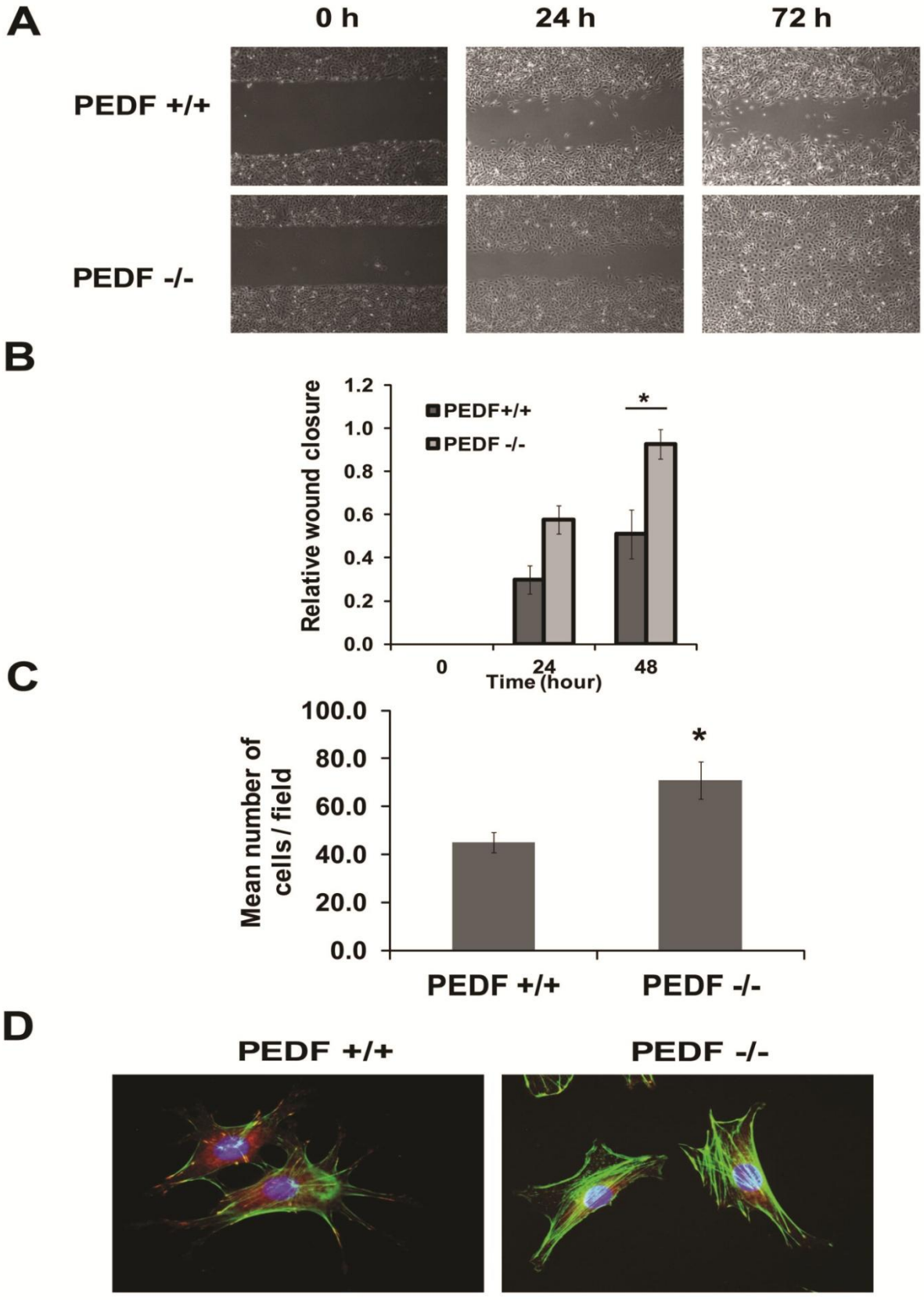
A
0 h
24 h
72 h
PEDF +/+
PEDF -/-
B
Relative wound closure
1.2
1.0
0.8
0.6
0.4
0.2
0.0
PEDF+/+
PEDF -/-
*
0
24
48
Time (hour)
C
Mean number of cells / field
100.0
80.0
60.0
40.0
20.0
0.0
*
PEDF +/+
PEDF -/-
D
PEDF +/+
PEDF -/-

Appendix Figure 3. The impact of PEDF-deficiency on the migration and formation of actin stress fibers and focal adhesions in lung EC.

A: Cell migration was determined by scratch wounding of a lung EC monolayer, and wound closure was monitored by photography. A representative experiment is shown. B: The quantitative assessment of the data in A (n=3,*p< 0.05). C: Transwell migration of lung EC. Please note that the PEDF -/- lung EC were significantly more migratory compared with PEDF +/+ cells (n=3,*p< 0.05). *D*: Examination of actin stress fibers and focal adhesions in lung EC. Lung EC were stained with anti-vinculin, phalloidin, and DAPI (×630). Please note reduced number of focal adhesions and increased actin stress fibers in PEDF -/- EC.

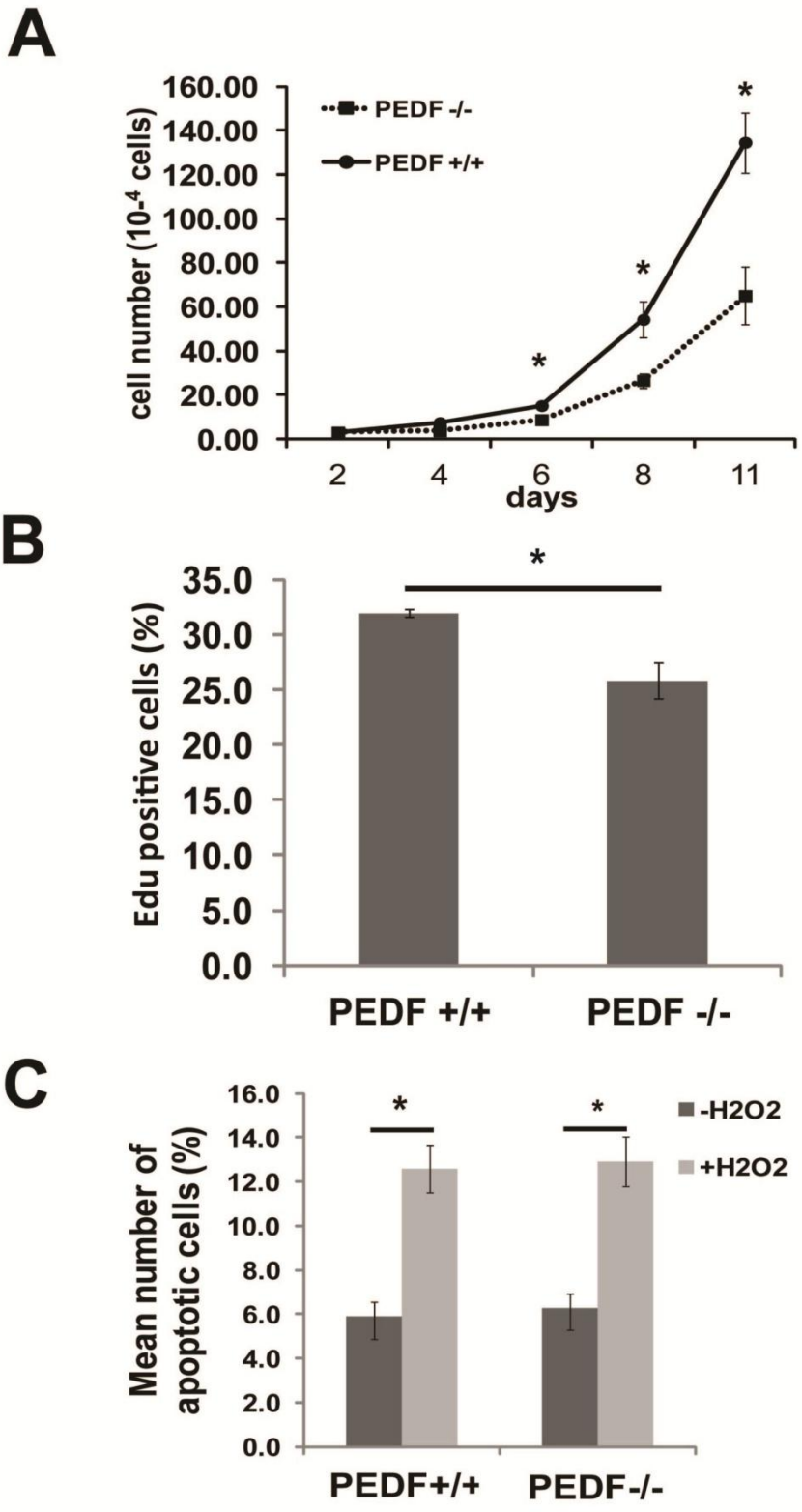
A
160.00
140.00
120.00
100.00
80.00
60.00
40.00
20.00
0.00
cell number (10-4 cells)
PEDF -/-
PEDF +/+
*
*
*
2
4
6
8
11
days
B
35.0
30.0
25.0
20.0
15.0
10.0
5.0
0.0
Edu positive cells (%)
*
PEDF +/+
PEDF -/-
C
16.0
14.0
12.0
10.0
8.0
6.0
4.0
2.0
0.0
Mean number of apoptotic cells (%)
*
*
-H2O2
+H2O2
PEDF+/+
PEDF-/-

Appendix Figure 4. The effect of PEDF deficiency on proliferation and apoptosis of lung EC. A and B: The rate of EC proliferation was determined by counting the number of cells in triplicates after different days in culture (A) and by analyzing the rate of DNA synthesis by FACScan flow cytometer analysis (A and B; *$p < 0.05$; $n = 3$). EdU is 5-ethynyl-2′-deoxyuridine. *C*: The rate of apoptosis was determined by TdT-dUTP Terminal Nick-End Labeling (TUNEL) staining. Positive cells were counted using a fluorescence microscope and calculated as percentage of total cell number per field. As an apoptotic stimulus, H_2O_2 in EC growth medium was added for 24 h (*$p<0.05$; $n=3$).

Attenuation of Capillary morphogenesis in PEDF -/- lung EC. EC undergo capillary morphogenesis when plated in Matrigel, which is a crucial feature of angiogenesis. PEDF +/+ EC exhibited well-organized capillary-like networks in Matrigel, whereas PEDF -/- EC failed to undergo capillary morphogenesis (Figure 5A). The quantification of the data is shown in Figure 5B.

PEDF -/- EC are more adherent. Alterations in migration of PEDF -/- EC implied that the deficiency in PEDF may affect adhesion of EC. We next investigated adhesion of PEDF +/+ and PEDF -/- EC to various extracellular matrix (ECM) proteins including collagen I, collagen IV, fibronectin and vitronectin. PEDF -/- EC adhered more strongly to collagen IV, fibronectin and vitronectin compared to PEDF +/+ EC. Neither PEDF +/+ nor PEDF -/- cells adhered to collagen I (Figure 6). Thus, PEDF deficiency had a significant impact on interaction of lung EC with various ECM proteins. These results suggested that lack of PEDF may affect expression levels and/or activity levels of various cell surface integrins involved in adhesion and migration. Expression levels of various integrins were determined by FACScan analysis (Figure 7). PEDF -/- EC expressed decreased levels of α3, α7 and αvβ3 integrins. PEDF +/+ and PEDF -/- EC expressed similar levels of α1-, α2-, α5-, α6-, β1- and β8- integrins. The mean fluorescence intensities are shown in each panel.

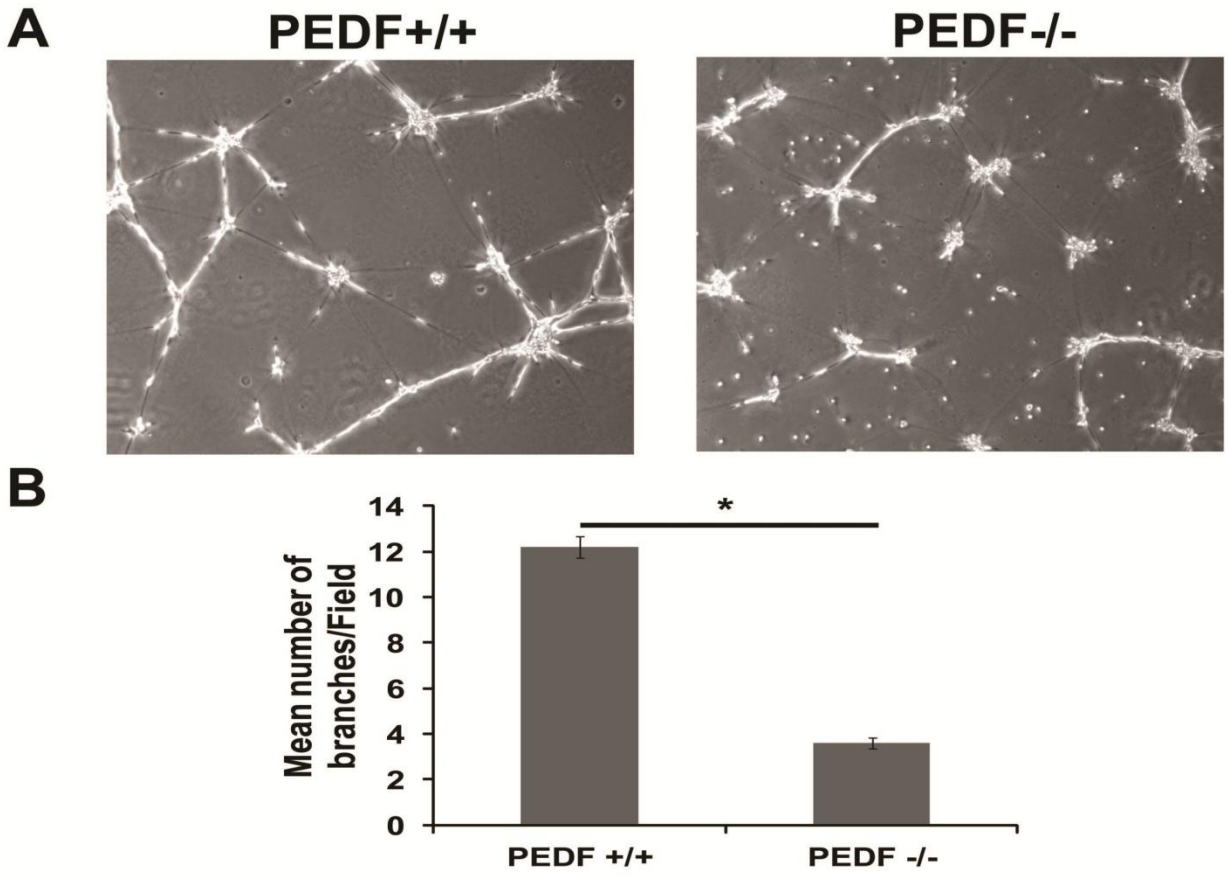

Appendix Figure 5. PEDF -/- lung EC fail to undergo capillary morphogenesis.

A: PEDF +/+ and PEDF -/- lung EC were plated in Matrigel and photographed in digital format. The quantitative assessment of the data is shown in B. Data are the mean number of branch points from 5 high-power fields (×100) ± SE. (*$p<0.05$; n=5).

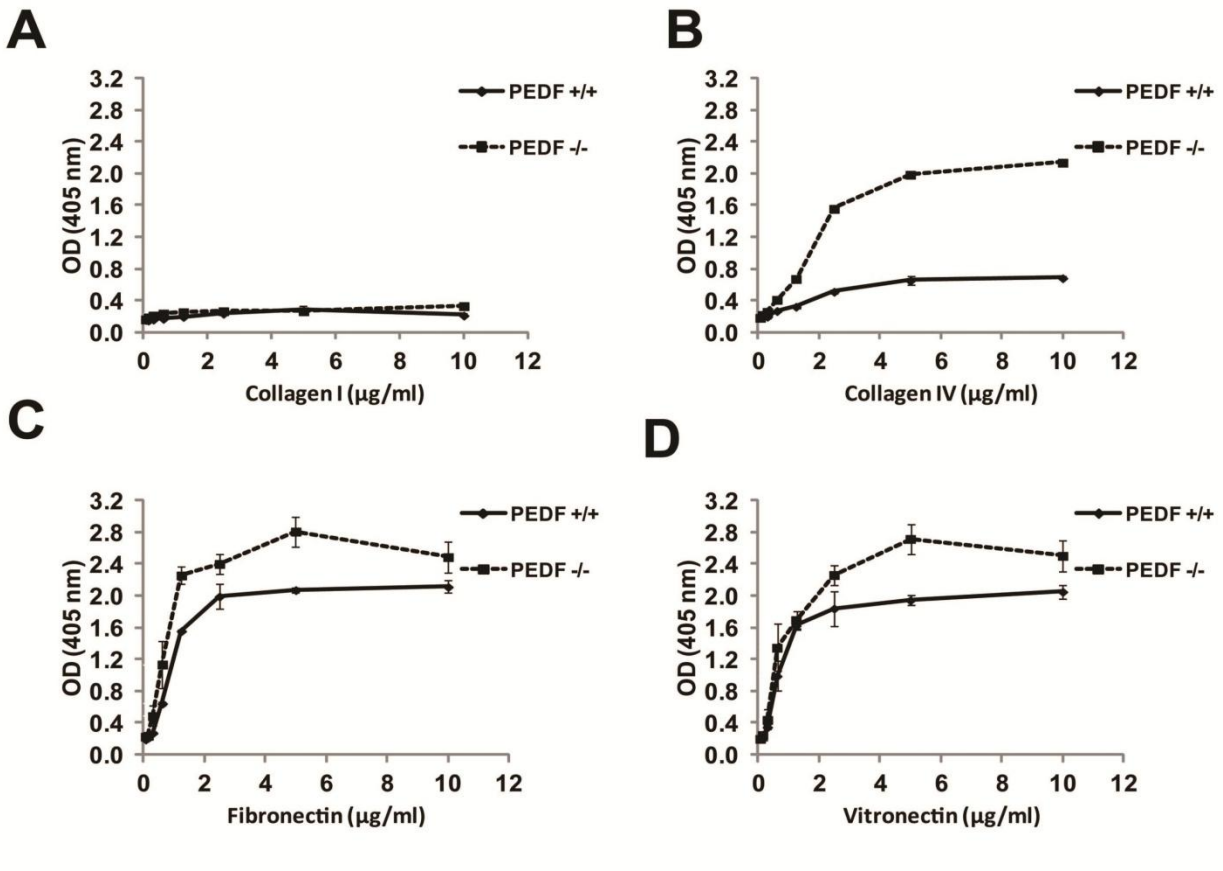

Appendix Figure 6. PEDF -/- lung EC exhibited enhanced adhesion to various extracellular matrix (ECM) proteins.

Adhesion of lung EC to collagen I (A), collagen IV(B), fibronectin, (C) and vitronectin (D) was determined by measuring number of adherent cells in each well coated with various concentration of ECM proteins. Number of adherent cells was quantified by measuring the cellular phosphatase activity as described in Methods.

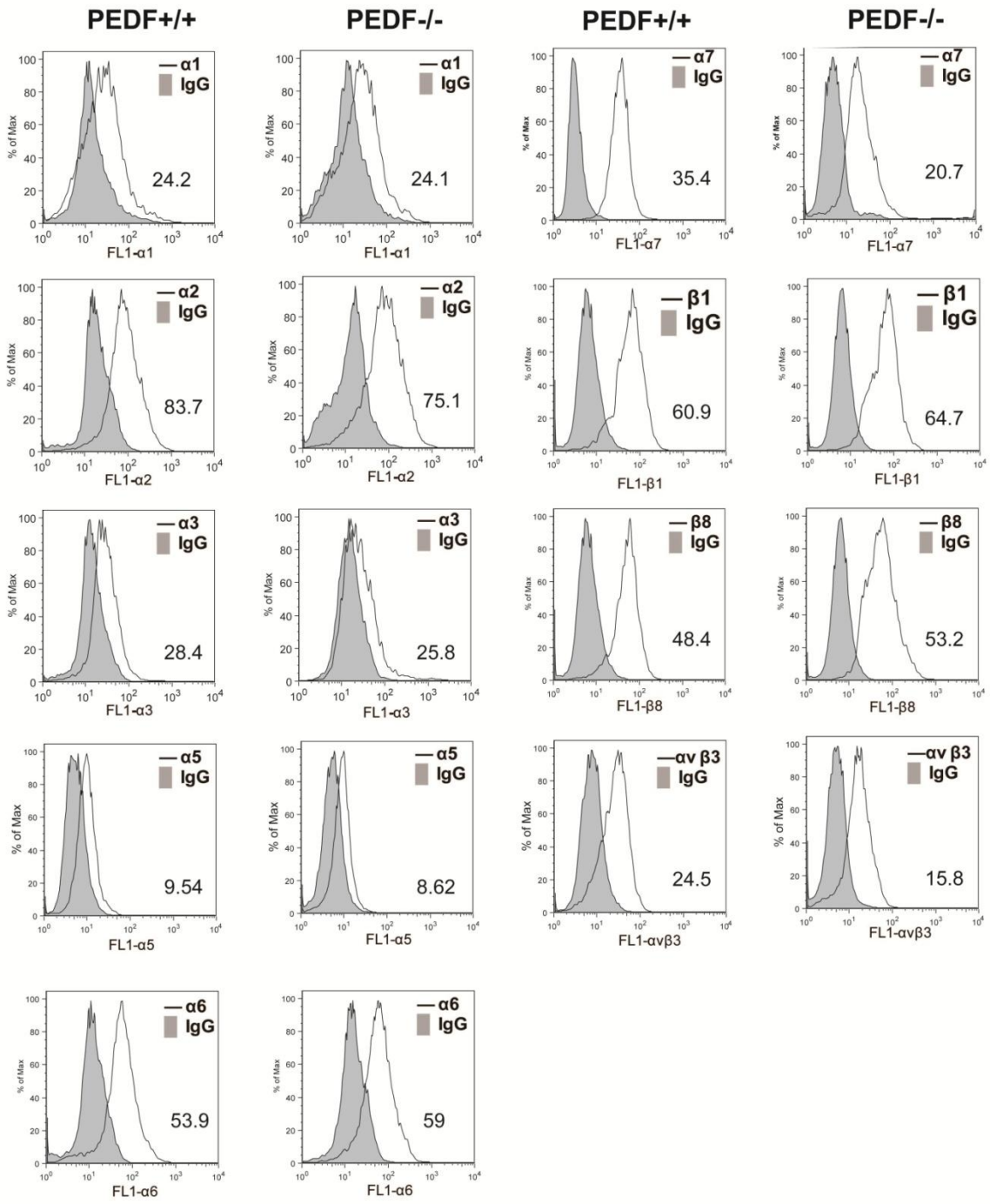
PEDF+/+
PEDF-/-
PEDF+/+
PEDF-/-
α1
IgG
24.2
FL1-α1
α1
IgG
24.1
FL1-α1
α7
IgG
35.4
FL1-α7
α7
IgG
20.7
FL1-α7
α2
IgG
83.7
FL1-α2
α2
IgG
75.1
FL1-α2
β1
IgG
60.9
FL1-β1
β1
IgG
64.7
FL1-β1
α3
IgG
28.4
FL1-α3
α3
IgG
25.8
FL1-α3
β8
IgG
48.4
FL1-β8
β8
IgG
53.2
FL1-β8
α5
IgG
9.54
FL1-α5
α5
IgG
8.62
FL1-α5
αv β3
IgG
24.5
FL1-αvβ3
αv β3
IgG
15.8
FL1-αvβ3
α6
IgG
53.9
FL1-α6
α6
IgG
59
FL1-α6
% of Max

Appendix Figure 7. Expression of integrins in retinal EC.

α1-, α2-, α3-,-α5-, α6-, α7-, β1-, β8- and $\alpha_v\beta_3$-integrin expression on lung EC was determined by FACS analysis . The geometric mean values are shown at the bottom corner of each graph. Similar results were observed using another isolation of EC.

Localization of VE-cadherin and β-catenin. VE-cadherin is a major component of the vascular EC adherens junctions and has a pivotal role in maintaining the integrity of vascular wall (240). VE-cadherin localized at sites of cell-cell contacts in PEDF +/+ EC as expected. However, VE-cadherin exhibited a diffused localization over the whole surface of PEDF -/- EC (Figure 8A). The localization of β-catenin was also examined by immunofluorescence staining in confluent and subconfluent cells. In confluent cells, PEDF +/+ EC showed a more punctate staining pattern compared with PEDF -/- EC. PEDF -/- EC exhibited more intact staining pattern at junction area (Fiugre 8A). In subconfluent cells, PEDF -/- EC exhibited an increase in the level of β-catenin localized in the nucleus. However, a strong nuclear localization of β-catenin was not observed in PEDF +/+ EC (Figure 8B).

The expression of ZO-1, occludin and β-catenin were also determined by Western blot analysis of total cell lysates. Cell lysates were prepared from confluent cells for examining ZO-1, occludin and β-catenin levels. PEDF -/- EC exhibited lower level of ZO-1 compared to PEDF +/+ EC. Although occludin levels were similar in PEDF +/+ and PEDF -/- EC, the size of the protein was different suggesting changes in phosphorylation state. The β-catenin level was increased in PEDF -/- EC compared to PEDF +/+ EC (Figure 8C). The increased expression and nuclear localization of β-catenin in PEDF -/- EC is consistent with activation of the canonical Wnt signaling pathway in the absence of PEDF as previously suggested (241).

We next determined the effect of PEDF re-expresion in PEDF -/- EC. When PEDF was re-expressed in PEDF -/- EC, the expression of level of β-catenin was suppressed (Supplementary figure 1A) compared with PEDF -/- EC transduced with vector control. In addition, junctional localization of β-catenin was examined. β-catenin was similar to PEDF +/+ EC exhibiting more punctate pattern compared with PEDF -/- EC transduced with vector control

(Supplementary figure 1B). Thus, PEDF expression has a significant impact on expression and localization of β-catenin.

Altered production of ECM proteins in PEDF -/- EC. The PEDF-deficiency mediated EC defects may be related to alteration in the synthesis and interactions of ECM proteins. TSP1 is a member of the thrombospondin (TSP) family of matricellular proteins with potent anti-angiogenic and inflammatory activity (222). PEDF -/- EC expressed slightly more TSP1 in their lysate. However, secreted TSP1 in conditioned medium (CM) collected from PEDF -/- EC was not detectable whereas PEDF +/+ EC secreted significant amount of TSP1 in CM (Figure 9). TSP2 is also antiangiogenic and is closely related to TSP1. PEDF -/- EC did not express detectable levels of TSP2 in their lysates or CM (Figure 9). We also determined the expression of other ECM proteins including fibronectin, tenascin-C, osteopontin and SPARC. PEDF -/- EC produced more cell-associated fibronectin than PEDF +/+ EC. However both cell types exhibited similar level of secreted fibronectin in CM. The level of tenascin-C and osteopontin were decreased in PEDF -/- EC compared to PEDF +/+ cells. Although PEDF -/- EC expressed more cell-associated SPARC than PEDF +/+ EC, the level of SPARC in CM of PEDF -/- EC was lower. Thus, overall level of SPARC was not altered by PEDF deficiency (Figure 9).

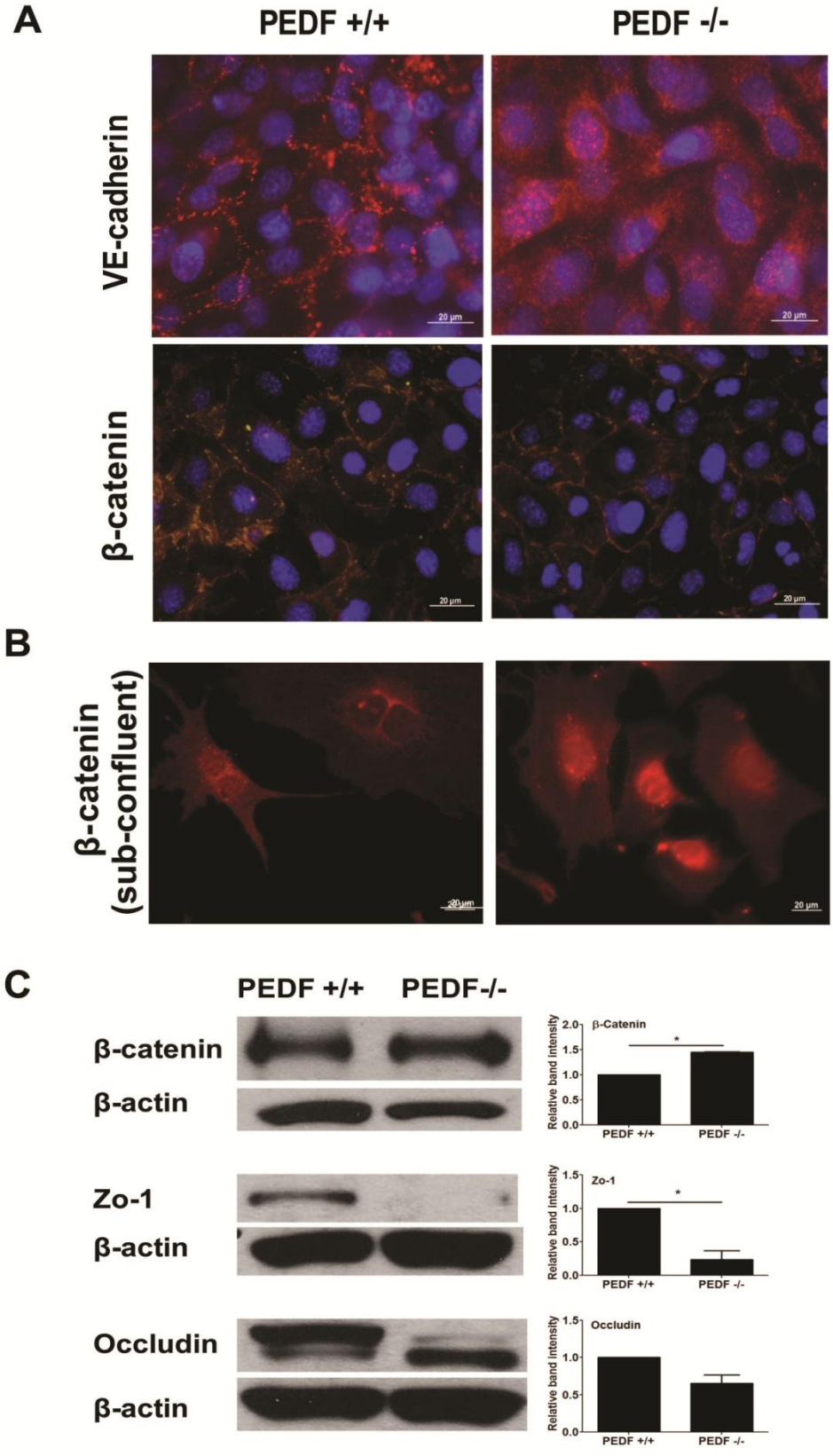
A
PEDF +/+
PEDF -/-
VE-cadherin
β-catenin
20 μm
B
β-catenin
(sub-confluent)
20 μm
C
PEDF +/+
PEDF-/-
β-catenin
β-actin
Zo-1
β-actin
Occludin
β-actin
β-Catenin
Zo-1
Occludin
Relative band intensity
PEDF +/+
PEDF -/-
*

Appendix Figure 8. Cellular localizations and expression of junctional proteins

Cellular localization of VE-cadherin and β-catenin in confluent cells (A) and β-catenin in subconfluent cells (B) were determined. PEDF+/+ and PEDF−/− lung EC were grown on fibronectin-coated chamber slides and stained with specific antibodies and DAPI as outlined in the Methods. Scale bar indicates 20 μm. *C*: Expression levels of β-catenin, ZO-1 and occludin in confluent cells were determined by Western blot analysis. β-actin was used for loading control. Relative band intensity was measured for quantification (*$p < 0.05$; $n = 3$).

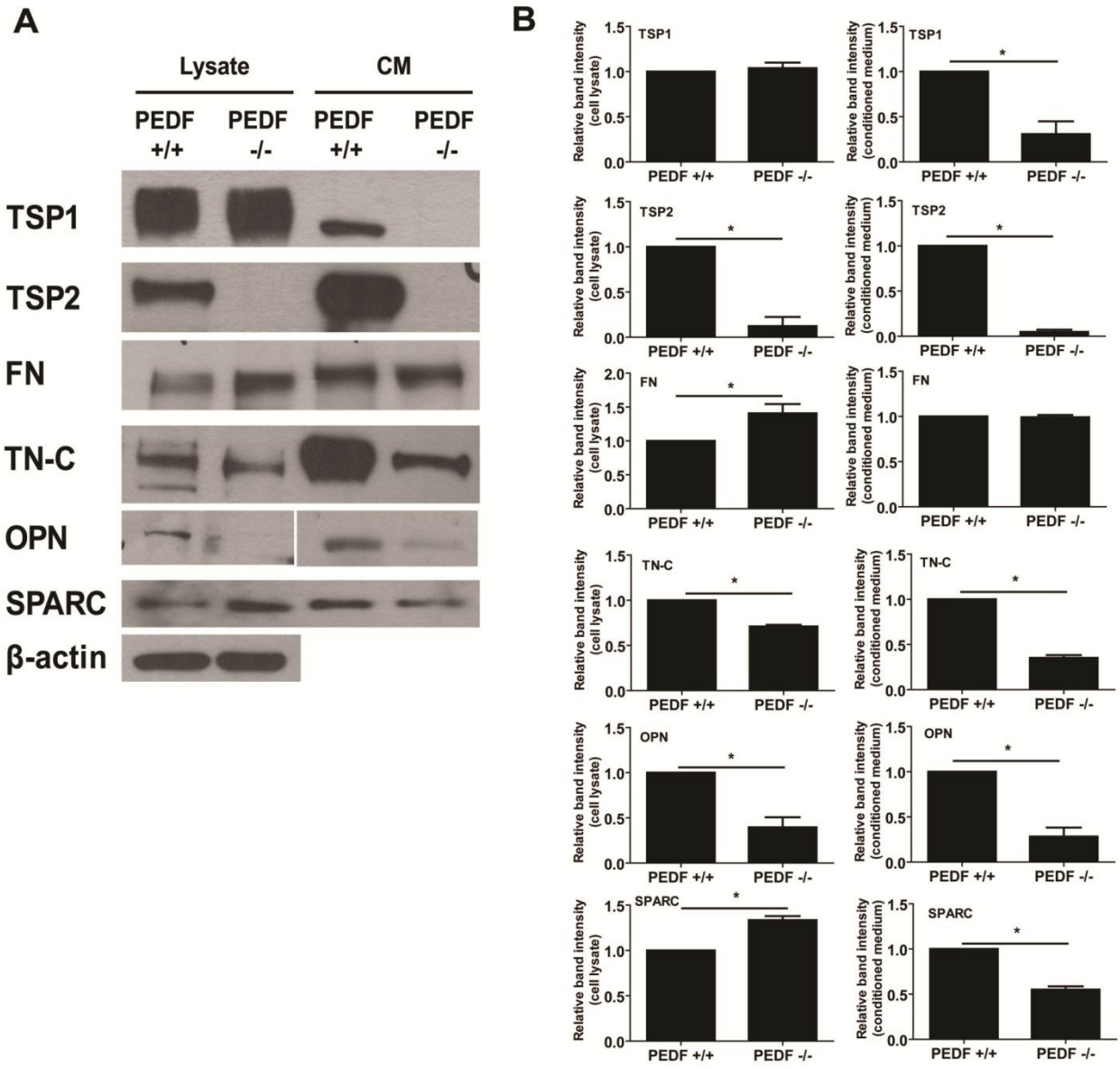

Appendix Figure 9. Altered production of ECM proteins in PEDF-/- EC.

A: Level of ECM proteins in PEDF +/+ and PEDF -/- lung EC was determined by Western blot analysis. The conditioned medium (CM) and cell lysates were analyzed by Western blotting for TSP1, TSP2, fibronectin, tenascin-C, osteopontin, and SPARC using specific antibodies. The β-actin was used for loading control. Quantifications are shown in B. Intensities were measured for quantification (*$p < 0.05$; $n = 3$).

PEDF deficiency impacts expression of nitric oxide synthase and NO production. Nitric oxide is a major player in VEGF-mediated angiogenesis and eNOS is the major source of NO production in the endothelium. Inhibition of eNOS activity attenuates capillary morphogenesis in vitro and VEGF-mediated angiogenesis in vivo (242, 243). Although iNOS is more efficient in NO production, it is generally associated with inflammatory conditions, and it is recognized as a marker of inflammation. We determined the expression and phosphorylation of eNOS in PEDF +/+ and PEDF -/- EC by Western blot analysis. Both cell types expressed similar level of total eNOS. However, phosphorylation of eNOS was significantly decreased in PEDF -/- EC compared to PEDF +/+ EC (Figure 10A). In contrast, the levels of iNOS and nNOS were dramatically increased in PEDF -/- EC (Figure 10A) along with a two-fold increase in NO level compared to PEDF +/+ EC (Figure 10B).

Decreased PECAM-1 expression and enhanced expression of inflammatory markers in the lung of PEDF -/- mice. We examined PECAM-1 expression in lung sections prepared form PEDF +/+ and PEDF -/ mice by immunofluorescence staining. In PEDF -/- lungs, a lower intensity of PECAM-1 staining was detected, consistent with decreased PECAM-1 expression in PEDF -/- lung EC. However, the ratio of vascular area in the lung of PEDF -/- mice was not significantly lower than in lung of PEDF +/+ mice (Figure 11A). Monoclonal antibody for F4/80 was used to detect the cell surface glycoprotein marker of macrophages to access the inflammation status of lungs from PEDF +/+ and PEDF -/- mice (244, 245). In the lung of PEDF -/- mice, expression level of F4/80 was significantly elevated compared with PEDF +/+ mice.

We also examined the expression of milk fat globule epidermal growth factor-8 (MFG-E8) in lungs from PEDF +/+ and PEDF -/- mice. In lungs of mice with acute lung injury, MFG-

E8 level is decreased and exogenous treatment with recombinant MFG-E8 alleviates acute lung injury induced by LPS instillation (246). Expression of MFG-E8 was also decreased in PEDF -/- mice compared with PEDF +/+ mice (Figure 11B). To further determine the inflammation status of lungs from PEDF +/+ and PEDF -/- mice, mRNA levels of monocyte chemotactic protein -1 (MCP-1) and Interleukin-1β (IL-1β) were also accessed by quantitative real time PCR., The levels of IL-1β (Figure 11C) and MCP-1 (Figure 11D) were significantly increased in the lung of PEDF -/- mice compared with PEDF +/+ mice.

The morphology of arterioles and venules in lung tissue were examined in sections stained by movat pentachrome. Arteriole wall in PEDF -/- mice was thicker than in PEDF +/+ mice (Figure 12 A, B). The similar result was also observed in venules (Figure 12 C, D). The ratios of wall area to lumen area in vessels were quantified (Figure 12 E, F). Vessel wall area in the lung of PEDF -/- mice was elevated compared with PEDF +/+ mice. However, the area of lumen in arterioles and venules were not significantly different in PEDF +/+ and PEDF -/- mice (not shown).

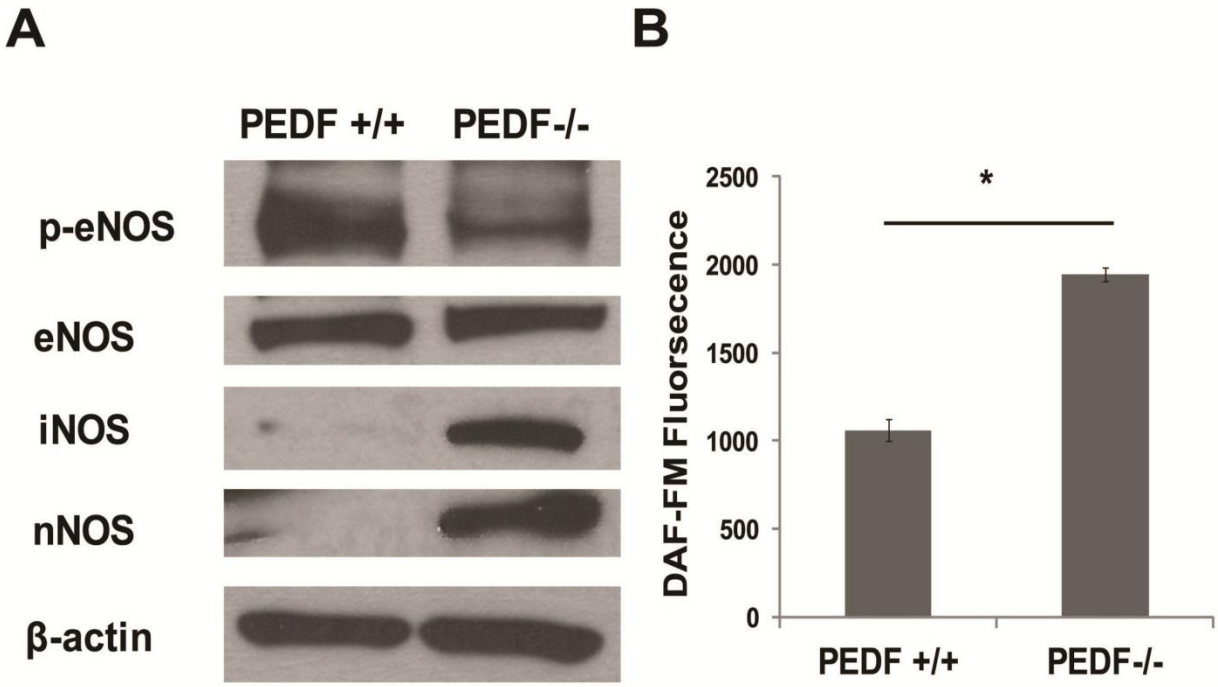

Appendix Figure 10. Alterations in the expression of NOS in PEDF-/- lung EC.

A: Phospho-eNOS, total eNOS, iNOS and nNOS in cell lysates were analyzed by Western blotting. Phosphorylation of eNOS was attenuated in PEDF -/- lung EC. Expression level of iNOS and nNOS was increased in PEDF -/- lung EC. The β-actin was used for loading control. These experiments were repeated using two different isolations of EC with similar results. B: Intracellular nitric oxide (NO) level in lung EC was measured using DAF-FM. Please note a significant increase in intracellular NO level in PEDF −/− lung EC compared with PEDF +/+ lung EC (*$p < 0.05$; $n = 3$).

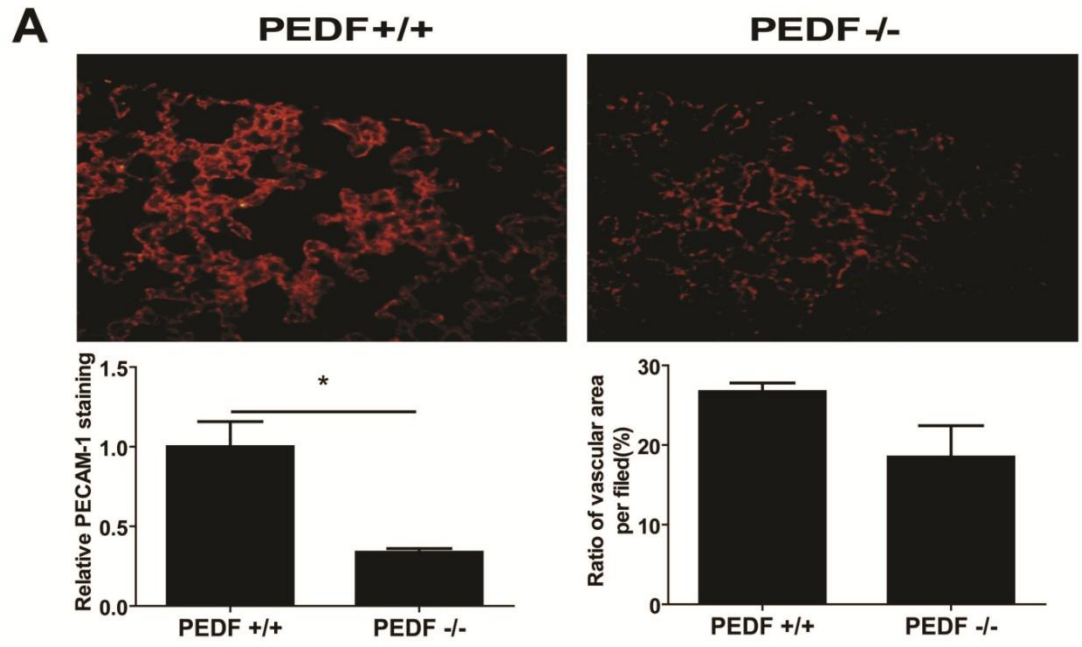
A
PEDF+/+
PEDF-/-
Relative PECAM-1 staining
1.5
1.0
0.5
0.0
*
PEDF +/+
PEDF -/-
Ratio of vascular area per filed(%)
30
20
10
0
PEDF +/+
PEDF -/-

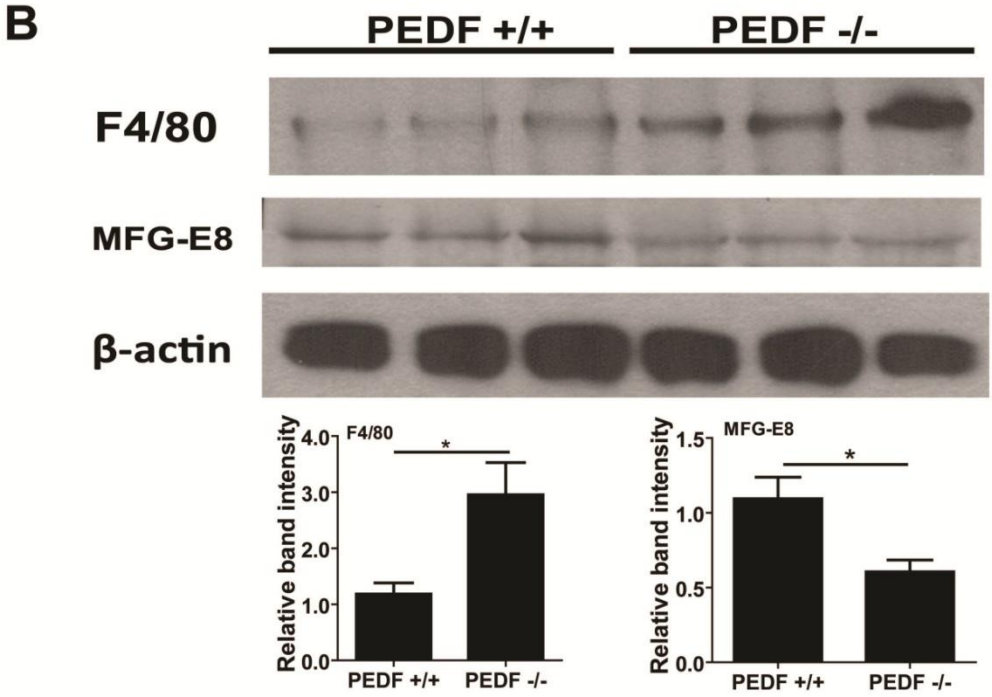
B
PEDF +/+
PEDF -/-
F4/80
MFG-E8
β-actin
F4/80
Relative band intensity
4.0
3.0
2.0
1.0
0.0
*
PEDF +/+
PEDF -/-
MFG-E8
Relative band intensity
1.5
1.0
0.5
0.0
*
PEDF +/+
PEDF -/-

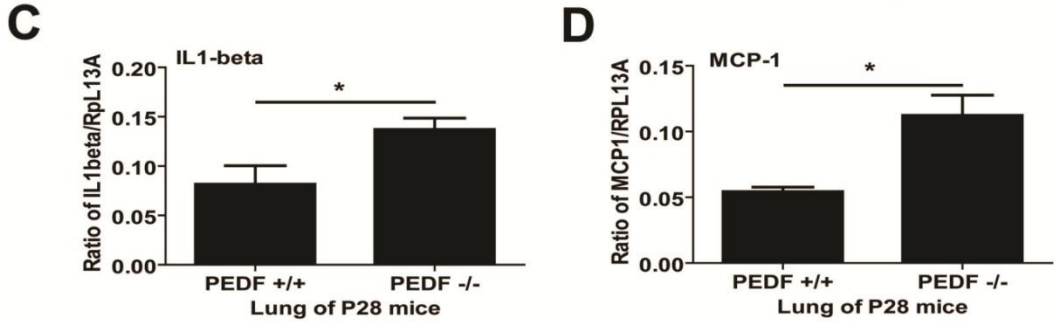
C
IL1-beta
Ratio of IL1beta/RpL13A
0.20
0.15
0.10
0.05
0.00
*
PEDF +/+
PEDF -/-
Lung of P28 mice
D
MCP-1
Ratio of MCP1/RPL13A
0.15
0.10
0.05
0.00
*
PEDF +/+
PEDF -/-
Lung of P28 mice

Appendix Figure 11. Expression of PECAM-1 and inflammatory markers in PEDF -/- lungs. A: Lung sections from P28 PEDF +/+ and PEDF -/- mice were stained with anti-PECAM-1 and fluorescence images were obtained in digital format (x400). Vascular PECAM-1 intensity in lung from PEDF -/- mice was lower compared with lungs from PEDF +/+ mice (*$p < 0.05$; $n = 4$). These results were consistent with reduced PECAM-1 levels detected in PEDF-/- lung EC. Vascular areas in lung from PEDF +/+ and PEDF -/- were not significantly different. B: Expression level of F4/80 and MFG-E8 was determined by Western blot analysis of lung lysates prepared from P28 PEDF +/+ and PEDF -/- mice. β-actin was used for loading control (*$p < 0.05$; $n = 3$). C and D: mRNA expressions of inflammatory cytokines in lung of P28 PEDF +/+ and PEDF -/- mice were investigated by quantitative real time PCR method. IL-1β (C) and MCP-1(D) level are shown ($n=3$, $p<0.05$). Please note increased expression of these cytokines in the lung of PEDF -/- mice.

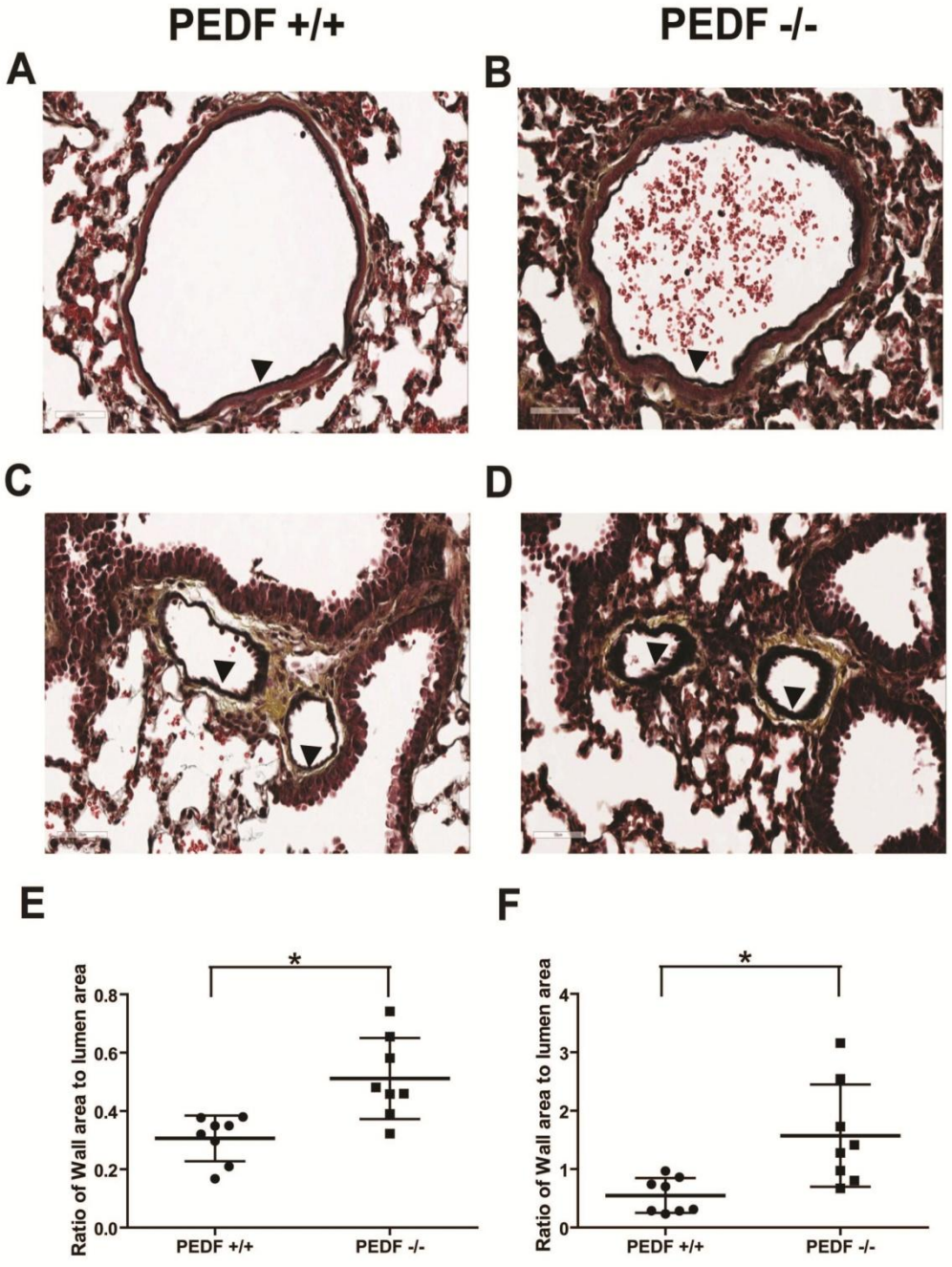
PEDF +/+
PEDF -/-
A
B
C
D
E
F
Ratio of Wall area to lumen area
0.0
0.2
0.4
0.6
0.8
*
PEDF +/+
PEDF -/-
Ratio of Wall area to lumen area
0
1
2
3
4
*
PEDF +/+
PEDF -/-

Appendix Figure 12. Vascular abnormities in PEDF-/- lungs.

Histological lung sections were prepared from P28 PEDF +/+ and PEDF -/- mice and stained with pentachrome movat. Arterioles are shown in *A* and *B*. Venules are shown in *C* and *D*. *A* and *C* are sections from PEDF +/+ mice and *B* and *D* are sections from PEDF -/- mice. Sections are obtained from comparable areas of lung tissue. Magnifications are x400. Arrow heads indicate vessel wall in arterioles and venules. Ratio of vessel wall area to lumen area are shown in E (arteriole) and F (venules) (*$p < 0.05$; $n = 8$).

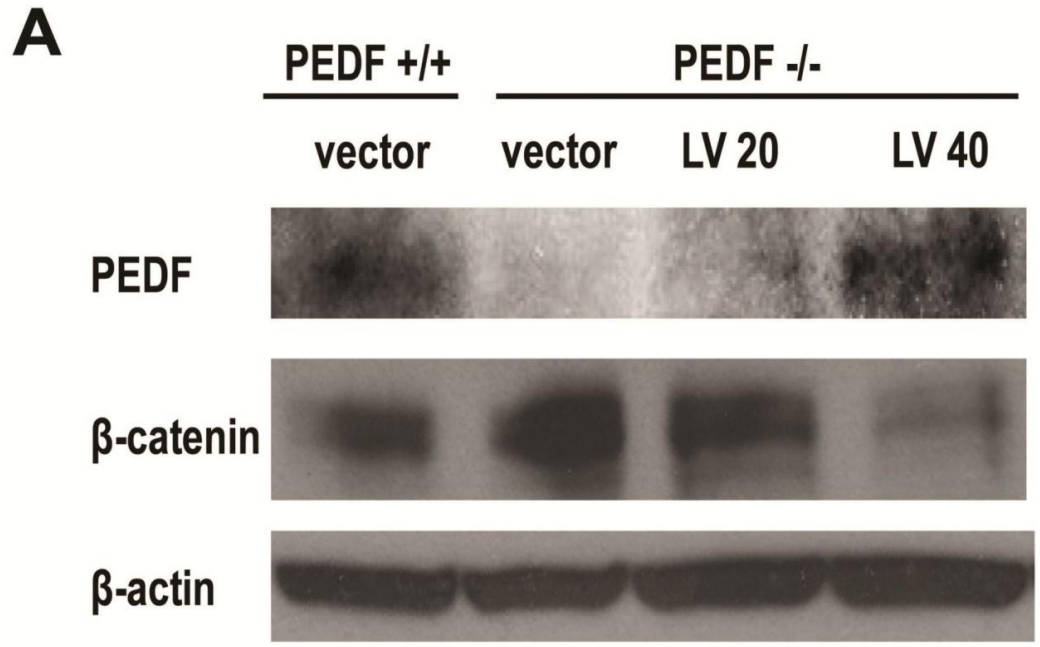
A
PEDF +/+
PEDF -/-
vector
vector
LV 20
LV 40
PEDF
β-catenin
β-actin

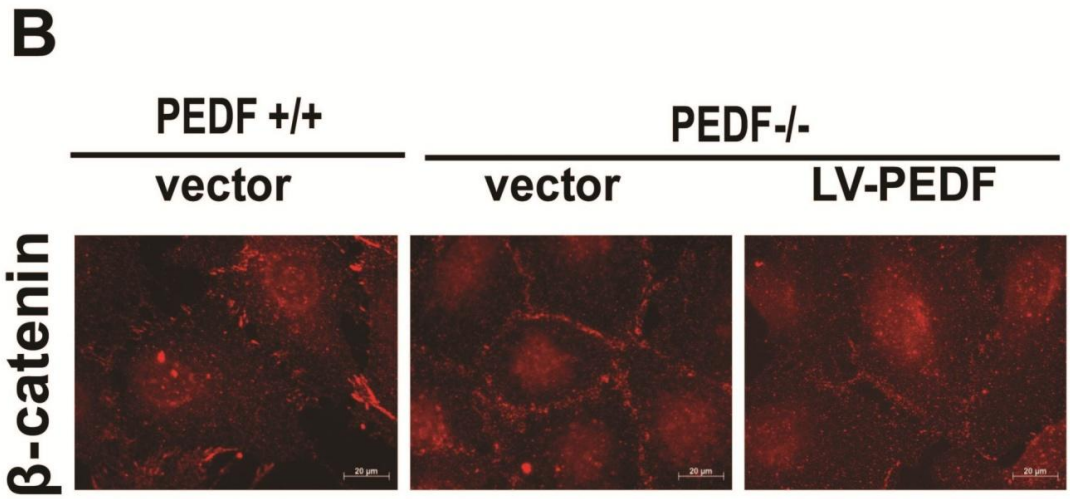
B
PEDF +/+
PEDF-/-
vector
vector
LV-PEDF
β-catenin

Appendix Supplementary Figure 1. Effect of PEDF re-expression in PEDF -/- EC on the expression and localization of β-catenin.

A: PEDF and β-catenin levels were determined by Western blot analysis. PEDF +/+ EC were infected with lenti viruses encoding vector control and PEDF -/- EC were infected with lenti viruses encoding vector control or lenti viruses at multiplicity of infection of 20 or 40 for the re-expression of PEDF. The β-actin was used for loading control. Two independent experiments were performed and showed similar results. B: Cellular localization of β-catenin in PEDF +/+ EC transfected with lenti viruses for vector control and PEDF -/- EC transfected with lenti viruses for vector controls or re-expression of PEDF. Scale bar indicates 20 μm.

Discussion

Here we addressed the cell autonomous effects of PEDF in the development and function of lung endothelium using PEDF+/+ and PEDF -/- mice and lung EC prepared from these mice. We found PEDF -/- lung EC were more migratory, proliferated at a slower rate, failed to undergo capillary morphogenesis, adhered more strongly to ECM proteins, and exhibited altered junctional properties along with a significant increase in β-catenin expression and nuclear localization. The PEDF-/- EC also produced increased levels of VEGF, altered ECM protein production, and expressed significantly higher levels of nNOS and iNOS with increased intracellular NO levels. In vivo, we observed decreased levels of PECAM-1 staining and increased levels of inflammatory cytokines including MCP-1 and IL-1β and F4/80, a marker of inflammatory macrophages. The level of MFG-E8, a protein with anti-inflammatory activity, was also decreased in lungs of PEDF-/- mice. These observations were also consistent with increased thickness of blood vessel walls in lung from PEDF -/- mice. Together our results support the pro-angiogenic and pro-inflammatory characteristics of lung endothelium in the absence of PEDF.

Expression of PEDF in lung endothelium has been studied to address the question whether lung endothelium produces PEDF. In human lung biopsies, PEDF is expressed in lung alveolus and its expression was colocalized with EC within microvessels (229). In contrast, PEDF was not included in the list of EC -enriched genes when expressed sequence tags obtained from lung EC fraction was analyzed to identify genes enriched in EC by Favre *et al* (247). However, mRNA expression of PEDF was detected by real time qPCR method in lung EC isolated from PEDF +/+ mice and secreted PEDF was detected in conditioned medium collected

from PEDF +/+ lung EC by western blot. Thus, PEDF is expressed in lung EC and secreted by lung EC.

Migration is fundamental to the ability of EC to form new blood vessels. The enhanced migration observed in PEDF-/- EC is consistent with the anti-angiogenic activity of PEDF, and increased levels of VEGF by PEDF -/- EC. The PEDF anti-migratory effect of PEDF has been previously demonstrated in human bone marrow EC (248). Cell migration is also closely associated with the formation of focal adhesions and actin stress fibers. PEDF -/- EC also showed increased levels of actin stress fibers and reduced number of focal adhesions consistent with their migratory phenotype (249, 250). The increased formation of actin stress fibers has been reported in rat microvascular lung endothelial cells after exposure to cigarette smoke to induce inflammation and human dermal microvascular endothelial cells incubated with inflammatory cytokines (244, 251). Thus, the increased actin stress fiber formation in PEDF -/- lung EC are consistent with the anti-inflammatory activity of PEDF and its deficiency may be conducive to production of inflammatory mediators.

We observed a four-fold increase in the amount of VEGF produced by PEDF -/- lung EC compared with PEDF +/+ lung EC. In addition, expression of VCAM-1, another marker of inflammation, was also increased in PEDF -/- lung EC. Others have shown that exposure of mice to lipopolysaccharide (LPS) results in inflammation and increased expression of VEGF in the lung (252). Furthermore, VCAM-1 expression is increased in LPS-treated mouse lung EC isolated from mice compared with non-treated cells (253). Thus, PEDF deficiency in the lung endothelium may promote the progression of inflammation.

In lungs, iNOS has been known for its crucial role during inflammation. iNOS is up-regulated by various inflammatory mediators including tumor necrosis factor (TNF)-α,

interferon(IFN)-γ and LPS. NO level is increased by up-regulation of iNOS expression in various inflammatory lung diseases including bronchial asthma and COPD. The lung iNOS is considered the major NO producing source in inflammatory pathways (254). In human retinal pericyte, PEDF attenuates iNOS expression and NO production induced by oxidized low density lipoprotein (255). In this study, the expression of iNOS and NO levels were significantly increased in PEDF -/- Lung EC. Taken together, PEDF may mediate its anti-inflammatory activity in the lung by regulating expression level of iNOS, perhaps through attenuation of canonical Wnt signaling pathway decreasing iNOS expression.

PEDF inhibits canonical Wnt signaling through interaction with LRP6 receptor, and regulates production of pro-angiogenic and pro-inflammatory factors including VEGF (241). Activation of canonical Wnt signaling pathway is followed by the nuclear translocation of β-catenin which drives the expression of target genes (210). We observed a significant increase in nuclear localization of β-catenin in PEDF -/- lung EC. In addition, the expression of iNOS is regulated by Wnt / β-catenin signaling pathway in hepatocytes and some cancer cells (256). Thus, our results suggest that up-regulation of iNOS and VEGF in PEDF-/- lung EC results from the activation of canonical Wnt signaling pathway as previously demonstrated for another member of serine protease inhibitor family (241).

PEDF is also known as contact inhibitory factor for its ability to arrest growth when cells reach confluence. Incubation of human umbilical vein endothelial cell (HUVEC) with PEDF-antibody enhanced their proliferation(257). However, the PEDF -/- EC have exhibited slower proliferation and DNA synthesis compared with PEDF +/+ EC. When iNOS is overexpressed in human coronary artery smooth muscle cell and HUVEC, their proliferation is decreased (258). In addition, iNOS-mediated NO overproduction results in inhibition of DNA synthesis(259).

Therefore, the increased expression of iNOS and production of NO may also attribute to attenuation of DNA synthesis and proliferation of PEDF -/- EC.

The PEDF -/- lung EC were more adherent on collagen IV, fibronectin and vitronectin. The alteration in adhesive properties of PEDF -/- lung EC may be contributed, at least in part, to decreased expression of tenascin-C. Tenascin-C has anti-adhesive activity through binding of the FN type III repeat and interfere with cell binding to fibronectin (260). Osteopontin also has anti-adhesive activity. In endothelial progenitor cells, osteopontin decreases cell adhesion (261). Thus, decreased production of tenascin-C and osteopontin may contribute to alterations in the adhesion properties of PEDF -/- EC. TSP1 and TSP2 are also ECM proteins with important roles in angiogenesis and inflammation. They have similar structural domains and exhibit anti-angiogenic activity (262), but their expression is differentially regulated during angiogenesis (263). Here expression of TSP2 was dramatically down regulated in PEDF -/- EC. A decrease in secreted level of TSP1 was also observed in PEDF -/- EC, despite similar expression of cell-associated TSP1. Thus, PEDF-deficiency had only a modest effect on the expression of TSP1, but completely suppressed TSP2 expression. These results imply that PEDF is involved in the regulation of TSP expression and perhaps their post-translational processing (203).

F4/80 is a cell surface glycoprotein on the macrophages and elevation of its level in the tissue suggests enhanced recruitment of macrophages (245). Lungs from PEDF -/- mice exhibited a pro-inflammatory phenotype revealed by a significant increase in the level of F4/80 antigen. In addition, the level of MFG-E8 was decreased in the lungs from PEDF -/- mice. MFG-E8 is a secreted molecule involved in the clearance of apoptotic cells along with anti-inflammatory activity, especially in the lung (264). After acute lung injury is induced by LPS instillation in mice, MFG-E8 mRNA and protein levels are attenuated in the lung (246). These

results suggest that lack of PEDF may be associated with the pro-inflammatory state of the lung in PEDF -/- mice. PEDF may inhibit inflammation by suppressing macrophage activation and ameliorates macrophage recruitment by inhibiting MCP-1 expression (265, 266). These results are consistent with our finding and a regulatory role for PEDF in lung inflammation.

Inflammation in the lung results in remodeling of the vascular structure. When inflammation is induced in the lung by infection, vessel wall thickness increases (267). We observed a significant increase in the vessel wall thickness of the lungs from PEDF-/- mice. These results further support an important role for PEDF in modulation of the inflammatory state of the lung. These results in lung are also consistent with those previously reported in the pancreas of PEDF -/- mice (232).

In summary, our studies demonstrated that lack of PEDF promotes the migratory activity of lung of EC consistent with the proposed PEDF anti-angiogenic activity. Furthermore, the absence of PEDF in EC was associated with the onset of an inflammatory phenotype. Lack of PEDF contributed to elevation of VEGF, iNOS and VCAM-1 levels in EC. The absence of PEDF also impacted the proliferation, adhesion and capillary morphogenesis of EC. These were concomitant with significant changes in the ECM proteins produced by EC, and activation of canonical Wnt signaling pathway. In vivo, PEDF-deficiency was associated with increase in vessel wall thickness and onset of inflammatory phenotypes in the lung. Together these results demonstrate an important role for PEDF expression in regulation of the pro-angiogenic and pro-inflammatory phenotype of the lung endothelium.

References

1. Runkle EA, Antonetti DA. The blood-retinal barrier: structure and functional significance. Methods in molecular biology. 2011;686:133-48.

2. Kaur C, Foulds WS, Ling EA. Blood-retinal barrier in hypoxic ischaemic conditions: basic concepts, clinical features and management. Prog Retin Eye Res. 2008;27(6):622-47.

3. Hosoya K-i, Tachikawa M. Inner Blood-Retinal Barrier Transporters: Role of Retinal Drug Delivery. Pharmaceutical Research. 2009;26(9):2055-65.

4. Klaassen I, Van Noorden CJF, Schlingemann RO. Molecular basis of the inner blood-retinal barrier and its breakdown in diabetic macular edema and other pathological conditions. Progress in Retinal and Eye Research. 2013;34(0):19-48.

5. Antonetti DA, Barber AJ, Bronson SK, Freeman WM, Gardner TW, Jefferson LS, et al. Diabetic retinopathy: seeing beyond glucose-induced microvascular disease. Diabetes. 2006;55(9):2401-11.

6. Diabetes Atlas. International Diabetes Federation; 2012 [updated 2012; cited 2013 September 18]; Available from: http://www.idf.org/diabetesatlas/.

7. Kempen JH, O'Colmain BJ, Leske MC, Haffner SM, Klein R, Moss SE, et al. The prevalence of diabetic retinopathy among adults in the United States. Arch Ophthalmol. 2004;122(4):552-63.

8. Roy MS, Klein R, O'Colmain BJ, Klein BK, Moss SE, Kempen JH. THe prevalence of diabetic retinopathy among adult type1 diabetic persons in the united states. Arch Ophthalmol. 2004;122(4):546-51.

9. Yau JWY, Rogers SL, Kawasaki R, Lamoureux EL, Kowalski JW, Bek T, et al. Global Prevalence and Major Risk Factors of Diabetic Retinopathy. Diabetes Care. 2012;35(3):556-64.

10. Bandello F, Lattanzio R, Zucchiatti I, Turco C. Pathophysiology and treatment of diabetic retinopathy. Acta Diabetol. 2013;50(1):1-20.

11. Bhagat N, Grigorian RA, Tutela A, Zarbin MA. Diabetic Macular Edema: Pathogenesis and Treatment. Survey of Ophthalmology. 2009;54(1):1-32.

12. Bandello F, Lattanzio R, Zucchiatti I, Del Turco C. Pathophysiology and treatment of diabetic retinopathy. Acta Diabetol. 2013;50(1):1-20.

13. Singh R, Barden A, Mori T, Beilin L. Advanced glycation end-products: a review. Diabetologia. 2001;44(2):129-46.

14. Yamagishi S-i, Takeuchi M, Matsui T, Nakamura K, Imaizumi T, Inoue H. Angiotensin II augments advanced glycation end product-induced pericyte apoptosis through RAGE overexpression. FEBS Letters. 2005;579(20):4265-70.

15. Kim J-H, Kim JH, Jun H-O, Yu YS, Kim K-W. Inhibition of Protein Kinase C δ Attenuates Blood-Retinal Barrier Breakdown in Diabetic Retinopathy. The American Journal of Pathology. 2010;176(3):1517-24.

16. Gardiner TA, Anderson HR, Stitt AW. Inhibition of advanced glycation end-products protects against retinal capillary basement membrane expansion during long-term diabetes. The Journal of Pathology. 2003;201(2):328-33.

17. Stitt AW, Hughes SJ, Canning P, Lynch O, Cox O, Frizzell N, et al. Substrates modified by advanced glycation end-products cause dysfunction and death in retinal pericytes by reducing survival signals mediated by platelet-derived growth factor. Diabetologia. 2004;47(10):1735-46.

18. Kowluru RA, Chan P-S. Oxidative Stress and Diabetic Retinopathy. Experimental Diabetes Research. 2007;2007.

19. Baynes JW. Role of oxidative stress in development of complications in diabetes. Diabetes. 1991;40(4):405-12.

20. Li J, Wang JJ, Yu Q, Chen K, Mahadev K, Zhang SX. Inhibition of Reactive Oxygen Species by Lovastatin Downregulates Vascular Endothelial Growth Factor Expression and Ameliorates Blood-Retinal Barrier Breakdown in db/db Mice: Role of NADPH Oxidase 4. Diabetes. 2010;59(6):1528-38.

21. Zheng Z, Chen H, Ke G, Fan Y, Zou H, Sun X, et al. Protective Effect of Perindopril on Diabetic Retinopathy Is Associated With Decreased Vascular Endothelial Growth Factor–to–Pigment Epithelium–Derived Factor Ratio: Involvement of a Mitochondria–Reactive Oxygen Species Pathway. Diabetes. 2009;58(4):954-64.

22. Al-Shabrawey M, Rojas M, Sanders T, Behzadian A, El-Remessy A, Bartoli M, et al. Role of NADPH Oxidase in Retinal Vascular Inflammation. Invest Ophthalmol Vis Sci. 2008;49(7):3239-44.

23. Warboys CM, Toh H-B, Fraser PA. Role of NADPH Oxidase in Retinal Microvascular Permeability Increase by RAGE Activation. Invest Ophthalmol Vis Sci. 2009;50(3):1319-28.

24. Pricci F, Leto G, Amadio L, Iacobini C, Cordone S, Catalano S, et al. Oxidative stress in diabetes-induced endothelial dysfunction involvement of nitric oxide and protein kinase C. Free Radical Biology and Medicine. 2003;35(6):683-94.

25. Zheng Z, Chen H, Li J, Li T, Zheng B, Zheng Y, et al. Sirtuin 1–Mediated Cellular Metabolic Memory of High Glucose Via the LKB1/AMPK/ROS Pathway and Therapeutic Effects of Metformin. Diabetes. 2012;61(1):217-28.

26. Du Y, Veenstra A, Palczewski K, Kern TS. Photoreceptor cells are major contributors to diabetes-induced oxidative stress and local inflammation in the retina. Proceedings of the National Academy of Sciences of the United States of America. 2013;110(41):16586-91.

27. Tang J, Kern TS. Inflammation in diabetic retinopathy. Progress in Retinal and Eye Research. 2011;30(5):343-58.

28. Zheng L, Du Y, Miller C, Gubitosi-Klug RA, Kern TS, Ball S, et al. Critical role of inducible nitric oxide synthase in degeneration of retinal capillaries in mice with streptozotocin-induced diabetes. Diabetologia. 2007;50(9):1987-96.

29. Mishra A, Newman EA. Inhibition of inducible nitric oxide synthase reverses the loss of functional hyperemia in diabetic retinopathy. Glia. 2010;58(16):1996-2004.

30. Mishra A, Newman EA. Aminoguanidine reverses the loss of functional hyperemia in a rat model of diabetic retinopathy. Frontiers in Neuroenergetics. 2012;3.

31. Perrone L, Devi TS, Hosoya KI, Terasaki T, Singh LP. Inhibition of TXNIP expression in vivo blocks early pathologies of diabetic retinopathy. Cell Death and Dis. 2010;1:e65.

32. Ayalasomayajula SP, Kompella UB. Subconjunctivally administered celecoxib-PLGA microparticles sustain retinal drug levels and alleviate diabetes-induced oxidative stress in a rat model. Eur J Pharmacol. 2005;511(2-3):191-8.

33. Krady JK, Basu A, Allen CM, Xu Y, LaNoue KF, Gardner TW, et al. Minocycline Reduces Proinflammatory Cytokine Expression, Microglial Activation, and Caspase-3 Activation in a Rodent Model of Diabetic Retinopathy. Diabetes. 2005;54(5):1559-65.

34. Li J, Wang JJ, Yu Q, Wang M, Zhang SX. Endoplasmic reticulum stress is implicated in retinal inflammation and diabetic retinopathy. FEBS Letters. 2009;583(9):1521-7.

35. Yang W, Yu X, Zhang Q, Lu Q, Wang J, Cui W, et al. Attenuation of streptozotocin-induced diabetic retinopathy with low molecular weight fucoidan via inhibition of vascular endothelial growth factor. Experimental Eye Research. 2013;115(0):96-105.

36. Hu Y, Chen Y, Ding L, He X, Takahashi Y, Gao Y, et al. Pathogenic role of diabetes-induced PPAR-α down-regulation in microvascular dysfunction. Proceedings of the National Academy of Sciences. 2013;110(38):15401-6.

37. Liu X, Chen HH, Zhang LW. Potential therapeutic effects of pigment epithelium-derived factor for treatment of diabetic retinopathy. Int J Ophthalmol. 2013;6(2):221-7. PMCID: 3633765.

38. Yoshida Y, Yamagishi S-I, Matsui T, Jinnouchi Y, Fukami K, Imaizumi T, et al. Protective role of pigment epithelium-derived factor (PEDF) in early phase of experimental diabetic retinopathy. Diabetes/Metabolism Research and Reviews. 2009;25(7):678-86.

39. Han Y, Bearse MA, Schneck ME, Barez S, Jacobsen CH, Adams AJ. Multifocal Electroretinogram Delays Predict Sites of Subsequent Diabetic Retinopathy. Invest Ophthalmol Vis Sci. 2004;45(3):948-54.

40. Barber AJ, Gardner TW, Abcouwer SF. The significance of vascular and neural apoptosis to the pathology of diabetic retinopathy. Invest Ophthalmol Vis Sci. 2011;52(2):1156-63. PMCID: 3053099.

41. El-Remessy AB, Al-Shabrawey M, Khalifa Y, Tsai N-T, Caldwell RB, Liou GI. Neuroprotective and Blood-Retinal Barrier-Preserving Effects of Cannabidiol in Experimental Diabetes. The American Journal of Pathology. 2006;168(1):235-44.

42. Kowluru RA, Engerman RL, Case GL, Kern TS. Retinal glutamate in diabetes and effect of antioxidants. Neurochemistry International. 2001;38(5):385-90.

43. Davalli AM, Perego C, Folli FB. The potential role of glutamate in the current diabetes epidemic. Acta Diabetol. 2012;49(3):167-83.

44. Ng JS, Bearse MA, Schneck ME, Barez S, Adams AJ. Local Diabetic Retinopathy Prediction by Multifocal ERG Delays over 3 Years. Invest Ophthalmol Vis Sci. 2008;49(4):1622-8.

45. Ngoh GA, Facundo HT, Zafir A, Jones SP. O-GlcNAc signaling in the cardiovascular system. Circ Res. 2010;107(2):171-85. PMCID: 2919351.

46. Gurel Z, Sieg KM, Shallow KD, Sorenson CM, Sheibani N. Retinal O-linked N-acetylglucosamine protein modifications: implications for postnatal retinal vascularization and the pathogenesis of diabetic retinopathy. Mol Vis. 2013;19:1047-59. PMCID: 3668662.

47. Kadiyala CSR, Zheng L, Du Y, Yohannes E, Kao H-Y, Miyagi M, et al. Acetylation of Retinal Histones in Diabetes Increases Inflammatory Proteins: EFFECTS OF MINOCYCLINE AND MANIPULATION OF HISTONE ACETYLTRANSFERASE (HAT) AND HISTONE DEACETYLASE (HDAC). Journal of Biological Chemistry. 2012;287(31):25869-80.

48. D'Cruz TS, Weibley BN, Kimball SR, Barber AJ. Post-Translational Processing of Synaptophysin in the Rat Retina Is Disrupted by Diabetes. PLoS One. 2012;7(9):e44711.

49. Kim YH, Kim YS, Roh GS, Choi WS, Cho GJ. Resveratrol blocks diabetes-induced early vascular lesions and vascular endothelial growth factor induction in mouse retinas. Acta Ophthalmologica. 2012;90(1):e31-e7.

50. Murakami T, Frey T, Lin C, Antonetti DA. Protein Kinase Cβ Phosphorylates Occludin Regulating Tight Junction Trafficking in Vascular Endothelial Growth Factor–Induced Permeability In Vivo. Diabetes. 2012;61(6):1573-83.

51. Mizutani M, Kern TS, Lorenzi M. Accelerated death of retinal microvascular cells in human and experimental diabetic retinopathy. The Journal of Clinical Investigation. 1996;97(12):2883-90.

52. Barber AJ, Antonetti DA, Kern TS, Reiter CEN, Soans RS, Krady JK, et al. The Ins2Akita Mouse as a Model of Early Retinal Complications in Diabetes. Investigative Ophthalmology & Visual Science. 2005;46(6):2210-8.

53. Enge M, Bjarnegard M, Gerhardt H, Gustafsson E, Kalen M, Asker N, et al. Endothelium-specific platelet-derived growth factor-B ablation mimics diabetic retinopathy. Embo J. 2002;21(16):4307-16. PMCID: 126162.

54. Engerman RL. Pathogenesis of diabetic retinopathy. Diabetes. 1989;38(10):1203-6.

55. Costa PZ, Soares R. Neovascularization in diabetes and its complications. Unraveling the angiogenic paradox. Life Sci. 2013;92(22):1037-45.

56. Miyamoto K, Khosrof S, Bursell SE, Rohan R, Murata T, Clermont AC, et al. Prevention of leukostasis and vascular leakage in streptozotocin-induced diabetic retinopathy via intercellular adhesion molecule-1 inhibition. Proc Natl Acad Sci U S A. 1999;96(19):10836-41. PMCID: 17969.

57. Bai N, Tang S, Ma J, Luo Y, Lin S. Increased expression of intercellular adhesion molecule-1, vascular cellular adhesion molecule-1 and leukocyte common antigen in diabetic rat retina. Yan Ke Xue Bao. 2003;19(3):176-83.

58. Villeneuve LM, Natarajan R. The role of epigenetics in the pathology of diabetic complications. Am J Physiol Renal Physiol. 2010;299(1):F14-25. PMCID: 2904177.

59. Chen S, Feng B, George B, Chakrabarti R, Chen M, Chakrabarti S. Transcriptional coactivator p300 regulates glucose-induced gene expression in endothelial cells. American Journal of Physiology - Endocrinology and Metabolism. 2009;298(1):E127-E37.

60. Zhong Q, Kowluru RA. Role of histone acetylation in the development of diabetic retinopathy and the metabolic memory phenomenon. Journal of Cellular Biochemistry. 2010;110(6):1306-13.

61. Zhong Q, Kowluru RA. Regulation of Matrix Metalloproteinase-9 by Epigenetic Modifications and the Development of Diabetic Retinopathy. Diabetes. 2013;62(7):2559-68.

62. He S, Li X, Chan N, Hinton DR. Review: Epigenetic mechanisms in ocular disease. Molecular vision. 2013;19:665-74. PMCID: 3611946.

63. McArthur K, Feng B, Wu Y, Chen S, Chakrabarti S. MicroRNA-200b Regulates Vascular Endothelial Growth Factor–Mediated Alterations in Diabetic Retinopathy. Diabetes. 2011;60(4):1314-23.

64. Murray AR, Chen Q, Takahashi Y, Zhou KK, Park K, Ma J-x. MicroRNA-200b Downregulates Oxidation Resistance 1 (Oxr1) Expression in the Retina of Type 1 Diabetes Model. Invest Ophthalmol Vis Sci. 2013;54(3):1689-97.

65. Kovacs B, Lumayag S, Cowan C, Xu S. microRNAs in Early Diabetic Retinopathy in Streptozotocin-Induced Diabetic Rats. Invest Ophthalmol Vis Sci. 2011;52(7):4402-9.

66. Ling S, Birnbaum Y, Nanhwan MK, Thomas B, Bajaj M, Ye Y. MicroRNA-dependent cross-talk between VEGF and HIF1α in the diabetic retina. Cellular Signalling. 2013;25(12):2840-7.

67. Gardner TW, Antonetti DA, Barber AJ, LaNoue KF, Levison SW. Diabetic retinopathy: more than meets the eye. Survey of ophthalmology. 2002;47 Suppl 2:S253-62.

68. Abbott NJ, Ronnback L, Hansson E. Astrocyte-endothelial interactions at the blood-brain barrier. Nature reviews Neuroscience. 2006;7(1):41-53.

69. Hamilton NB, Attwell D, Hall CN. Pericyte-mediated regulation of capillary diameter: a component of neurovascular coupling in health and disease. Frontiers in neuroenergetics. 2010;2. PMCID: 2912025.

70. Armulik A, Genove G, Mae M, Nisancioglu MH, Wallgard E, Niaudet C, et al. Pericytes regulate the blood-brain barrier. Nature. 2010;468(7323):557-61.

71. Al Ahmad A, Gassmann M, Ogunshola OO. Maintaining blood–brain barrier integrity: Pericytes perform better than astrocytes during prolonged oxygen deprivation. Journal of Cellular Physiology. 2009;218(3):612-22.

72. Dejana E. Endothelial cell-cell junctions: happy together. Nat Rev Mol Cell Biol. 2004;5(4):261-70.

73. Vestweber D. VE-Cadherin: The Major Endothelial Adhesion Molecule Controlling Cellular Junctions and Blood Vessel Formation. Arteriosclerosis, Thrombosis, and Vascular Biology. 2008;28(2):223-32.

74. Taddei A, Giampietro C, Conti A, Orsenigo F, Breviario F, Pirazzoli V, et al. Endothelial adherens junctions control tight junctions by VE-cadherin-mediated upregulation of claudin-5. Nat Cell Biol. 2008;10(8):923-34.

75. Gonzalez-Mariscal L, Betanzos A, Nava P, Jaramillo BE. Tight junction proteins. Prog Biophys Mol Biol. 2003;81(1):1-44.

76. Wolburg H, Noell S, Mack A, Wolburg-Buchholz K, Fallier-Becker P. Brain endothelial cells and the glio-vascular complex. Cell Tissue Res. 2009;335(1):75-96.

77. Sawada N, Murata M, Kikuchi K, Osanai M, Tobioka H, Kojima T, et al. Tight junctions and human diseases. Med Electron Microsc. 2003;36(3):147-56.

78. Dejana E, Giampietro C. Vascular endothelial-cadherin and vascular stability. Curr Opin Hematol. 2012;19(3):218-23.

79. Nagasawa K, Chiba H, Fujita H, Kojima T, Saito T, Endo T, et al. Possible involvement of gap junctions in the barrier function of tight junctions of brain and lung endothelial cells. Journal of Cellular Physiology. 2006;208(1):123-32.

80. Quaegebeur A, Segura I, Carmeliet P. Pericytes: blood-brain barrier safeguards against neurodegeneration? Neuron. 2010;68(3):321-3.

81. Armulik A, Abramsson A, Betsholtz C. Endothelial/pericyte interactions. Circ Res. 2005;97(6):512-23.

82. Bobbie MW, Roy S, Trudeau K, Munger SJ, Simon AM. Reduced connexin 43 expression and its effect on the development of vascular lesions in retinas of diabetic mice. Invest Ophthalmol Vis Sci. 2010;51(7):3758-63. PMCID: 2904019.

83. Shepro D, Morel NM. Pericyte physiology. The FASEB Journal. 1993;7(11):1031-8.

84. Tomasek JJ, Haaksma CJ, Schwartz RJ, Vuong DT, Zhang SX, Ash JD, et al. Deletion of Smooth Muscle α-Actin Alters Blood–Retina Barrier Permeability and Retinal Function. Invest Ophthalmol Vis Sci. 2006;47(6):2693-700.

85. Darland DC, Massingham LJ, Smith SR, Piek E, Saint-Geniez M, D'Amore PA. Pericyte production of cell-associated VEGF is differentiation-dependent and is associated with endothelial survival. Developmental Biology. 2003;264(1):275-88.

86. Simonavicius N, Ashenden M, van Weverwijk A, Lax S, Huso DL, Buckley CD, et al. Pericytes promote selective vessel regression to regulate vascular patterning. Blood. 2012;120(7):1516-27.

87. Walshe TE, Saint-Geniez M, Maharaj ASR, Sekiyama E, Maldonado AE, D'Amore PA. TGF-β Is Required for Vascular Barrier Function, Endothelial Survival and Homeostasis of the Adult Microvasculature. PLoS One. 2009;4(4):e5149.

88. Ejaz S, Chekarova I, Ejaz A, Sohail A, Lim CW. Importance of pericytes and mechanisms of pericyte loss during diabetic retinopathy. Diabetes, Obesity and Metabolism. 2008;10(1):53-63.

89. Watanabe T, Raff MC. Retinal astrocytes are immigrants from the optic nerve. Nature. 1988;332(6167):834-7.

90. Schnitzer J. Retinal astrocytes: their restriction to vascularized parts of the mammalian retina. Neuroscience Letters. 1987;78(1):29-34.

91. Chan-Ling T, Stone J. Degeneration of astrocytes in feline retinopathy of prematurity causes failure of the blood-retinal barrier. Invest Ophthalmol Vis Sci. 1992;33(7):2148-59.

92. Choi YK, Kim KW. Blood-neural barrier: its diversity and coordinated cell-to-cell communication. BMB Rep. 2008;41(5):345-52.

93. Gardner TW, Lieth E, Khin SA, Barber AJ, Bonsall DJ, Lesher T, et al. Astrocytes increase barrier properties and ZO-1 expression in retinal vascular endothelial cells. Invest Ophthalmol Vis Sci. 1997;38(11):2423-7.

94. Choi YK, Kim K-W. AKAP12 in astrocytes induces barrier functions in human endothelial cells through protein kinase Cζ. FEBS Journal. 2008;275(9):2338-53.

95. Nishikiori N, Osanai M, Chiba H, Kojima T, Mitamura Y, Ohguro H, et al. Glial Cell–Derived Cytokines Attenuate the Breakdown of Vascular Integrity in Diabetic Retinopathy. Diabetes. 2007;56(5):1333-40.

96. Alvarez JI, Dodelet-Devillers A, Kebir H, Ifergan I, Fabre PJ, Terouz S, et al. The Hedgehog Pathway Promotes Blood-Brain Barrier Integrity and CNS Immune Quiescence. Science. 2011;334(6063):1727-31.

97. Kim JH, Kim JH, Yu YS, Kim DH, Kim K-W. Recruitment of pericytes and astrocytes is closely related to the formation of tight junction in developing retinal vessels. Journal of Neuroscience Research. 2009;87(3):653-9.

98. Joussen AM, Smyth N, Niessen C. Pathophysiology of diabetic macular edema. Dev Ophthalmol. 2007;39:1-12.

99. Cui Y, Xu X, Bi H, Zhu Q, Wu J, Xia X, et al. Expression modification of uncoupling proteins and MnSOD in retinal endothelial cells and pericytes induced by high glucose: The role of reactive oxygen species in diabetic retinopathy. Experimental Eye Research. 2006;83(4):807-16.

100. Trudeau K, Molina AJA, Guo W, Roy S. High Glucose Disrupts Mitochondrial Morphology in Retinal Endothelial Cells: Implications for Diabetic Retinopathy. The American Journal of Pathology. 2010;177(1):447-55.

101. Du Y, Kowluru A, Kern TS. PP2A contributes to endothelial death in high glucose: inhibition by benfotiamine. American Journal of Physiology - Regulatory, Integrative and Comparative Physiology. 2010;299(6):R1610-R7.

102. Leal EC, Aveleira CA, Castilho ÁF, Serra AM, Baptista FI, Hosoya K-I, et al. High glucose and oxidative/nitrosative stress conditions induce apoptosis in retinal endothelial cells by a caspase-independent pathway. Experimental Eye Research. 2009;88(5):983-91.

103. Li A-F, Roy S. High Glucose–Induced Downregulation of Connexin 43 Expression Promotes Apoptosis in Microvascular Endothelial Cells. Invest Ophthalmol Vis Sci. 2009;50(3):1400-7.

104. Spoerri PE, Afzal A, Li Calzi S, Shaw LC, Cai J, Pan H, et al. Effects of VEGFR-1, VEGFR-2, and IGF-IR hammerhead ribozymes on glucose-mediated tight junction expression in cultured human retinal endothelial cells. Mol Vis. 2006;12:32-42.

105. Bhattacharjee PS, Huq TS, Potter V, Young A, Davenport IR, Graves R, et al. High-Glucose-Induced Endothelial Cell Injury Is Inhibited by a Peptide Derived from Human Apolipoprotein E. PLoS One. 2012;7(12):e52152.

106. Tien T, Barrette KF, Chronopoulos A, Roy S. Effects of High Glucose-Induced Cx43 Downregulation on Occludin and ZO-1 Expression and Tight Junction Barrier Function in Retinal Endothelial Cells. Invest Ophthalmol Vis Sci. 2013.

107. Chen X, Li J, Li M, Zeng M, Li T, Xiao W, et al. KH902 suppresses high glucose-induced migration and sprouting of human retinal endothelial cells by blocking VEGF and PIGF. Diabetes, Obesity and Metabolism. 2013;15(3):224-33.

108. Huang Q, Sheibani N. High glucose promotes retinal endothelial cell migration through activation of Src, PI3K/Akt1/eNOS, and ERKs. American Journal of Physiology - Cell Physiolog. 2008;295(6):C1647-C57.

109. Yuan L, Hu J, Luo Y, Liu Q, Li T, Parish CR, et al. Upregulation of heparanase in high-glucose-treated endothelial cells promotes endothelial cell migration and proliferation and correlates with Akt and extracellular-signal-regulated kinase phosphorylation. Molecular vision. 2012;18:1684-95. PMCID: 3388982.

110. Romeo G, Liu W-H, Asnaghi V, Kern TS, Lorenzi M. Activation of Nuclear Factor-κB Induced by Diabetes and High Glucose Regulates a Proapoptotic Program in Retinal Pericytes. Diabetes. 2002;51(7):2241-8.

111. Takamura Y, Tomomatsu T, Kubo E, Tsuzuki S, Akagi Y. Role of the Polyol Pathway in High Glucose–Induced Apoptosis of Retinal Pericytes and Proliferation of Endothelial Cells. Invest Ophthalmol Vis Sci. 2008;49(7):3216-23.

112. Geraldes P, Hiraoka-Yamamoto J, Matsumoto M, Clermont A, Leitges M, Marette A, et al. Activation of PKC-delta and SHP-1 by hyperglycemia causes vascular cell apoptosis and diabetic retinopathy. Nat Med. 2009;15(11):1298-306. PMCID: 3290906.

113. Fu D, Wu M, Zhang J, Du M, Yang S, Hammad SM, et al. Mechanisms of modified LDL-induced pericyte loss and retinal injury in diabetic retinopathy. Diabetologia. 2012;55(11):3128-40.

114. Devi TS, Hosoya K-I, Terasaki T, Singh LP. Critical role of TXNIP in oxidative stress, DNA damage and retinal pericyte apoptosis under high glucose: Implications for diabetic retinopathy. Exp Cell Res. 2013;319(7):1001-12.

115. Li Y, Smith D, Li Q, Sheibani N, Huang S, Kern T, et al. Antibody-Mediated Retinal Pericyte Injury: Implications for Diabetic Retinopathy. Invest Ophthalmol Vis Sci. 2012;53(9):5520-6.

116. Trudeau K, Molina AJA, Roy S. High Glucose Induces Mitochondrial Morphology and Metabolic Changes in Retinal Pericytes. Invest Ophthalmol Vis Sci. 2011;52(12):8657-64.

117. Beltramo E, Berrone E, Giunti S, Gruden G, Perin PC, Porta M. Effects of mechanical stress and high glucose on pericyte proliferation, apoptosis and contractile phenotype. Experimental Eye Research. 2006;83(4):989-94.

118. Pfister F, Feng Y, vom Hagen F, Hoffmann S, Molema G, Hillebrands J-L, et al. Pericyte Migration: A Novel Mechanism of Pericyte Loss in Experimental Diabetic Retinopathy. Diabetes. 2008;57(9):2495-502.

119. Tu Z, Li Y, Smith DS, Sheibani N, Huang S, Kern T, et al. Retinal Pericytes Inhibit Activated T Cell Proliferation. Invest Ophthalmol Vis Sci. 2011;52(12):9005-10.

120. Rungger–Brändle E, Dosso AA, Leuenberger PM. Glial Reactivity, an Early Feature of Diabetic Retinopathy. Invest Ophthalmol Vis Sci. 2000;41(7):1971-80.

121. Feit-Leichman RA, Kinouchi R, Takeda M, Fan Z, Mohr S, Kern TS, et al. Vascular Damage in a Mouse Model of Diabetic Retinopathy: Relation to Neuronal and Glial Changes. Invest Ophthalmol Vis Sci. 2005;46(11):4281-7.

122. Iandiev I, Pannicke T, Reichenbach A, Wiedemann P, Bringmann A. Diabetes alters the localization of glial aquaporins in rat retina. Neuroscience Letters. 2007;421(2):132-6.

123. Ly A, Yee P, Vessey KA, Phipps JA, Jobling AI, Fletcher EL. Early Inner Retinal Astrocyte Dysfunction during Diabetes and Development of Hypoxia, Retinal Stress, and Neuronal Functional Loss. Invest Ophthalmol Vis Sci. 2011;52(13):9316-26.

124. Lind KR, Ball KK, Cruz NF, Dienel GA. The unfolded protein response to endoplasmic reticulum stress in cultured astrocytes and rat brain during experimental diabetes. Neurochemistry International. 2013;62(5):784-95.

125. Gariano RF, Gardner TW. Retinal angiogenesis in development and disease. Nature. 2005;438(7070):960-6.

126. Frank RN. Diabetic Retinopathy. New England Journal of Medicine. 2004;350(1):48-58.

127. The Diabetes Control and Complications Trial Research G. The Effect of Intensive Treatment of Diabetes on the Development and Progression of Long-Term Complications in Insulin-Dependent Diabetes Mellitus. New England Journal of Medicine. 1993;329(14):977-86.

128. Gerhardt H, Betsholtz C. Endothelial-pericyte interactions in angiogenesis. Cell Tissue Res. 2003;314(1):15-23.

129. Feng Y, vom Hagen F, Lin J, Hammes HP. Incipient diabetic retinopathy--insights from an experimental model. Ophthalmologica. 2007;221(4):269-74.

130. Hammes HP, Feng Y, Pfister F, Brownlee M. Diabetic retinopathy: targeting vasoregression. Diabetes. 2011;60(1):9-16. PMCID: 3012202.

131. Hayden MR, Yang Y, Habibi J, Bagree SV, Sowers JR. Pericytopathy: oxidative stress and impaired cellular longevity in the pancreas and skeletal muscle in metabolic syndrome and type 2 diabetes. Oxid Med Cell Longev. 2010;3(5):290-303.

132. Aiello LP, Gardner TW, King GL, Blankenship G, Cavallerano JD, Ferris FL, 3rd, et al. Diabetic retinopathy. Diabetes Care. 1998;21(1):143-56.

133. Lomonosova E, Chinnadurai G. BH3-only proteins in apoptosis and beyond: an overview. Oncogene. 2008;27 Suppl 1:S2-19. PMCID: 2928556.

134. Ren D, Tu HC, Kim H, Wang GX, Bean GR, Takeuchi O, et al. BID, BIM, and PUMA are essential for activation of the BAX- and BAK-dependent cell death program. Science. 2010;330(6009):1390-3. PMCID: 3163443.

135. Valverde AM, Miranda S, Garcia-Ramirez M, Gonzalez-Rodriguez A, Hernandez C, Simo R. Proapoptotic and survival signaling in the neuroretina at early stages of diabetic retinopathy. Mol Vis. 2013;19:47-53. PMCID: 3541044.

136. Scheef EA, Sorenson CM, Sheibani N. Attenuation of proliferation and migration of retinal pericytes in the absence of thrombospondin-1. Am J Physiol Cell Physiol. 2009;296(4):C724-34.

137. Han JH, Ha SW, Lee IK, Kim BW, Kim JG. High glucose-induced apoptosis in bovine retinal pericytes is associated with transforming growth factor beta and betaIG-H3: betaIG-H3 induces apoptosis in retinal pericytes by releasing Arg-Gly-Asp peptides. Clin Experiment Ophthalmol. 2010;38(6):620-8.

138. Huang Q, Sheibani N. High glucose promotes retinal endothelial cell migration through activation of Src, PI3K/Akt1/eNOS, and ERKs. Am J Physiol Cell Physiol. 2008;295(6):C1647-57. PMCID: 2603562.

139. Su X, Sorenson CM, Sheibani N. Isolation and characterization of murine retinal endothelial cells. Mol Vis. 2003;9:171-8.

140. Tang Y, Scheef EA, Wang S, Sorenson CM, Marcus CB, Jefcoate CR, et al. CYP1B1 expression promotes the proangiogenic phenotype of endothelium through decreased intracellular oxidative stress and thrombospondin-2 expression. Blood. 2009;113(3):744-54. PMCID: 2628380.

141. Lin S, Sahai A, Chugh SS, Pan X, Wallner EI, Danesh FR, et al. High glucose stimulates synthesis of fibronectin via a novel protein kinase C, Rap1b, and B-Raf signaling pathway. Journal of Biological Chemistry. 2002;277(44):41725-35.

142. Varma S, Lal BK, Zheng R, Breslin JW, Saito S, Pappas PJ, et al. Hyperglycemia alters PI3k and Akt signaling and leads to endothelial cell proliferative dysfunction. American Journal of Physiology - Heart and Circulatory Physiology. 2005;289(4):H1744-H51.

143. Wang S, Park S, Fei P, Sorenson CM. Bim is responsible for the inherent sensitivity of the developing retinal vasculature to hyperoxia. Developmental Biology. 2011;349(2):296-309. PMCID: 3021136.

144. King GL, Loeken MR. Hyperglycemia-induced oxidative stress in diabetic complications. Histochemistry and Cell Biology. 2004;122(4):333-8.

145. Kanwar M, Chan PS, Kern TS, Kowluru RA. Oxidative damage in the retinal mitochondria of diabetic mice: possible protection by superoxide dismutase. Investigative Ophthalmology and Visual Science. 2007;48(8):3805-11.

146. Tsai GY, Cui JZ, Syed H, Xia Z, Ozerdem U, McNeill JH, et al. Effect of N-acetylcysteine on the early expression of inflammatory markers in the retina and plasma of diabetic rats. Clin Experiment Ophthalmol. 2009;37(2):223-31.

147. El-Remessy AB, Behzadian MA, Abou-Mohamed G, Franklin T, Caldwell RW, Caldwell RB. Experimental diabetes causes breakdown of the blood-retina barrier by a mechanism involving tyrosine nitration and increases in expression of vascular endothelial growth factor and urokinase plasminogen activator receptor. Am J Pathol. 2003;162(6):1995-2004.

148. Ryer EJ, Sakakibara K, Wang C, Sarkar D, Fisher PB, Faries PL, et al. Protein kinase C delta induces apoptosis of vascular smooth muscle cells through induction of the tumor suppressor p53 by both p38-dependent and p38-independent mechanisms. Journal of Biological Chemistry. 2005;280(42):35310-7.

149. Gschwendt M, Muller HJ, Kielbassa K, Zang R, Kittstein W, Rincke G, et al. Rottlerin, a Novel Protein Kinase Inhibitor. Biochemical and Biophysical Research Communications. 1994;199(1):93-8.

150. Kato K, Yamanouchi D, Esbona K, Kamiya K, Zhang F, Kent KC, et al. Caspase-mediated protein kinase C-δ cleavage is necessary for apoptosis of vascular smooth muscle cells. American Journal of Physiology - Heart and Circulatory Physiology. 2009;297(6):H2253-H61.

151. Mavria G, Vercoulen Y, Yeo M, Paterson H, Karasarides M, Marais R, et al. ERK-MAPK signaling opposes Rho-kinase to promote endothelial cell survival and sprouting during angiogenesis. Cancer Cell. 2006;9(1):33-44.

152. Kroll J, Epting D, Kern K, Dietz CT, Feng Y, Hammes HP, et al. Inhibition of Rho-dependent kinases ROCK I/II activates VEGF-driven retinal neovascularization and sprouting angiogenesis. Am J Physiol Heart Circ Physiol. 2009;296(3):H893-9.

153. Bryan BA, Dennstedt E, Mitchell DC, Walshe TE, Noma K, Loureiro R, et al. RhoA/ROCK signaling is essential for multiple aspects of VEGF-mediated angiogenesis. FASEB Journal. 2010;24(9):3186-95. PMCID: 2923346.

154. Pathak MK, Yi T. Sodium stibogluconate is a potent inhibitor of protein tyrosine phosphatases and augments cytokine responses in hemopoietic cell lines. Journal of Immunology. 2001;167(6):3391-7.

155. Wang S, Sorenson CM, Sheibani N. Attenuation of retinal vascular development and neovascularization during oxygen-induced ischemic retinopathy in Bcl-2-/- mice. Developmental Biology. 2005;279(1):205-19.

156. Moore F, Santin I, Nogueira TC, Gurzov EN, Marselli L, Marchetti P, et al. The transcription factor C/EBP delta has anti-apoptotic and anti-inflammatory roles in pancreatic beta cells. PLoS One. 2012;7(2):e31062. PMCID: 3275575.

157. Barthson J, Germano CM, Moore F, Maida A, Drucker DJ, Marchetti P, et al. Cytokines tumor necrosis factor-alpha and interferon-gamma induce pancreatic beta-cell apoptosis through STAT1-mediated Bim protein activation. J Biol Chem. 2011;286(45):39632-43. PMCID: 3234786.

158. Tajima K, Takaishi H, Takito J, Tohmonda T, Yoda M, Ota N, et al. Inhibition of STAT1 accelerates bone fracture healing. Journal of Orthopaedic Research. 2010;28(7):937-41.

159. Bjarnegård M, Enge M, Norlin J, Gustafsdottir S, Fredriksson S, Abramsson A, et al. Endothelium-specific ablation of PDGFB leads to pericyte loss and glomerular, cardiac and placental abnormalities. Development. 2004;131(8):1847-57.

160. Armulik A, Abramsson A, Betsholtz C. Endothelial/Pericyte Interactions. Circulation Research. 2005;97(6):512-23.

161. Okazaki J, Mawatari K, Liu B, Kent KC. The effect of protein kinase C and its alpha subtype on human vascular smooth muscle cell proliferation, migration and fibronectin production. Surgery. 2000;128(2):192-7.

162. Yi T, Pathak MK, Lindner DJ, Ketterer ME, Farver C, Borden EC. Anticancer activity of sodium stibogluconate in synergy with IFNs. Journal of Immunology. 2002;169(10):5978-85.

163. Neviani P, Santhanam R, Trotta R, Notari M, Blaser BW, Liu S, et al. The tumor suppressor PP2A is functionally inactivated in blast crisis CML through the inhibitory activity of the BCR/ABL-regulated SET protein. Cancer Cell. 2005;8(5):355-68.

164. Palenski TL, Sorenson CM, Sheibani N. Inflammatory cytokine-specific alterations in retinal endothelial cell function. Microvascular Research. 2013;89(0):57-69.

165. Huang J-S, Chuang L-Y, Guh J-Y, Huang Y-J, Hsu M-S. Antioxidants attenuate high glucose-induced hypertrophic growth in renal tubular epithelial cells. American Journal of Physiology - Renal Physiology. 2007;293(4):F1072-F82.

166. Torella D, Curcio A, Gasparri C, Galuppo V, De Serio D, Surace FC, et al. Fludarabine prevents smooth muscle proliferation in vitro and neointimal hyperplasia in vivo through specific inhibition of STAT-1 activation. Am J Physiol Heart Circ Physiol. 2007;292(6):H2935-43.

167. Qian L, Van Laake LW, Huang Y, Liu S, Wendland MF, Srivastava D. miR-24 inhibits apoptosis and represses Bim in mouse cardiomyocytes. J Exp Med. 2011;208(3):549-60. PMCID: 3058576.

168. Guo L, Xu J, Qi J, Zhang L, Wang J, Liang J, et al. MicroRNA-17-92a upregulation by estrogen leads to Bim targeting and inhibition of osteoblast apoptosis. Journal of Cell Science. 2013;126(4):978-88.

169. Xie X, Peng J, Chang X, Huang K, Huang J, Wang S, et al. Activation of RhoA/ROCK regulates NF-κB signaling pathway in experimental diabetic nephropathy. Molecular and Cellular Endocrinology. (0).

170. Mustapha NM, Tarr JM, Kohner EM, Chibber R. NADPH Oxidase versus Mitochondria-Derived ROS in Glucose-Induced Apoptosis of Pericytes in Early Diabetic Retinopathy. Journal of Ophthalmology. 2010;2010.

171. Stratman AN, Schwindt AE, Malotte KM, Davis GE. Endothelial-derived PDGF-BB and HB-EGF coordinately regulate pericyte recruitment during vasculogenic tube assembly and stabilization. Blood. 2010;116(22):4720-30. PMCID: 2996127.

172. Saunders WB, Bohnsack BL, Faske JB, Anthis NJ, Bayless KJ, Hirschi KK, et al. Coregulation of vascular tube stabilization by endothelial cell TIMP-2 and pericyte TIMP-3. J Cell Biol. 2006;175(1):179-91. PMCID: 2064509.

173. Tarallo S, Beltramo E, Berrone E, Dentelli P, Porta M. Effects of high glucose and thiamine on the balance between matrix metalloproteinases and their tissue inhibitors in vascular cells. Acta Diabetologica. 2010;47(2):105-11.

174. Quaegebeur A, Lange C, Carmeliet P. The neurovascular link in health and disease: molecular mechanisms and therapeutic implications. Neuron. 2011;71(3):406-24.

175. Nedergaard M, Ransom B, Goldman SA. New roles for astrocytes: Redefining the functional architecture of the brain. Trends in Neurosciences. 2003;26(10):523-30.

176. Huang Q, Sheibani N. High glucose promotes retinal endothelial cell migration through activation of Src, PI3K/Akt1/eNOS, and ERKs. American journal of physiology Cell physiology. 2008;295(6):C1647-57. PMCID: 2603562.

177. Kumar S, Zhuo L. Longitudinal in vivo imaging of retinal gliosis in a diabetic mouse model. Exp Eye Res. 2010;91(4):530-6.

178. Lamers ML, Almeida MES, Vicente-Manzanares M, Horwitz AF, Santos MF. High Glucose-Mediated Oxidative Stress Impairs Cell Migration. PLoS One. 2011;6(8):e22865.

179. Li W, Febbraio M, Reddy SP, Yu D-Y, Yamamoto M, Silverstein RL. CD36 participates in a signaling pathway that regulates ROS formation in murine VSMCs. The Journal of Clinical Investigation. 2010;120(11):3996-4006.

180. Kraft AD, Johnson DA, Johnson JA. Nuclear Factor E2-Related Factor 2-Dependent Antioxidant Response Element Activation by tert-Butylhydroquinone and Sulforaphane Occurring Preferentially in

Astrocytes Conditions Neurons against Oxidative Insult. The Journal of Neuroscience. 2004;24(5):1101-12.

181. Scheef E, Wang S, Sorenson CM, Sheibani N. Isolation and characterization of murine retinal astrocytes. Mol Vis. 2005;11:613-24.

182. Ziehr J, Sheibani N, Sorenson CM. Alterations in cell-adhesive and migratory properties of proximal tubule and collecting duct cells from bcl-2 -/- mice. Am J Physiol Renal Physiol. 2004;287(6):F1154-63.

183. Middeldorp J, Hol EM. GFAP in health and disease. Prog Neurobiol. 2011;93(3):421-43.

184. Serini G, Valdembri D, Bussolino F. Integrins and angiogenesis: a sticky business. Exp Cell Res. 2006;312(5):651-8.

185. Clemmons DR, Maile LA, Ling Y, Yarber J, Busby WH. Role of the integrin alphaVbeta3 in mediating increased smooth muscle cell responsiveness to IGF-I in response to hyperglycemic stress. Growth Horm IGF Res. 2007;17(4):265-70. PMCID: 2366026.

186. van Strien ME, Breve JJ, Fratantoni S, Schreurs MW, Bol JG, Jongenelen CA, et al. Astrocyte-derived tissue transglutaminase interacts with fibronectin: a role in astrocyte adhesion and migration? PLoS One. 2011;6(9):e25037. PMCID: 3174992.

187. Nandi J, Saud B, Zinkievich JM, Yang ZJ, Levine RA. TNF-alpha modulates iNOS expression in an experimental rat model of indomethacin-induced jejunoileitis. Mol Cell Biochem. 2010;336(1-2):17-24.

188. Hsieh H-L, Lin C-C, Hsiao L-D, Yang C-M. High Glucose Induces Reactive Oxygen Species-Dependent Matrix Metalloproteinase-9 Expression and Cell Migration in Brain Astrocytes. Mol Neurobiol. 2013:1-14.

189. Christopherson KS, Ullian EM, Stokes CCA, Mullowney CE, Hell JW, Agah A, et al. Thrombospondins Are Astrocyte-Secreted Proteins that Promote CNS Synaptogenesis. Cell. 2005;120(3):421-33.

190. Dawson DW, Pearce SFA, Zhong R, Silverstein RL, Frazier WA, Bouck NP. CD36 Mediates the In Vitro Inhibitory Effects of Thrombospondin-1 on Endothelial Cells. The Journal of Cell Biology. 1997;138(3):707-17.

191. Sheibani N, Frazier WA. Thrombospondin-1, PECAM-1, and regulation of angiogenesis. Histology and histopathology. 1999;14(1):285-94.

192. Asnaghi V, Gerhardinger C, Hoehn T, Adeboje A, Lorenzi M. A Role for the Polyol Pathway in the Early Neuroretinal Apoptosis and Glial Changes Induced by Diabetes in the Rat. Diabetes. 2003;52(2):506-11.

193. Yang C, Iyer RR, Yu ACH, Yong RL, Park DM, Weil RJ, et al. β-Catenin signaling initiates the activation of astrocytes and its dysregulation contributes to the pathogenesis of astrocytomas. Proceedings of the National Academy of Sciences. 2012;109(18):6963-8.

194. Elobeid A, Bongcam-Rudloff E, Westermark B, Nister M. Effects of inducible glial fibrillary acidic protein on glioma cell motility and proliferation. J Neurosci Res. 2000;60(2):245-56.

195. Palenski TL, Sorenson CM, Sheibani N. Inflammatory cytokine-specific alterations in retinal endothelial cell function. Microvasc Res. 2013;89:57-69. PMCID: 3764503.

196. Cogswell JP, Godlevski MM, Wisely GB, Clay WC, Leesnitzer LM, Ways JP, et al. NF-kappa B regulates IL-1 beta transcription through a consensus NF-kappa B binding site and a nonconsensus CRE-like site. The Journal of Immunology. 1994;153(2):712-23.

197. Barca O, Seoane M, Senaris RM, Arce VM. Fas/CD95 ligation induces proliferation of primary fetal astrocytes through a mechanism involving caspase 8-mediated ERK activation. Cell Physiol Biochem. 2013;32(1):111-20.

198. Wakabayashi N, Slocum SL, Skoko JJ, Shin S, Kensler TW. When NRF2 talks, who's listening? Antioxid Redox Signal. 2010;13(11):1649-63. PMCID: 2966480.

199. Fan J, Xu G, Jiang T, Qin Y. Pharmacologic induction of heme oxygenase-1 plays a protective role in diabetic retinopathy in rats. Investigative Ophthalmology & Visual Science. 2012;53(10):6541-56.

200. Kang DH, Lee DJ, Lee KW, Park YS, Lee JY, Lee SH, et al. Peroxiredoxin II is an essential antioxidant enzyme that prevents the oxidative inactivation of VEGF receptor-2 in vascular endothelial cells. Mol Cell. 2011;44(4):545-58.

201. Otani A, Kojima H, Guo C, Oishi A, Yoshimura N. Low-Dose-Rate, Low-Dose Irradiation Delays Neurodegeneration in a Model of Retinitis Pigmentosa. The American Journal of Pathology. 2012;180(1):328-36.

202. Yonezawa T, Hattori S, Inagaki J, Kurosaki M, Takigawa T, Hirohata S, et al. Type IV collagen induces expression of thrombospondin-1 that is mediated by integrin α1β1 in astrocytes. Glia. 2010;58(7):755-67.

203. Nita-Lazar A, Haltiwanger RS. Methods for Analysis of O-Linked Modifications on Epidermal Growth Factor-Like and Thrombospondin Type 1 Repeats. In: Minoru F, editor. Methods in Enzymology: Academic Press; 2006. p. 93-111.

204. Cheung N, Mitchell P, Wong TY. Diabetic retinopathy. Lancet. 2010;376(9735):124-36.

205. Liu Y, Leo LF, McGregor C, Grivitishvili A, Barnstable CJ, Tombran-Tink J. Pigment epithelium-derived factor (PEDF) peptide eye drops reduce inflammation, cell death and vascular leakage in diabetic retinopathy in Ins2(Akita) mice. Mol Med. 2012;18:1387-401. PMCID: 3533643.

206. Wang S, Gottlieb JL, Sorenson CM, Sheibani N. Modulation of thrombospondin 1 and pigment epithelium-derived factor levels in vitreous fluid of patients with diabetes. Arch Ophthalmol. 2009;127(4):507-13. PMCID: 2819322.

207. Sheibani N, Sorenson CM, Cornelius LA, Frazier WA. Thrombospondin-1, a natural inhibitor of angiogenesis, is present in vitreous and aqueous humor and is modulated by hyperglycemia. Biochem Biophys Res Commun. 2000;267(1):257-61.

208. Christine M Sorenson SW, Robert Gendron, Helene Paradis, Nader Sheibani. Thrombospondin-1 Deficiency Exacerbates the Pathogensis of Diabetic Retinopathy. Journal of Diabetes and Metabolism. 2013;S12(005).

209. Zhang B, Abreu JG, Zhou K, Chen Y, Hu Y, Zhou T, et al. Blocking the Wnt pathway, a unifying mechanism for an angiogenic inhibitor in the serine proteinase inhibitor family. Proceedings of the National Academy of Sciences. 2010;107(15):6900-5.

210. Clevers H, Nusse R. Wnt/beta-catenin signaling and disease. Cell. 2012;149(6):1192-205.

211. Park K, Lee K, Zhang B, Zhou T, He X, Gao G, et al. Identification of a novel inhibitor of the canonical Wnt pathway. Mol Cell Biol. 2011;31(14):3038-51. PMCID: 3133395.

212. Chen Y, Hu Y, Zhou T, Zhou KK, Mott R, Wu M, et al. Activation of the Wnt Pathway Plays a Pathogenic Role in Diabetic Retinopathy in Humans and Animal Models. The American Journal of Pathology. 2009;175(6):2676-85.

213. Kato M, Castro NE, Natarajan R. MicroRNAs: potential mediators and biomarkers of diabetic complications. Free Radic Biol Med. 2013;64:85-94. PMCID: 3762900.

214. Guo L, Xu J, Qi J, Zhang L, Wang J, Liang J, et al. MicroRNA-17-92a upregulation by estrogen leads to Bim targeting and inhibition of osteoblast apoptosis. Journal of Cell Science. 2013;126(Pt 4):978-88.

215. Ho J, Pandey P, Schatton T, Sims-Lucas S, Khalid M, Frank MH, et al. The pro-apoptotic protein Bim is a microRNA target in kidney progenitors. J Am Soc Nephrol. 2011;22(6):1053-63. PMCID: 3103725.

216. Ozcan S, Andrali SS, Cantrell JE. Modulation of transcription factor function by O-GlcNAc modification. Biochim Biophys Acta. 2010;1799(5-6):353-64. PMCID: 2881704.

217. Donath MY, Böni-Schnetzler M, Ellingsgaard H, Halban PA, Ehses JA. Cytokine production by islets in health and diabetes: cellular origin, regulation and function. Trends in Endocrinology & Metabolism. 2010;21(5):261-7.

218. Yang WH, Park SY, Nam HW, Kim do H, Kang JG, Kang ES, et al. NFkappaB activation is associated with its O-GlcNAcylation state under hyperglycemic conditions. Proceedings of the National Academy of Sciences of the United States of America. 2008;105(45):17345-50. PMCID: 2582288.

219. Gewinner C, Hart G, Zachara N, Cole R, Beisenherz-Huss C, Groner B. The Coactivator of Transcription CREB-binding Protein Interacts Preferentially with the Glycosylated Form of Stat5. Journal of Biological Chemistry. 2004;279(5):3563-72.

220. Han RNN, Stewart DJ. Defective Lung Vascular Development in Endothelial Nitric Oxide Synthase-Deficient Mice. Trends in Cardiovascular Medicine. 2006;16(1):29-34.

221. Holderfield MT, Hughes CCW. Crosstalk Between Vascular Endothelial Growth Factor, Notch, and Transforming Growth Factor-β in Vascular Morphogenesis. Circulation Research. 2008;102(6):637-52.

222. Sheibani N, Frazier WA. Thrombospondin-1, PECAM-1, and regulation of angiogenesis. Histol Histopathol. 1999;14(1):285-94.

223. Wang S, Gottlieb JL, Sorenson CM, Sheibani N. Modulation of Thrombospondin 1 and Pigment Epithelium-Derived Factor Levels in Vitreous Fluid of Patients With Diabetes. Arch Ophthalmol. 2009;127(4):507-13.

224. Lee CG, Ma B, Takyar S, Ahangari F, DelaCruz C, He CH, et al. Studies of Vascular Endothelial Growth Factor in Asthma and Chronic Obstructive Pulmonary Disease. Proceedings of the American Thoracic Society. 2011;8(6):512-5.

225. Becerra SP, Sagasti A, Spinella P, Notario V. Pigment epithelium-derived factor behaves like a noninhibitory serpin. Neurotrophic activity does not require the serpin reactive loop. J Biol Chem. 1995;270(43):25992-9.

226. Steele FR, Chader GJ, Johnson LV, Tombran-Tink J. Pigment epithelium-derived factor: neurotrophic activity and identification as a member of the serine protease inhibitor gene family. Proc Natl Acad Sci U S A. 1993;90(4):1526-30. PMCID: 45907.

227. Tombran-Tink J, Chader GG, Johnson LV. PEDF: a pigment epithelium-derived factor with potent neuronal differentiative activity. Exp Eye Res. 1991;53(3):411-4.

228. Tombran-Tink J, Barnstable CJ. PEDF: a multifaceted neurotrophic factor. Nat Rev Neurosci. 2003;4(8):628-36.

229. Cosgrove GP, Brown KK, Schiemann WP, Serls AE, Parr JE, Geraci MW, et al. Pigment Epithelium–derived Factor in Idiopathic Pulmonary Fibrosis. American Journal of Respiratory and Critical Care Medicine. 2004;170(3):242-51.

230. Kawaguchi T, Yamagishi S, Itou M, Okuda K, Sumie S, Kuromatsu R, et al. Pigment epithelium-derived factor inhibits lysosomal degradation of Bcl-xL and apoptosis in HepG2 cells. Am J Pathol. 2010;176(1):168-76. PMCID: 2797879.

231. Ueda S, Yamagishi S, Matsui T, Jinnouchi Y, Imaizumi T. Administration of pigment epithelium-derived factor inhibits left ventricular remodeling and improves cardiac function in rats with acute myocardial infarction. Am J Pathol. 2011;178(2):591-8. PMCID: 3278887.

232. Doll JA, Stellmach VM, Bouck NP, Bergh AR, Lee C, Abramson LP, et al. Pigment epithelium-derived factor regulates the vasculature and mass of the prostate and pancreas. Nat Med. 2003;9(6):774-80.

233. Dawson DW, Volpert OV, Gillis P, Crawford SE, Xu H, Benedict W, et al. Pigment epithelium-derived factor: a potent inhibitor of angiogenesis. Science. 1999;285(5425):245-8.

234. Chen L, Zhang SS-M, Barnstable CJ, Tombran-Tink J. PEDF induces apoptosis in human endothelial cells by activating p38 MAP kinase dependent cleavage of multiple caspases. Biochemical and Biophysical Research Communications. 2006;348(4):1288-95.

235. Park K, Jin J, Hu Y, Zhou K, Ma JX. Overexpression of pigment epithelium-derived factor inhibits retinal inflammation and neovascularization. Am J Pathol. 2011;178(2):688-98. PMCID: 3070578.

236. Wang JJ, Zhang SX, Mott R, Chen Y, Knapp RR, Cao W, et al. Anti-inflammatory effects of pigment epithelium-derived factor in diabetic nephropathy. Am J Physiol Renal Physiol. 2008;294(5):F1166-73.

237. Ahn JK, Moon HJ. Changes in Aqueous Vascular Endothelial Growth Factor and Pigment Epithelium-derived Factor after Ranibizumab Alone or Combined with Verteporfin for Exudative Age-related Macular Degeneration. American Journal of Ophthalmology. 2009;148(5):718-24.e1.

238. Kasahara Y, Tuder RM, Taraseviciene-Stewart L, Le Cras TD, Abman S, Hirth PK, et al. Inhibition of VEGF receptors causes lung cell apoptosis and emphysema. J Clin Invest. 2000;106(11):1311-9. PMCID: 387249.

239. Zudaire E, Gambardella L, Kurcz C, Vermeren S. A Computational Tool for Quantitative Analysis of Vascular Networks. PLoS One. 2011;6(11):e27385.

240. Julie G. Breaking the VE-cadherin bonds. FEBS Letters. 2009;583(1):1-6.

241. Park K, Lee K, Zhang B, Zhou T, He X, Gao G, et al. Identification of a novel inhibitor of the canonical Wnt pathway. Mol Cell Biol. 2011;31(14):3038-51. PMCID: 3133395.

242. Tang Y, Scheef EA, Gurel Z, Sorenson CM, Jefcoate CR, Sheibani N. CYP1B1 and endothelial nitric oxide synthase combine to sustain proangiogenic functions of endothelial cells under hyperoxic stress. Am J Physiol Cell Physiol. 2010;298(3):C665-78. PMCID: 2838582.

243. Morais C, Ebrahem Q, Anand-Apte B, Parat MO. Altered angiogenesis in caveolin-1 gene-deficient mice is restored by ablation of endothelial nitric oxide synthase. Am J Pathol. 2012;180(4):1702-14.

244. Qiao J, Huang F, Naikawadi RP, Kim KS, Said T, Lum H. Lysophosphatidylcholine impairs endothelial barrier function through the G protein-coupled receptor GPR4. American Journal of Physiology - Lung Cellular and Molecular Physiology. 2006;291(1):L91-L101.

245. Savale L, Tu L, Rideau D, Izziki M, Maitre B, Adnot S, et al. Impact of interleukin-6 on hypoxia-induced pulmonary hypertension and lung inflammation in mice. Respiratory Research. 2009;10(1):6.

246. Aziz M, Matsuda A, Yang WL, Jacob A, Wang P. Milk fat globule-epidermal growth factor-factor 8 attenuates neutrophil infiltration in acute lung injury via modulation of CXCR2. J Immunol. 2012;189(1):393-402. PMCID: 3382007.

247. Favre CJ, Mancuso M, Maas K, McLean JW, Baluk P, McDonald DM. Expression of genes involved in vascular development and angiogenesis in endothelial cells of adult lung. Am J Physiol Heart Circ Physiol. 2003;285(5):H1917-38.

248. Bernard A, Gao-Li J, Franco CA, Bouceba T, Huet A, Li Z. Laminin receptor involvement in the anti-angiogenic activity of pigment epithelium-derived factor. J Biol Chem. 2009;284(16):10480-90. PMCID: 2667735.

249. Devallière J, Chatelais M, Fitau J, Gérard N, Hulin P, Velazquez L, et al. LNK (SH2B3) is a key regulator of integrin signaling in endothelial cells and targets α-parvin to control cell adhesion and migration. The FASEB Journal. 2012;26(6):2592-606.

250. Oviedo PJ, Sobrino A, Laguna-Fernandez A, Novella S, Tarín JJ, García-Pérez M-A, et al. Estradiol induces endothelial cell migration and proliferation through estrogen receptor-enhanced RhoA/ROCK pathway. Molecular and Cellular Endocrinology. 2011;335(2):96-103.

251. Schweitzer KS, Hatoum H, Brown MB, Gupta M, Justice MJ, Beteck B, et al. Mechanisms of lung endothelial barrier disruption induced by cigarette smoke: role of oxidative stress and ceramides. Am J Physiol Lung Cell Mol Physiol. 2011;301(6):L836-46. PMCID: 3233827.

252. Karmpaliotis D, Kosmidou I, Ingenito EP, Hong K, Malhotra A, Sunday ME, et al. Angiogenic growth factors in the pathophysiology of a murine model of acute lung injury. American Journal of Physiology - Lung Cellular and Molecular Physiology. 2002;283(3):L585-L95.

253. O'Dea KP, Dokpesi JO, Tatham KC, Wilson MR, Takata M. Regulation of monocyte subset proinflammatory responses within the lung microvasculature by the p38 MAPK/MK2 pathway. Am J Physiol Lung Cell Mol Physiol. 2011;301(5):L812-21. PMCID: 3213987.

254. Sugiura H, Ichinose M. Nitrative stress in inflammatory lung diseases. Nitric Oxide. 2011;25(2):138-44.

255. Zhang SX, Wang JJ, Dashti A, Wilson K, Zou MH, Szweda L, et al. Pigment epithelium-derived factor mitigates inflammation and oxidative stress in retinal pericytes exposed to oxidized low-density lipoprotein. J Mol Endocrinol. 2008;41(3):135-43. PMCID: 2714421.

256. Du Q, Park KS, Guo Z, He P, Nagashima M, Shao L, et al. Regulation of human nitric oxide synthase 2 expression by Wnt beta-catenin signaling. Cancer Res. 2006;66(14):7024-31.

257. Matsumoto K, Ishikawa H, Nishimura D, Hamasaki K, Nakao K, Eguchi K. Antiangiogenic property of pigment epithelium-derived factor in hepatocellular carcinoma. Hepatology. 2004;40(1):252-9.

258. Cooney R, Hynes SO, Duffy AM, Sharif F, O'Brien T. Adenoviral-mediated gene transfer of nitric oxide synthase isoforms and vascular cell proliferation. J Vasc Res. 2006;43(5):462-72.

259. Tomko RJ, Jr., Azang-Njaah NN, Lazo JS. Nitrosative stress suppresses checkpoint activation after DNA synthesis inhibition. Cell Cycle. 2009;8(2):299-305. PMCID: 2752830.

260. Van Obberghen-Schilling E, Tucker RP, Saupe F, Gasser I, Cseh B, Orend G. Fibronectin and tenascin-C: accomplices in vascular morphogenesis during development and tumor growth. Int J Dev Biol. 2011;55(4-5):511-25.

261. Yu M, Liu Q, Yi K, Wu L, Tan X. Effects of osteopontin on functional activity of late endothelial progenitor cells. Journal of Cellular Biochemistry. 2011;112(7):1730-6.

262. Hiscott P, Paraoan L, Choudhary A, Ordonez JL, Al-Khaier A, Armstrong DJ. Thrombospondin 1, thrombospondin 2 and the eye. Progress in Retinal and Eye Research. 2006;25(1):1-18.

263. Lin T-n, Kim G-M, Chen J-J, Cheung W-M, He YY, Hsu CY. Differential Regulation of Thrombospondin-1 and Thrombospondin-2 After Focal Cerebral Ischemia/Reperfusion. Stroke. 2003;34(1):177-86.

264. Cui T, Miksa M, Wu R, Komura H, Zhou M, Dong W, et al. Milk Fat Globule Epidermal Growth Factor 8 Attenuates Acute Lung Injury in Mice after Intestinal Ischemia and Reperfusion. American Journal of Respiratory and Critical Care Medicine. 2010;181(3):238-46.

265. Zamiri P, Masli S, Streilein JW, Taylor AW. Pigment Epithelial Growth Factor Suppresses Inflammation by Modulating Macrophage Activation. Investigative Ophthalmology & Visual Science. 2006;47(9):3912-8.

266. Zhang SX, Wang JJ, Dashti A, Wilson K, Zou M-H, Szweda L, et al. Pigment epithelium-derived factor mitigates inflammation and oxidative stress in retinal pericytes exposed to oxidized low-density lipoprotein. Journal of Molecular Endocrinology. 2008;41(3):135-43.

267. Hopkins N, Cadogan E, Giles S, McLoughlin P. Chronic airway infection leads to angiogenesis in the pulmonary circulation. Journal of Applied Physiology. 2001;91(2):919-28.